UNIVERSITA' DEGLI STUDI DI SIENA
DIPARTIMENTO Biotecnologie, Chimica e Farmacia

DOTTORATO DI RICERCA IN
Chemical and Pharmaceutical Sciences
CICLO XXXIV
COORDINATORE Prof. Maurizio Taddei

TITOLO DELLA TESI:

COMPARTMENTALIZED ALGAL-BASED NANOCARRIERS AS VECTORS FOR ANTIOXIDANTS: STRUCTURAL AND FUNCTIONAL CHARACTERIZATION

SETTORE SCIENTIFICO-DISCIPLINARE: CHIM 02

DOTTORANDO
Ilaria Clemente

TUTOR
Prof. Claudio Rossi
Co-tutor Prof.ssa Sandra Ristori (Università degli Studi di Firenze & CSGI)

ANNO ACCADEMICO: 2020/2021

Summary

Chapter 1

1.Introduction

1.1 Drug delivery of bioactive compounds

The delivery of bioactive molecules with poor or limited solubility in aqueous environments is an active field of research and a challenge in formulation and delivery science.[1,2,3,4] Hydrophobic bioactive agents display a broad spectrum of potential activity against many diseases, possessing antimicrobial, neuroprotective, anti-inflammatory and antioxidant properties and thus constituting an interesting and vast class of compounds. In fact, most of the existing drugs nowadays fall under this category, since the methods applied in the process of discovery often generate poorly water-soluble molecules as drug candidates.[5,6,7] This directly derives from the fact that longtime experimental evidence has shown that most natural bioactive drugs possess hydrophobic character and are thus scarcely soluble in aqueous environments, which is due to functional reasons. Since the biological compartments in living organisms are defined and separated by amphiphilic barriers with hydrophobic inner core, it is necessary for drug molecules to have the ability to cross them to be available for absorption at the target site.[3,4,8] Thus, the nature of the delivery issue lies in the experimental constraints encountered in the attempt to solubilize bioactive compounds. Several widely known drugs with high therapeutic success, such as doxorubicin and paclitaxel, are poorly water-soluble and would have never been marketed without the help of improved solubilization techniques.[9,10,11] Various delivery systems have been developed specifically and are today commercially available for both of these representative hydrophobic bioactives. Based on these premises, synthetic drug candidates are selected to possess certain properties typical of natural bioactives that were experimentally known to produce an effective therapeutic outcome, which usually results in a high number of hydrophobic and scarcely soluble compounds.[5,12] Consequently, computational methods such as combinatorial chemistry and high throughput screening techniques are particularly affected by this outcome. The scarce solubility in aqueous media of many drugs is a longtime drawback in pharmaceutics, since it usually result in poor bioavailability and large fluctuations in the rate of absorption by patients, that frequently is not balanced by permeability.[4,13,14] Thus, the application on commercial scale of several bioactives is hindered by this obstacle, that additionally can be correlated with stability issues. The complexity of the solubility problem lies first and foremost in the experimental assessment of the problem itself. Indeed, even though the nature of this issue has been studied for several decades, the empirical testing and predictive ability of the available methods is still partially lacking.[12,15] The quantitative assessment of solvation limits in

water, biological activity and pharmacokinetics of poorly water-soluble drugs was recently tackled by combining experimental and computational approaches.[16] Nevertheless, the incompleteness of reliable and reproducible experimental data limits the full exploitation of these techniques.

The main issues regarding solubility are the experimental identification of scarcely soluble bioactive molecules and their solvation limits, the classification of the relevant physicochemical properties that determine these limits and how the balance among these latter should work to improve this constraint.[12,4] Indeed, experimental data obtained on bioactives established that some characteristics connected to scarce solubility are necessary for functionality. Several efforts were dedicated through the years to establish reliable experimental, and later, computational approaches to recognize unfailingly these molecules and evidence the relevant parameters determining their behavior.[17,18] Indeed, many poorly water-soluble bioactives remained undetected as solvation-problematic for long time since the experimental methods to measure solubility were generally not appropriate, too simplistic and no analytical standard technique was established, leading to lack of data and consequent delivery issues and scarce efficacy.[19,20] Particularly, there is often limited availability on the quantity of synthetized compound to be experimentally analyzed so that the extracted information is generally not accurate, which influences also computational methods when it is fed to the algorithms. Even when the direct measurement is carried out by solvating the molecule at different concentrations and prolonging the experimental duration to ensure that the solubility equilibrium is reached, detection limits and reproducibility of the measured values, plus masking effects given by organic solvents can still constitute an issue. The obtained experimental results on solubility are usually complemented by evidence from other physicochemical studies to describe appropriately the eventual existing correlations, and thus improve the synthetic procedures and the predictive ability of the algorithms. This data is nowadays then treated with computational approaches to determine reliable molecular descriptors to identify bioactive scarcely soluble compounds and calculate which ones could likely get to the end of the drug development process and be formulated in a suitable form for delivery.

Regarding the correlation with other factors, through the years several experimentally measured and then calculated properties were analyzed to determine what physicochemical characteristics constituted relevant parameters related to poor aqueous solubility of bioactive molecules.[21,13] Among evaluated factors the molecular size, the lipophilicity, the polarizability, the presence and number of H-bond donors and acceptors, the partition coefficient, and the energy difference between the HOMO and LUMO were deemed to be some of the most significant. Some of these parameters were also included in the well-known rule in drug discovery, the so-called rule of five that considers these

quantities to impose to the algorithm, and sets range of values to predict the poor absorption and permeation of drug candidates[22,13] on the basis of previously observed empirical evidence. According to this famous rule proposed by Lipinski et al., the above mentioned properties are the most important parameters determining favorable or scarce solubility. This hypothesis found additional confirmation in subsequent studies that evidenced the correlation between each factor and the experimentally measured solubility values, obtaining energy-related considerations on the favorability of these properties.[23] In fact, the molecular size and its related descriptors such as molecular weight, polarizability and nonpolar surface area had already all been found empirically to be decreasing factors for solubility in several bioactives. Thus, analytical measurements combined with calculations can manage to identify the solubility limits of bioactive compounds to be efficiently screened as drug candidates, even though the computational data must be once again validated by experimental results. The two aspects discussed above are employed to assess the extent of the poor solubility of potentially interesting bioactives and thus elaborate a delivery strategy.

Nevertheless, also the stability and permeability play a relevant role in determining the efficacy of orally active drugs. Several poorly-soluble compounds were selected in the past for drug development and thanks to formulation design strategies they could still be marketed despite their scarce solubility. Indeed, to obtain an orally active formulation a balance of solubility, stability and permeability should be achieved.[3,4] There are a number of approaches that can be adopted to improve these properties, in particular for certain lipophilic compounds, referred to in the literature as “grease balls” due to their high hydrophobicity.[12] Appropriate solubilizing agents can be added to obtain a suitable formulation to increase the solubility and successfully obtain their therapeutic effect.[24] Among the available delivery strategies, the formulation of the compound of interest with the addition of excipients, e. g. wetting agents, solubility enhancers, disintegrants, surfactants, lipids and encapsulants in general are usually very effective options.[4,25,26] Moreover, it has been shown that also bile salts and other surface-active components present in the intestinal fluid are able to improve solubility and concur to the successful drug development process of highly lipophilic molecules.[27] Besides, the improvement of stability and circulation time in the organism often represents a limiting step in the development of adequate formulations. Indeed, several biomolecules present low resistance to degradation and chemical or physical instability in physiological conditions.[28] Chemical instability to dissolution, pH and ionic force shifts, temperature, etc. typically results in drug oxidation, reduction, hydrolysis and isomerization. Physical instability of the bioactive molecules in the system occurs when these latter are susceptible to phase changes (e. g. crystallization-melting or polymorphic transitions), gravitational separation and aggregation. These shortcomings can be solved through various approaches, for example protecting the drug by loading in the carrier system or retarding aggregation

and phase changes to increase physical stability.[28] The identification of the main actors causing the instability is fundamental to design and formulate effective delivery systems able to protect the cargo and prevent degradation. Generally, the formulation method is selected by adapting the best suited approach according to the drug and the biological target, since the vector-target compatibility plays a major role in successful drug administration.

Among the most popular techniques are the ones based on nanoformulations such as encapsulation or co-delivery of hydrophobic drugs in nanoparticle-based carriers fabricated from either inorganic (i. e. metal-based complexes, mineral crystals) or organic (i. e. colloidal systems from lipids, surfactants, polymers or proteins/polysaccharide complexes) matter, that are able to solubilize and protect the guest compound thus elongating its circulation time.[4,29] Even though a universal encapsulation method capable of increasing notably the bioavailability of most drugs is still yet to be found, nanotechnology-based approaches have been considered the most appropriate to improve the applicability of natural hydrophobic drugs.[30] Encapsulation methods highly rely on the affinity and association between the carrier system and the guest compound, that are needed to achieve both high rate of loading and solubilization/dispersion of the drug and to ensure stability of the formulation against aspecific disruption or degradation conditions. In fact, affinity is a fundamental requisite since no chemical covalent bonds are formed between the encapsulant aggregate and the guest molecule, but instead the formation of the formulation is governed by physicochemical forces and geometrical constraints.[31,32] The necessary requirement is the presence of a suitable association or positioning of the guest molecule to be enclosed in the host aggregate. The intermolecular forces at play during the encapsulation process are mostly hydrophobic interactions, van der Waals and London dispersion forces and hydrogen bonding which all concur to the association. Eventually, the exclusion of water from the apolar moieties of the assembly and conformational adjustments may contribute as well to the process.[29,33] The host aggregate should possess adequate topological properties such as size and surface-to-volume ratio to fit the guest molecule, as well as compatible charges and polarity to ensure the proper positioning and intermolecular association during encapsulation. The stereochemistry and dipolar orientation of both host aggregate and guest compound are concurring conditions that affect the efficacy of the loaded system formation, together with the employed solvent and temperature. The combination of these concomitant forces generates a significantly stable aggregate between the two components, associating together through strong interactions.[33] Thus, nano-encapsulation and dispersion are favored by several stability and thermodynamic contributes that should be carefully considered to control the formation of the loaded system. Indeed, as reported in the literature, it is possible to change the experimental conditions such as temperature, pH, concentration and solvent and naturally, the selected host carrier according to the desired outcome, in order to tune certain

desired properties of the vector-guest assembly in course of formation.[26] As an example, the attempt to obtain more biocompatible and biomimetic delivery systems has been the focus of the attention in recent years. Since the use of encapsulation techniques is particularly popular in pharmaceutical applications where the drug of interest should be orally administrated and absorbed by the gastrointestinal tract or in food science as well, the biocompatibility of the obtained formulation is a particularly relevant aspect.[29]

In general, the source materials should be readily accessible, while the fabrication process should be relatively inexpensive, reproducible and easy to perform and scale-up for large-scale production. The nano-fabrication methods use a variety of approaches that can be classified into top-down, bottom-up or a combination of both, depending on the physicochemical processes employed.[34] The former methods involve the modification of massive materials to obtain dispersions, as an example by phase homogenization procedures, grinding of bulk matter to reduce size or by injecting a liquid phase into a different phase, whereas in the bottom-up processes the assembly proceeds from smaller building blocks to form larger aggregates. Frequently, it is not uncommon to employ a combination of both methods to obtain delivery systems with the desired composition, structural and physicochemical properties.[35] Since these attributes are the main parameters influencing the stability, biocompatibility and bioavailability of the obtained nano-formulation, careful optimization of the steps of the preparation procedure is required. A successful delivery nanosystem must then stabilize the hydrophobic drug in the carrier aggregate and release it in a bioactive form once the site of absorption is reached. In particular, the choice of the composition of the building blocks that should fall into the "generally recognized as safe" (GRAS) FDA definition, greatly impacts on the formulation structural and functional properties i. e. its dimensions, morphology, molecular interactions, encapsulation and loading capacity, cargo protection, retention and release efficiency.[25] As a consequence, the biocompatibility and bioavailability will be influenced accordingly. Indeed, if the formulation should be orally administrated and release its cargo in the intestinal tract, then the aggregate components should remain intact until that point and then be processed by intestinal enzymes and release the guest drug upon digestion. So, the building blocks components should be selected to design a delivery system that can improve the overall bioavailability by increasing the fraction of drug that is present in a bioactive form in the gastrointestinal tract, that is accessible during digestion and that is then absorbed.[36] Moreover, the encapsulated molecule should be kept isolated and protected to avoid interactions with other bioactives. This is true both for pharmaceutical dosage forms and food-grade colloids such as dietary supplements and micronutrient carriers.[28] Many available examples can be found in the literature since the choice of the most appropriate system should be made on a case-by-

case basis, even though the main focus is generally on the use of natural-derived soft matter aggregates, be it surfactant-, lipid-, carbohydrate-, or protein-based.[37]

Surfactants are quite popular solubilizing agents thanks to their amphiphilicity and general biocompatibility, and their use as building blocks for microemulsions and micellar systems is rather common.[33] Indeed, both types of systems are self-assembly aggregates of the surfactant itself, with the presence of an oil phase in the former case, that display amphiphilic character thus are particularly suited to encapsulate lipophilic bioactives and solubilize them in aqueous environments. Moreover, their ability to form complexes with drugs also in solid form has proven to be an effective method to increase solubility and wettability. The so-called drug solid dispersions with amphiphilic surfactants showed many advantages in increasing the dissolution properties and the stability of drugs and are often reported as one of the most promising approaches.[38] The solid dispersion is formed by mixing the powdered drug with the surfactant and it is then loaded in an inert carrier such as a polymeric matrix, that will then transport the bioactive molecule-surfactant system. In fact, surfactants can interact with the drug and form micellar aggregates that increase the drug solubility and stability thanks to the action of the amphiphilic component, that inhibits the precipitation and controls the dissolution rate. Clearly, screening tests are available to select the most appropriate surfactant and preparation method for the drug of interest and the intended application.

Lipids are one of the main classes of molecules employed as building blocks of many nanocarriers in pharmaceutics and food industry e. g. liposomes, nanoemulsions, solid lipid nanoparticles (SLNs), lipid nanovectors of varied symmetry.[39] These aggregates present the advantage of being often formed from natural-derived substances, since lipids can be extracted from food ingredients like egg, soy, dairy, sunflower, microorganisms or cultivation biomasses, thus granting biocompatibility of the prepared systems. Liposomes are generally obtained from self-assembled phospholipids bilayers in aqueous environments by energy input which induces the formation of out-of-equilibrium vesicles. These aggregates present one or more compartments having an onion-like organization with aqueous core and quasi-spherical shape.[33,40] The presence of both a hydrophilic and hydrophobic phase is particularly favorable for the incorporation of a variety of different molecules, that can be encapsulated either in the aqueous core or in the lipidic membrane by loading them during liposome formation.[40] Single- or multi-nanoemulsions are nanosized nonequilibrium colloidal dispersions formed from emulsifiers that disperse and stabilize an oil phase in droplets into an aqueous medium. The so-formed core–shell nanostructures possess an inner hydrophobic phase formed by oil components and the non-polar moieties of emulsifiers, whereas the polar shell consists of the polar parts of the emulsifiers at the interface with the aqueous continuous phase.[41] Lipophilic bioactives

are usually encapsulated in the hydrophobic core to solubilize them and improve bioavailability. Solid lipid nanoparticles are prepared like conventional O/W (oil/water) emulsions and then cooled down to induce lipid crystallization and partial or complete solidification of the lipid phase.[42] The nature of the interfacial layer surrounding the lipid phase can be modulated according to the desired outcome like in conventional emulsions and the bioactives can be encapsulated in the solid matrix for enhanced protection and retention.

Other types of inclusion complexes, even though based on single-molecule structures instead of nanocarriers, are carbohydrates such as cyclodextrins, a class of starch-derived cyclic carbohydrates often employed as complexating agents. They are generally non-toxic and are not absorbed in the upper gastrointestinal tract but metabolized in the colon, and they are labelled as GRAS to be used as food additives. Indeed, they can be used as flavor carriers and preserving agents thanks to their ability to form molecular interactions with several compounds and encapsulate them both in solid and aqueous phases.[43] Cyclodextrins possess a truncated cone structure with a hollow cavity inside with low polarity groups that can be considered a hydrophobic environment, whereas the external groups are hydrophilic, thus granting the aqueous solubility. This property can be exploited to form molecular inclusion assemblies with poorly water-soluble compounds, consequently achieving increased drug solubilization and stabilization.[44] Moreover, considering the natural origin of cyclodextrins that grants good biocompatibility, these encapsulating compounds are particularly suitable to incorporate food-grade and anti-bacterial molecules such as essential oils and volatiles.

Also proteins and biopolymers are often employed in combination to obtain biocompatible carriers with appropriate stability and incorporation capability for non-polar bioactives. A frequently found combination is the use of zein, a hydrophobic protein from corn that is able to assemble in nanoaggregates, stabilized by coatings of various types of polysaccharides e. g. chitosan, pectin, alginate, carrageenan.[45] These polysaccharides have been reported to improve the stability of protein nanoparticles by preventing excessive aggregation and increasing their resistance to shifts in environmental conditions, particularly when cross-linked themselves to form compact gel-like structures on the surface. Indeed, these co-delivery systems were able to improve the water-dispersibility, stability, and bioavailability of some investigated hydrophobic nutraceuticals, thus offering an alternative carrier for oral administration from natural-derived components.

In this thesis, lipid-based nanocarriers were selected over single molecule complexes due to the above mentioned advantageous properties, such as the use of nature-derived building blocks and bioavailability. Moreover, their polymorphism and assembly flexibility grant several design possibilities to better adapt the nanocarriers to the delivery purposes.

1.2 Soft matter (lipid) nanosystems

Among soft matter lipid nanosystems suitable as drug delivery vectors, lipid mesophases possess ideal characteristics of biocompatibility and biodegradability and generally high surface-to-volume ratio, which leads to good bioactive encapsulation capability. Moreover, their easily tunable character concurs to optimal control over retention and release properties. These systems are supramolecular assemblies with two- or three-dimensional periodicity particularly interesting for their rich mesomorphism and ability to self-organize in various architectures.[46] They are classified as lyotropic liquid crystals since they share with crystals the presence of short-range positional order at the molecular/particle scale, like the well-known thermotropic ones, but similarly to liquids they also display long-range positional and motional disorder.[47,48] Due to the polymorphic properties of lipids, upon hydration these molecules can self-assemble in various supramolecular arrangements deriving from the subtle balance between their hydrophilic and hydrophobic moieties. The interplay of several contributions such as interfacial curvature, lipid packing frustration, headgroup hydrophilicity and functionality, tail group hydrophobicity and fluidity determine the self-assembly, in particular for structures deviating from the planar and fluid lamellar phase (L_α) with zero mean curvature.[49] Indeed, the lamellar phase is formed by amphiphilic bilayer stackings in two dimensions intercalated by aqueous environment. The Lα lamellar phase, that is the simplest and most commonly found phase, possesses disordered lipid tails in the two-dimensional layers whereas for the Lβ the tails display a lattice organization. The single bilayer unit, that is then found also in other more articulated nonlamellar architectures, is composed by two monolayers tightly packed together to keep segregated from water, with the hydrophobic tails facing each other in the inner core and the polar heads hydrated by water.[46,50] In fact, the self-assembly is spontaneously driven by the hydrophobic effect, that leads to interaction and segregation of the hydrophobic tails in water, and by the entropic contribution given by the water molecules excluded from the hydrocarbon chains volume. The confinement of the tails in the inner bilayer core is functional to minimize the interactions between apolar molecules, that interact to form the lipid aggregate, and the polar aqueous solvent, that structures itself around the hydrophobic assembly to minimize the surface area of contact with the lipid phase as well.[51] Indeed, the disruption of strongly bound and structured water molecules to solubilize the single lipid molecules in a mixture would involve a much higher energy cost. On the contrary, the organization of hydrophobic lipid moieties in a network or aggregate surrounded by a self-interacting continuous water medium results in a much lower Gibbs free energy, thus leading to the spontaneous self-assembly of lipid molecules above a certain critical aggregation concentration upon hydration by water. The polar headgroup moieties interacting with water will then position at the interface with the aqueous environment. However, these aggregates maintain a dynamics that allows rearrangements

both at the bilayer and supramolecular scale, and various conformational or fluidity states are possible upon changes in the environmental conditions e. g. water content, monomer concentration, temperature etc.[47,48] Generally, the aggregation in the energetically lower architecture according to the lipid type, the temperature and dilution conditions will be favored. The global aggregate topology is greatly influenced by the lipid type since the local geometry and shape are relevant factors for the molecular packing in the aggregates. The geometric relationship between the molecular volume and surface area at the interface for a particular molecular length is defined as critical packing parameter (CPP), that is the ratio between the volume of the hydrophobic chain and its length, times the cross-section of the molecular area.[52] The values obtained for this parameter can define qualitatively and reasonably predict the resulting topology of the self-assembled aggregate. The packing parameter thus defines a local geometrical constraint which directs the orientation of the interfacial membrane towards positive or negative curvatures, with respect to the reference zero curvature of the lamellar phase that corresponds to a packing parameter equal to unity, typical of cylindrical-shaped lipids. Thus, this property is dependent on the intrinsic shape and chemical functionality of the amphiphile. Packing parameters significantly different from unity will result in highly curved lipid surfaces, leading to complex 2- or 3-D bilayer organizations that are defined as direct or Type I for positive curvature, and inverse or Type II for negative curvature.[53] The former or latter type depends on the lateral pressure on the interfacial monolayer exerted either on the headgroups or the tails, respectively, pushing the curvature towards the opposite moiety. Moreover, cone-shaped amphiphiles with large headgroup volume tend to favor positive mean curvature (Type I), whereas negative mean curvature (Type II) is preferred by wedge-shaped amphiphiles, which possess splayed tails that increase the hydrophobic volume.[47] This simple parameter is able to give a fairly reliable predictive tool of the available topologies for a certain molecular shape in certain conditions of temperature, hydration, steric and molecular interactions. Other models taking into account the contribution of the free energies of monolayer curvature, hydrocarbon tail packing frustration and intermolecular forces are generally able to give more accurate predictions of the achievable symmetries.

Among the different existing arrangements some of the most investigated and applied, apart from the flat lamellar phases, are the hexagonal and cubic phases that form two- and three-dimensional structures, respectively.[54] Both types are nonlamellar structures where the order of increasingly negative interfacial curvature with respect to the lamellar phase goes from the cubic phases, that possesses three mainly studied topologies, to the hexagonal phases (see Figure 1). More negative curvatures can be reached by the micellar cubic phases, that are however less commonly found architectures.[46,55] The hexagonal phases are two-dimensional architectures constituted by infinitely long rod-like cylindrical micelles densely packed at the vertices of an hexagonal lattice with one

cylinder in the middle. The water-lipid headgroups are disposed around the cylinders whereas the lipid hydrophobic tails fill the continuous region. Since their first observations in the 60s, the possibility to obtain cubic phases of different symmetries in aqueous dispersions has been largely explored.[56] The interest in these structures led to the categorization of several types of cubic symmetries identified by their crystallographic space group that differentiates the spacing of the repeat unit cell. The main phases identified so far include the micellar type I with three different space groups, the inverse micellar type II and the three best-known bicontinuous inverted cubic phases with space groups Q224 (Pn3m double-diamond), Q229 (Im3m primitive), and Q230 (Ia3d gyroid).[57,58] These nonlamellar mesophases are formed by classes of lipids with critical packing parameters different from unity which allows both positive and negative curvature of the lipid-water interface. This property generates a surface of contiguous lipid bilayers draped around two non-interconnected water channels, that can be described with the theory of infinitely periodic minimal surfaces (IPMS). The mathemathical concept of minimal surface can be described as a surface curved in three-dimensional space where every point is a saddle point of the two main curvatures that are equal in value with opposite sign, giving a mean zero curvature in each surface point. If the surface is extended in 3-D space, infinitely periodic minimal surfaces are obtained. Following this representation, the bicontinuous cubic phases can be described as an highly curved triply periodic lipidic bilayer, with a zero mean curvature at each point on the bilayer midplane surface, so that the interfacial energy and the frustration of the lipid chains can be minimized. The aqueous environment surrounding the phase is then subdivided in two sets of interpenetrating but nonintersecting channel networks.[59,60] The three bicontinuous phases are termed as diamond, primitive and gyroid following the surface geometry nomenclature used in the IPMS theory[61] and referring to the connectivity of the water channels systems. Indeed, the Ia3d double gyroid displays threefold connectivity of aqueous channels, the Pn3m double diamond has a fourfold connectivity and the Im3m primitive sixfold, respectively. The three topologies are related to each other by an isometric relationship, meaning that each phase can be continuously deformed into another via stretching transformation while maintaining constant average curvature and constant Gaussian curvature, which determines the topological membrane type, due to their flexibility.[46] The structured networks formed by these phases are optically isotropic (non birefringent) and optically transparent, with varied viscosity in the optimal range to act as drug depot.

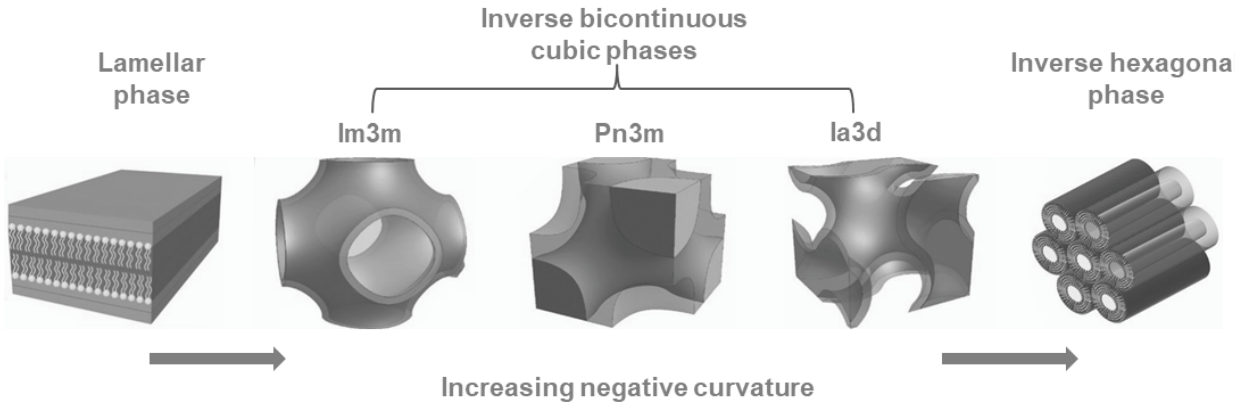

Figure 1. Lipid mesophases in order of increasing negative curvature from left to right, i. e. lamellar phase, the three inverse bicontinuous cubic Im3m, Pn3m and Ia3d, and the inverse hexagonal phase.

The critical packing parameter alone cannot fully describe the bicontinuous cubic phases due to the complexity of these structures. Nevertheless, some lipid classes are known for their tendency to favor the assembly in these architectures. In particular, neutral lipids with wedge-shaped structures such as glycerols and triglycerides are usually employed to obtain these phases in water, since they can assemble with either positive or negative curvatures of the interfacial layer and their ability to transit from one phase to the other is known from their phase diagrams.[47] Indeed, by increasing the water content in the system or the temperature, transitions from the Ia3d gyroid to the Pn3m double diamond were observed. The swelling of this latter until the point of maximum hydration of the water channels results in a state of thermodynamic equilibrium where the excess water outside the Pn3m cubic phase coexists with it. The same lyotropic-liquid-crystalline behavior was observed for transitions from the Ia3d gyroid to the primitive Im3m at increasing water content and temperature as well, even though additional increase of this latter parameter leads to transitions from cubic to inverse hexagonal phase.[46] This behavior is generally shared among all types of cubic, hexagonal and micellar bicontinuous phases also depending on the employed lipids. Nevertheless, at excess water content beyond the maximum swelling of lipid bicontinuous phases, the two most commonly observed at thermodynamic equilibrium with the water outside the channels are the Pn3m and Im3m cubic. The ability to coexist with excess water in equilibrium is a crucial property of lipid mesophases, that makes these systems particularly appropriate as drug delivery vectors. In fact, this results in enhanced stability of the lipid structured networks for the entire duration of the drug transportation and administration, thus resulting in an advantageous attribute with respect to other complexes, e. g. trasport by a single molecule, such as carbohydrates or proteins. Moreover, when the bulk lipid mesophases are in this state of maximum hydration in coexistence with the excess water, a dispersed nanostructured system can be obtained by adding stabilizing agents or energy. Indeed, these dispersed lipid mesophases in dilute regimes are generally obtained by high-energy input through sonication or

addition of stabilizing molecules to the dispersion, until an homogeneous nanostructure is obtained and kinetically stabilized. This is commonly done for cubic and hexagonal mesophases, which also thanks to their high surface-to-volume ratio and high fraction of compartmentalization possess better encapsulation efficiency with respect to other phases. The obtained dispersed forms of bulk cubic and hexagonal phases are termed cubosomes and hexosomes respectively, and they exhibit analogous nanostructured organization at the supramolecular level so that the same topological descriptors and terminology apply.[47] On the other hand, they show enhanced properties as drug delivery carriers with respect to the parent bulk mesophases e. g. optical transparency, lower turbidity, improved fluidity deriving from lower viscosity and larger surface area with the same available volume. The long-term stability is usually granted by the employed stabilizers so that they possess optimal shelf-life and due to their flexibility they can be destined to several applications. In particular, through the years several functionalized hexosomes and cubosomes were proposed to be used as stimuli-responsive carriers to precisely release their cargo following various environmental stimuli e. g. light, pH, molecular detection, magnetic fields, etc. At the same time, even though these systems generally show biodegradable and biocompatible attributes, growing attention has been recently focused on the use of safe sources of lipid building blocks to obtain GRAS classified commercial products to deliver poorly-water soluble molecules for human and environmental applications.

1.3 Suitable sources of soft matter

The use of natural-derived materials as a source of building blocks for soft matter nanosystems has been lately the focus of many research efforts. Two main reasons are the drivers of this interest, i. e. (i) the quest for bioinspired and biomimetic formulations for safe human and animal use, so that these latter should be at the same time biocompatible with living organisms and easily biodegradable, and (ii) the possibility of employing natural biomasses as sources to potentially generate a virtuous cycle for waste materials with no other end use or to extract additional value from already exploited materials. From the applicative point of view, the potential of biomimetic membrane-based systems in translational science has been shown already by liposomal carriers, that have been approved in several pharmaceutic formulations with more currently on trial phases.[9] Even though these latter are generally built from synthetic building blocks, the interest for nature-derived biomembranes and their innate functionality as cellular active entities has been growing ever since. Among the most common options, the exploitation of extracellular vesicles (EVs) and extracted plasma membranes as building blocks for membrane-based lipid nanosystems has attracted considerable attention to obtain nanocarriers able to perform biomimetic functions e. g. surface recognition, cellular adhesion, active

signaling and molecule transportation through membrane.[62] Indeed, these lipidic biological entities are able to preserve and retain their original membrane protein profile and fragments of their biological contents throughout the extraction process, so that their cellular behavior can still be mimicked when they are applied for in-vivo nanocarrier coating and decoration. It has been reported that both plasma membrane-coated nanovectors or extracellular vesicles employed as drug vehicles possess advantageous properties due to the exposure on their surface of functional protein moieties, e. g. immunomodulatory proteins conferring longer systemic circulation times or recognition fragments that can enable the intrinsic targeting of specific cells or sites.[63] Particularly, it is known that EVs still maintain a biological relationship with the original parent cell, which potentially represents an asset for engineering and targeting methods. Moreover, the possibility to employ autologous formulations for patients in clinical practice ensures a full carrier-target biocompatibility, thus achieving minimal risk of immunogenicity and opening opportunities for personalized medicine. As recently reported in the literature,[62] the combination of these intrinsic cellular activities with advanced engineered functionalities already employed in liposome nanotechnology can result in the design of innovative bionanomaterials for formulation science.

However, some crucial points in the preparation process of such systems still need implementation to reach large-scale applicability. Indeed, plasma membranes are usually extracted from living cells to be engineered as surface coatings or membrane units onto lipidic carriers and the extraction process involves treatments able to yield an empty membrane without its cellular contents. Then the extracted membranes are extruded to obtain nanovesicles or coated core-shell nanoparticles. Since no established protocol for standardized large-scale production exists at the moment, the scalability and reproducibility of these precision techniques can constitute a criticality in plasma membranes application.[62] Similar concerns regard the use of extracellular vesicles, that are nano- or sub-micron vesicles regularly secreted during various cellular processes by most types of living cells. Even though their properties as mediators of cell-cell communication and signaling are rather interesting, the complex surface molecular profile affects their adaptability to chemical modification and engineering.[62] Moreover, it was observed that even when EVs are fused with liposomes to manipulate their activity, the in vivo behavior is still influenced by the original parental cell and it is complex to predict. Thus, the evidently advantageous characteristics of biomimetics and biocompatibility of cell-derived lipid nanocarriers are currently still counterbalanced by the need of extensive and systematic investigation of their in vivo properties and functionality for safe large-scale use.

An alternative strategy to mammalian cell-derived building blocks for natural-based lipid nanosystems is the exploitation of microorganism or plant biomasses, either as an added value use or

for recycling purposes of waste materials. This approach could be beneficial both from the biocompatibility and biodegradability aspect and from a sustainable perspective. Several researchers have reported in the latest years novel procedures to obtain lipid nanovectors from microbial phospholipids, generally from prokaryote membranes (e.g. Prokaryote Derived PD-liposomes) obtained from bacteria with low-cost production requirements and easily scalable procedures. Thus, the microbial lipids are extracted and re-assembled to build lipid nanovectors.[64,65] This technique was established considering the necessity of a composition-based approach to obtain compatible nanovectors for use against pathogenic microorganisms. Particularly, their use was envisaged for medical applications to enhance the efficacy of currently available antibiotics. Since it is known that most bacteria naturally produce functional lipid vesicles, the extraction and remodulation of this lipid content to exploit its properties is considered a viable engineering strategy, particularly for the delivery of antibiotics, anticancer drugs and DNA.

Another popular source of lipids are the biomasses from plant material, that have been extensively used in the latest years for the production of safe, biocompatible and sustainable lipid nanosystems to be applied as drug carriers. Indeed, this approach seems rather promising to obtain natural-derived nanovectors for drug delivery applications in medicine, food preservation and dietary supplements and agronomics.[66,67] These biomasses offer the unparalleled advantage of being largely available and low-cost materials, sometime constituting waste products not recycled for any added value process, that can be easily obtained in large quantities thus offering the potential for scalability. Moreover, the natural origin usually from edible plants ensures the nontoxic nature of the synthesized systems and the general environmental-friendly methodology. As seen above for microorganisms, also edible plants are known to spontaneously produce and secrete nano-sized lipid vesicles known as plant-derived edible nanoparticles (PDNPs), recently isolated from various sources e. g. grape, ginger and lemon. The extracted lipids are then reassembled to achieve a uniform size distribution of nanovectors that are preferentially applied in the medical field.[68] Indeed, the benefits of such systems over artificial or mammalian cell lipids include the absence of immunogenicity, the low-cost production and the efficient encapsulating and delivery capacity. Moreover, some lipid nanocarriers from plants possess intrinsic therapeutic properties that can be exploited particularly in the clinical practice, as reported for example for leaf extracts of Ficus and broccoli that resulted protective against hepatic diseases. Another interesting type of delivery vehicles are the nanostructured lipid carriers (NLCs) fabricated from vegetable oils, recently reported and applied as encapsulating agents for natural plant extracts, thus exploiting the bioactive effect obtained by the synergy of the carrier and cargo components.[68] Among the main applications in biomedicine of recent years, grapefruit-derived nanovectors (GNVs) were shown to be effective carriers for in vivo delivery of chemotherapeutic drugs and small

interfering RNA (siRNA). These systems were also able to precisely administer therapeutics to inflammatory cancer tissues. Ginger-derived nanoparticles (GDNPs) displayed good encapsulation capability for a variety of guest components e. g. miRNAs, some proteins and high quantities of lipids and ginger bioactive components, that were then delivered to the digestive mucosa. Lemon juice-obtained lipid nanocarriers proved as well to be efficient delivery agents for protein contents.[68] Beyond the applications in the biomedical field, an emerging sector for biocompatible lipid formulations is the delivery of bioactives for agricultural purposes. Olive pomace, that is a waste material of the olive oil production line has been employed as an extraction source to obtain lipids, that were then used as building blocks for novel formulations to deliver root promoting hormones to rooting recalcitrant olive tree species. This strategy allows to exploit the total biocompatibility between the carrier and target thus maximizing the delivery efficacy, while at the same time envisaging a sustainable procedure to recycle this waste material in the perspective of circular economy processes.[67]

At the crossing between the properties of bacterial microorganisms and plants, algae are considered a promising source of biomass for several purposes, since many species are able to spontaneously produce and accumulate lipids in relevant amounts. The metabolic flexibility, biocompatible and biodegradable character and the cost-effective production of these microorganisms represent desirable properties to employ these materials at large scale for pharmaceutical/biomedical applications, tissue engineering, regenerative medicine and other biological activities.

1.4 Scope of the work

In this thesis work, soft matter lipid nanovectors were designed and prepared as biocompatible and biodegradable drug carriers for a commercially valuable but poorly water-soluble antioxidant, i. e. curcumin, which was loaded alone or in combination with adjuvants (α-tocopherol or piperine), to investigate possible synergistic effects and enhancing properties. The design strategy adopted for these formulations involved the use of natural-derived building blocks for carriers composition to favor the compatibility with the cargo and increase the encapsulation efficiency, while at the same time exploiting the combined bioactivity. Two natural biomasses from algal origin were employed as source to extract different classes of lipids, to devise an added value application for this industrially attracting material. Lipids were chosen as building blocks to exploit their spontaneous self-assembly and rich polymorphic attributes, as well as their membrane-like character and nontoxicity. Both polar and nonpolar lipid classes were used and consequently, the obtained aggregates displayed different supramolecular symmetries. In particular, polar lipids assembled preferentially in a lamellar mesophase organization, whereas nonpolar (neutral) lipids self-organized in cubic architectures. Since these nanosystems were dissolved in water dilute regime, the obtained nanoformulations were termed liposomes and cubosomes, respectively. The high surface-to-volume ratio and loading efficiency granted successful encapsulation of the guest molecules. Finally, the so-formed nanoformulations were extensively characterized both from the physico-chemical and functional point of view in an integrated structure-function perspective.

Chapter 2

2.Materials and methods

Materials: algal biomasses and natural antioxidants

2.1. Source of biomass and determination of microalgal lipids

Microalgae are photosynthetic organisms present in all aquatic environments and they possess a rich composition of biomolecules, that can be modulated thanks to their metabolic flexibility and the noticeable technological achievements in algal biotechnology. Indeed, algae are widely cultivated to obtain biomass and its derivatives for commercial purposes such as feed, food adjuvants and cosmetics, and potentially biofuel production. Particularly, oleaginous species i. e. algae with oil-rich composition are interesting for industrial purposes and can be easily manipulated since they possess both autotrophic and heterotrophic metabolisms, according to the chosen culture conditions. In general, the maximum oil yield achievable with microalgae cultures is strongly dependent on various parameters such as the chosen alga, the geographical location, and the selected growth conditions, varying from less than 10% to more than 80% of dry weight.[69] Nevertheless, it was estimated that potentially the oil yield from microalgae production could be up to 20 times higher than the most productive crops actually available at the industrial scale.[70] Microalgae grown in standard conditions i. e. fed with a nutrient sufficient medium, are already able to synthetize a commercially relevant amount of lipids, often mainly composed by large percentages of polar lipids such as glycolipids and phospholipids.[69] Since often for industrial purposes e. g. biofuel production the interest is driven on high yields of glycerides or free fatty acids, an appealing alternative from the economical aspect is represented by the nitrogen starvation technique to obtain biomasses richer in this oil composition. In fact, some algae species are well known for their stress behavior in condition of nitrogen source removal from the growth medium as the cell division is slowed down, the cells increase their size and there is an accumulation of neutral lipids in the cytoplasm, mainly constituted of triglycerides and mono- and diglycerides.[70] Among the algal strains known for such ability, the marine microalgae *Nannochloropsis* sp. is particularly suitable as potential source rich in oil content. Indeed, *Nannochloropsis oceanica* sp. is a genus of autotrophic microalgae known for its high constitutional lipid content and the capability to accumulate oils under nitrogen starvation conditions by shifting its metabolism. Specifically, it has been reported that using a two-phase cultivation process where a nutrient sufficient phase is followed by nitrogen deprivation, it was possible to achieve much higher lipid productivity and to increase the crude lipid content up to 60–70% of the biomass. In such conditions, a shift of the accumulated lipid was observed towards higher percentages of neutral lipids

(in particular triglycerides) with respect to polar glycolipids and phospholipids.[70] Moreover, it was found that the increase in neutral lipids was not only due to transformation of other classes of lipids e. g. phospholipids, but mostly they were produced by de novo synthesis.[71] These findings confirmed that when oleaginous algae are exposed to nutritional conditions limiting growth, they are able to store surplus energy under the form of neutral fats, while at the same time preserving the content of structural lipids. On the contrary, when the microalga is fed with complete or even nutrient sufficient medium, the most abundant lipid class is represented by phospholipids.[71] The possibility to exploit the metabolism to obtain chemically different, albeit slightly, lipid compositions makes this microalga particularly attractive not only for fuel production but also as natural lipid source to design and prepare soft matter nanosystems. Indeed, these lipid classes thanks to their packing parameters assemble preferentially into nonlamellar aggregates or lamellar vesicles, respectively and then dilute cubosome or liposomes can be obtained.

Nannochloropsis oceanica F&M-M24, from the Fotosintetica & Microbiologica (F&M) S.r.l. culture collection, was cultivated outdoors at F&M facility in Sesto Fiorentino (Florence, Italy) in a 100 m^2 GWP®-II (Green Wall Panel) photobioreactor in two different conditions, namely in nitrogen deprivation and nitrogen sufficient state to obtain two biomasses with varied lipid compositions. Regarding the nitrogen-starved biomass, the employed growth medium was artificial seawater from the Adriatic Sea Aquarium & Equipment (Rimini, Italy) at 30 g L^{-1} salinity, filtered (filters at pore size 10 μM and 1 μM) and administered with F medium nutrients without the nitrogen source.[71] The nitrogen content brought in the medium at the inoculum (8.2 mg L^{-1}) was consumed right away. Then, after 5 days of cultivation in nitrogen deprived F medium the culture was harvested by centrifugation and the biomass stored at -20 °C, then lyophilized and powdered for analyses and use.[72] The nitrogen sufficient biomass was grown in the same conditions in GWP and fed complete culture medium with nitrogen source. Two biomasses were obtained with different composition, i. e. a triglycerides-rich biomass from the microalga grown in nitrogen deprivation conditions, and the other one with lipid content shifted towards phospholipids from the microalga grown with nitrogen sufficient medium. The lyophilized biomasses were extracted and analyzed as reported in Table 1 (starved biomass) and in previous works from our collaborators (nitrogen sufficient biomass).[71,73]

2.2 Lipid determination by GC-MS

The lipid composition of nitrogen starved *Nannochloropsis* sp. was determined through advanced analytical measurements to identify the major classes of lipids present in the extracted mixture and their respective ratios. An Agilent 7820 Gas Chromatograph system equipped with a 5975C MSD with EI ionization was employed. Dry lipid extract was weighted, resuspended in chloroform and vortexed. Then 100 µL were introduced in a chromatography column (Bond Elut SI, Agilent) and three different fractions (neutral, glycolipids and polar lipids) were collected in order of polarity, washing the column respectively with equal volumes of chloroform, acetone and methanol. Samples were heated at 60 °C and evaporated under liquid nitrogen. The esterified fatty acids obtained for each lipid class were transformed in the corresponding methyl esters via alkaline transmethylation reaction. The analytes were identified comparing their Retention Time (RT) with those of the standard mix and matching the mass spectra acquired with those obtained from the standards and/or published in the NIST Mass Spectral Database.

The results for the nitrogen starved biomass, as expected from the literature on *Nannochloropsis* and from previous analyses of our collaborators,[71,73] showed a strong prevalence of neutral lipids that constituted about 76% of the total, followed by glycolipids (19.37%) and phospholipids (4.73%) (Table 1). Considering TAGs are known for self-assembling in nonlamellar structures, these results gave insights on the plausible supramolecular architecture of the obtained nanosystems.
Regarding the fatty acids composition, the C 16:0 and C 16:1 n 7 chains that are typical in TAGs were the most representative in the neutral lipid fraction, together with C 18:1 n 9 (Tab. 1). The saturated palmitic acid was predominant in all the fractions, up to 62% of the phospholipid fraction, as seen in the literature.[73] Oleic acid (C 18:1 n 9; 26%), myristic acid (C 14:0; 17%) and stearic acid (C 18:0; 12%) were the most represented in the glycolipid fraction together with the palmitic acid. In the phospholipid fraction instead myristic acid (13%) was more abundant than oleic acid (10%). Long chain fatty acids (8.58%) were detected in lower amounts in the three fractions. Glycolipid and phospholipid fractions contained mostly saturated fatty acids, while on the contrary unsaturated fatty acids were more present in the neutral lipid fraction (Tab.1).

	Lipid class			
	NL fraction	GL fraction	PL fraction	TOTAL
Fatty acid	75.90%	19.37%	4.73%	(%)
C 10:0	0.10	0.17	0.00	0.10
C 14:0	14.31	17.25	13.03	14.54
C 15:0	0.78	0.91	0.62	0.78
C 16:0	25.34	35.85	61.62	28.61
C 16:1 n 7	17.85	3.72	4.03	14.31
C 17:0	1.90	1.67	0.82	1.77
C 18:0	5.26	12.08	8.42	6.56
C 18:1 n 9 c	23.61	26.40	10.28	15.46
C 20:0	0.36	0.31	0.19	0.34
C 20:3 n 6	0.99	0.31	0.42	0.82
C 20:4 n 6	2.62	0.43	0.25	2.06
C 20:5 n 3	6.82	0.85	0.28	5.30
C 22:0	0.07	0.05	0.06	0.06
Total (%)	75.90	19.37	4.73	100.00
total saturated	48.10	68.29	84.75	
total unsaturated	51.90	31.71	15.25	

Table 1. Fatty acid composition (%) of the three lipid classes, i. e. neutral lipids (NL), glycolipids (GL), and phospholipids (PL) of starved *Nannochloropsis oceanica* F&M-M24 biomass.

2.3 Design and preparation of nanovectors

Hydrophobic drugs of natural origin are the ideal guest molecules for lipid nanovectors obtained from microorganism biomasses. Indeed, despite the potential advantageous properties held by this class of compounds and their fairly diffused popularity, their effective use for commercial applications on the industrial scale is often hindered by several issues, as seen in the previous chapter. The main concern is that these molecules show poor water solubility and chemical instability in physiological media which results in poor bioavailability and absorption from the organism, to name just a few. These matters represent an open challenge and a major drawback in the assessment of the biological activity of these compounds, and they have elicited great effort from formulation scientists to overcome these limitations. As seen in the Introduction, encapsulation and complexation/co-delivery are among the most popular techniques to improve the solubility, circulation time and absorption of these compounds by living organisms thus increasing their efficacy. Among such molecules a prominent place is held by natural antioxidants whose anti-radical, anti-inflammatory, anti-mutagenic, anti-microbial, and anti-cancer activities made them popular since ancient times in traditional medicine, particularly in Asian countries as medicinal herbs. Curcumin (1,7-bis(4-hydroxy-3-methoxyphenyl)-1,6-heptadien-3,5-dione) (Figure 2a), a lipophilic polyphenol usually extracted from the rhizome of turmeric (*Curcuma longa*), is nowadays one of the most popular antioxidant compounds used as dietary supplement, food additive and pharmaceutical prodrug, very attractive for potential

application for neurodegenerative, cardiovascular, and neoplastic diseases thanks to its antioxidant and anti-inflammatory properties.[74] In fact, the downregulatory pathways of curcumin include the expression of many pro-inflammatory cytokines (e. g. the TNF-α tumor necrosis factor), chemokines and interleukins (IL-1, IL-2, IL-6, IL-8, IL-12) and the inactivation of the nuclear factor (NF)-κB. Together with other turmeric products, that are also used as food preservatives, curcumin has been deemed as safe by some of the main institutions that assess safety and regulate use and distribution of drugs and food products worldwide, such as the FDA (USA), the FAO/WHO and the Natural Health Products Directorate (Canada).[74] These assessments allowed also its global distribution as an over-the-counter supplement. Nevertheless, despite evidence is not lacking on the investigation of its action at the biochemical level and regarding the preclinical and clinical studies, its poor aqueous solubility, membrane permeability and thus bioavailability in the systemic circulation makes its therapeutic action difficult to assess. Such issue is likely due to its rather fast metabolism and excretion from the human body that hinders proper distribution and absorption, thus the effort at the formulation level lies in the elongation of its bioactivity and circulation time.[74]

α-Tocopherol is another popular lipophilic antioxidant (Figure 2b) and together with γ-tocopherol is the most abundant vitamin E component, even though only the α- form is absorbed by the human organism and thus usually employed as a dietary supplement. In fact, for in vivo purposes dietary requirements of vitamin E are currently limited to α-tocopherol, being the only form that reverses vitamin E deficiency and no other vitamin E components are interconverted to α-tocopherol in humans. The other compounds (i.e., β, δ, and γ, both tocopherols and tocotrienols) are commonly used as preservatives in cosmetics and foods, as vitamin E components are known to be one of the most powerful preservative available on the market when combined with water-soluble ascorbic acid.[75] Regarding the in vivo antioxidant action of α-tocopherol, it was hypothesized that it could protect highly vulnerable polyunsaturated phospholipids (PUPL) and polyunsaturated fatty acids (PUFA), with production of a tocopheroxyl radical generated by taking the hydroxyl hydrogen from the phenolic hydroxyl group. Moreover, α-Tocopherol is known to inhibit key events in inflammatory signaling such as platelet aggregation, release of IL-1β from lipopolysaccharide-activated macrophages, adhesion of monocytes to endothelial cells, production of monocyte chemoattractant protein-1 and IL-8 in human aortic endothelial cells, LDL-induced proliferation of smooth muscle cells and activation of NADPH oxidase in human monocytes.[75]

Finally, another interesting natural antioxidant is piperine, a simple dietary alkaloid (Figure 2c) mainly isolated from the seeds, fruits and roots of *Piper nigrum* Linn and *Piper longum* Linn. Piperine

and its derivatives exhibit a wide range of biological properties, such as anti-tumor, antioxidant, anti-inflammatory, anti-mycobacterial, insecticidal activities, etc. Moreover, it is known to act as an inhibitor of glucuronidation in the liver and intestine and to be able to modulate membrane dynamics, thus modifying permeation properties.[76] Interestingly, it is widely known and employed as an oral absorption enhancer of bioavailability to improve the bioactivity of several other drugs when co-administrated with them. Particularly, it was reported in the literature that it was able to increase the maximum plasma concentration of curcumin, and it is often used with this latter to obtain synergic pharmacological effect.[76,77]

Considering these advantageous properties, curcumin was chosen as the designated natural antioxidant of interest for this investigation. α-Tocopherol and piperine were selected as adjuvants for curcumin since these two compounds have been used in the past for co-encapsulation and co-delivery of curcumin,[77] to facilitate incorporation and co-administration by acting synergistically as bio-enhancers. These three antioxidants were then encapsulated in our designed lipid nanocarriers to improve their biodistribution and bioavailability. In fact, the use of lipids extracted from natural sources represents a feasible approach to increase compatibility between vectors and natural cargo and facilitate insertion. The possibility to obtain biomasses with different lipid class composition allows to investigate the contribution of both supramolecular arrangement and guest molecules on the delivery efficacy, while also providing a potentially more cost-effective alternative to industrial-scale purified molecules.

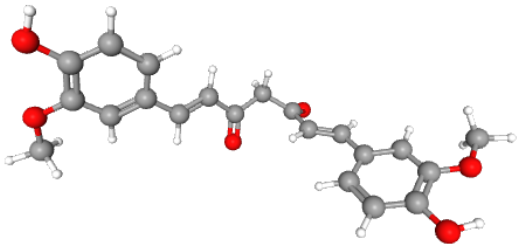

a)

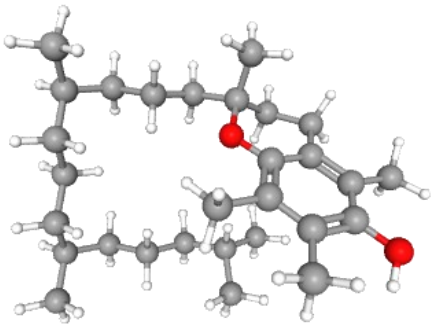

b)

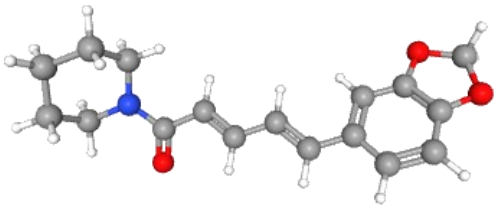

c)

Figure 2 (a, b, c). Balls and sticks representations of the molecular structures of curcumin a), α-tocopherol b), and piperine c).

Curcumin, piperine and α-tocopherol were purchased from Sigma-Aldrich and used as received. The two dried algal biomasses were stored in freezer at −20 ± 1 °C and de-frozen before use to prevent degradation, then lipid extraction was performed in Folch solution ($CHCl_3/CH_3OH$ 2:1 v/v) by weighing 25 mg/mL for samples with lower concentration, and 40 mg/mL for samples loaded at higher concentration, which were employed for SAXS studies. The solutions were stirred for 24 h at room temperature, then the organic solvents were evaporated to obtain a lipid film. Stock solutions of the three antioxidants in acetone were added to the dry film in the appropriate concentrations. Subsequent evaporation was performed under vacuum to obtain a dry lipid film which was then rehydrated, using MilliQ water and equilibrated for 12 h. The obtained suspensions were subjected to extensive vortexing followed by eight freeze-and-thaw cycles. Finally, high-power sonication using a Bandelin Sonopuls HD 4050 probe sonicator (frequency 20 kHz) was employed to downsize the lipid nanovectors, as previously described.[72] The applied protocol constituted of 5 cycles of 3 min each in pulse mode, alternated by 2–3 min intervals to let the samples cool down to prevent

overheating and damaging. Two series of diluted systems were studied in this work, namely cubosomes and liposomes. The composition of each sample in terms of type of supramolecular structure and loaded antioxydants (curcumin, piperine and α-tocopherol) is reported in Table 2.

Sample name	Supramolecular structure	Loaded compound	Loaded concentration
Empty-cub	cubosome	-	-
C1-cub	cubosome	Curcumin (C)	10^{-2}M
CT-cub	cubosome	C+ α-tocopherol (T)	10^{-2}M C, 5x10^{-3}M T
CP-cub	cubosome	C+ piperine (P)	10^{-2}M C, 5x10^{-3}M P
C2.5-cub	cubosome	Curcumin (C)	2.5 x 10^{-2}M
C2.5T-cub	cubosome	C+ α-tocopherol (T)	2.5 x 10^{-2}M, 1.25 x10^{-3}M
C2.5P -cub	cubosome	C+ piperine (P)	2.5 x 10^{-2}M, 1.25 x10^{-3}M
Empty-lip	liposome	-	-
C1-lip	liposome	Curcumin (C)	10^{-2}M
CT -lip	liposome	C+ α-tocopherol (T)	10^{-2}M C, 5x10^{-3}M T
CP -lip	liposome	C+ piperine (P)	10^{-2}M C, 5x10^{-3}M P
C2.5 -lip	liposome	Curcumin (C)	2.5 x 10^{-2}M
C2.5T -lip	liposome	C+ α-tocopherol (T)	2.5 x 10^{-2}M, 1.25 x10^{-3}M
C2.5P-lip	liposome	C+ piperine (P)	2.5 x 10^{-2}M, 1.25 x10^{-3}M

Table 2. Sample list, loaded compounds and concentrations

Methods: characterization and analyses

For a comprehensive understanding from the physico-chemical and bioanalitical perspectives, various characterization techniques can be used to investigate the structural and morphological properties of dispersed lipid nanosystems, their interactions with guest molecules and how the structure and interactions impact on the functionality as delivery systems. First of all, as a preliminary structural characterization of soft matter systems Dynamic Light Scattering is generally employed to assess the nanoscale range of the systems and their size dispersity. From the structural and morphological point of view, high-resolution techniques such as Small Angle X-ray Scattering and Cryo-TEM are generally the most appropriate choice to obtain in-depth, comprehensive knowledge of supramolecular architectures.[78,79] Though both techniques are powerful and informative, their use is complementary since SAXS is able to give structural details of the whole sample offering simultaneously high spatial and temporal resolution, albeit in reciprocal space, so that the data obtained generally needs elaborate processing to extract a valuable model. On the other hand, Cryo-TEM measures directly real-space structures thus allowing direct visualization of the morphology and size distribution, though the sampling is performed point by point in different regions and sample

preparation can be often laborius and might potentially generate artifacts. Considering that SAXS probes nanostructures in the reciprocal and cryo-TEM in the real space, the Fourier transform of the lipid structures in cryo-TEM micrographs equals the phase assignment obtained with SAXS. The study of the interactions of the carrier with guest molecules can give insightful knowledge on the synergy of the complex. It can be investigated by spectroscopic techniques such as Nuclear Magnetic Resonance, that provides structural information at molecular level as well as knowledge on molecular dynamics and host-guest interactions. Calorimetric techniques such as Isothermal Titration Calorimetry can elucidate the thermodynamics governing the above mentioned interactions and the thermal transitions of the aggregates, thus complementing structural and dynamical data with energetical understanding of the system. The influence of physico-chemical properties on the functionality of nanocarrier systems can be studied approaching two levels of testing as drug delivery vectors. In particular, these nanosystems can be evaluated from the point of view of (i) the stability and release behavior in biologically relevant media and (ii) the applicability to in vitro studies e.g. on cells. The stability in various conditions is a rather relevant aspect, since to be effecive a drug carrier must be able to encapsulate and protect its cargo during the transport and release it only when the target is reached. Moreover, the release profile should be preferably slow and sustained, so to achieve a continuos administration of the drug molecule in the appropriate concentration range for optimal uptake. The analysis of the nanovectors loading and stability to evaluate drug delivery efficacy is generally carried out by employing biomimetic media, either commercial or prepared in-house, that simulate physiologically relevant conditions e. g. the digestive environment of stomach and intestine with various degrees of complexity.[80] This model is generally the selected one since the administration via oral distribution is one of the most common delivery methods for drug systemic absorption. The simplest media only involve non-specific parameters such as temperature and pH, moving forwards to progressively more complex models involving ionic force, flow profiles, and finally, in gastrointestinal tract models (GIT) also enzyme activity and surface-active components such as bile salts and other solubilizing agents are included. These simulations are quite useful to assess the impact of the passage through these conditions on the stability of the systems and the bioaccessibility of the loaded cargo.[77,81,82] These experiments can be also complemented by parallel structural analyses to follow the destabilization profile of the carrier through time. Release experiments generally involve the assessment of the release profile in various media in concomitant evaluation with the stability, as the loaded drug is then delivered to the target while the aggregate carrier experiences destabilization and disruption. Several aspects of release can be investigated, considering not only the kinetics of the discharge profile but also the bioactivity and delivery efficacy towards some selected targets. In the case of antioxidant molecules, the efficacy of the encapsulating

formulations to preserve and even enhance this property of the loaded cargo can be tested through radical scavenging assays and antioxidant capability tests in vitro on cells, to evaluate the bioactivity towards different targets and conditions.

Structural techniques

2.4 Dynamic Light Scattering

Dynamic Light Scattering (also known as Photon Correlation Spectroscopy) is used to assess the range of dimensions of the aggregates by analyzing the size distribution profile of the particles in suspension at the nanoscale and the dispersity of the system irradiated by light.[83] Brownian motion of non-interacting particles due to random collisions with the molecules of the liquid surrounding the particles is assumed, so it is appropriate for the study of disordered diluted systems. The time scale of movement of the particles is used to derive dynamic information about the scattering objects, since small particles diffuse quickly and vice versa large particles diffuse more slowly, as it is defined by the Stokes-Einstein equation (1) which relates the particle size and its speed. Fluctuations over time of the scattered light intensity due to diffusing particles in suspension are measured by means of photon-autocorrelation function, which measures the degree of correlation between two intensity signals over a period of time. The exponential decay in the autocorrelation function over time is related to particle size, as the rate of decay is much faster for small particles since it depends on the diffusion coefficient of the scattering objects, thus allowing to derive the distribution of sizes and consequently its dispersity.

$$D = \frac{kT}{6\pi\eta r}$$

(1)

where k is the Boltzmann constant, T is the absolute temperature, and η is the local viscosity of dispersant.

In this thesis DLS measurements of lipid nanocarriers were performed on a Malvern Zetasizer (Nano ZS) equipped with a He–Ne 633 nm, 4 mW laser and backscattering optics, after diluting all samples 1:200 with MilliQ water to adjust optical turbidity. The cumulant expansion method was employed to analyze the autocorrelation function of the scattered intensity and to obtain the mean size and polydispersity index of the samples. All measurements were recorded in triplicate (n=3) and averaged.

2.5 Small Angle X-Ray Scattering

Conceptually similar to other (static) light scattering techniques, in Small Angle X-ray Scattering (SAXS) the nature of the interaction with matter is the scattering of X-rays from the electrons, so that electron-rich atoms generate higher scattered intensity. In synchrotron X-ray sources a highly collimated and monochromatic beam impacts on the irradiated sample and it is scattered in the forward direction, where a two-dimensional detector collects the signal. Then, the radial integration of the two-dimensional scattering pattern gives the one-dimensional scattering intensity I as a function of q, that is the length of the scattering vector (i.e. the momentum transfer) defined by:

$$q = \frac{4\pi}{\lambda} \sin \frac{\theta}{2}$$

(2)

where λ is the incident wavelength (typically of the order ~1 Å) and θ the scattering angle. The length scale probed by the experiment is set by the spanning q-range. According to the probed scattering vectors that are generally available in synchrotron sources, X-ray instrumental range is defined USAXS for ultralow angles, SAXS for small angles and WAXS for wide angles. SAXS is one of the designated techniques to investigate the structure for different lipid–water systems, both with nonlamellar or lamellar organization, and determine the lipid phase. Particularly, for ordered mesophase structures at the repeat unit cell scale, this procedure relies on constructive interferences in the reciprocal space from the ordered scattering planes of the mesophase.[84] When these systems are irradiated the resulting X-ray scattering pattern gives a characteristic set of intensity rings (2D) or maxima (1D) corresponding to Bragg reflections or peaks, whose positions in the reciprocal space identifies the symmetry of the mesophase at the unit cell scale, as above mentioned in the Introduction. These data can then be used to extract other relevant parameters reflecting the structural organization at the supramolecular scale.[85] In the case of non-intercorrelated bilayer structures such as unilamellar assemblies, the aggregate identification is possible through typical patterns of the intensity plot, particularly ascribable to the form factor term at multiple q-ranges. The broad q-range available at synchrotron SAXS instruments together with sub-millisecond time resolution allows a variety of dynamical studies from the molecular level to the upper limit of the colloidal scale, making this technique the selected one for such systems.[86] Moreover, the long collimation distances employed with synchrotron SAXS reduces the background over the conventional SAXS range, thus enabling

investigation of systems in extremely dilute regimes, such as the dispersed forms of mesophase structures, e. g. cubosomes, hexosomes, etc.

SAXS experiments for all samples listed in Table 2 were performed at the high-brilliance ID02 beamline of the European Synchrotron (Grenoble, France), currently the most powerful beamline worldwide for soft matter studies.[86] The wavelength of the incoming beam was 1 Å, and the sample-to-detector distances were 0.8, 10, and 31 m, which covered a wide total q range, i.e. 3×10^{-3} to 7.5 nm^{-1}. The parameter q is the magnitude of the scattering vector, as defined by equation (2). The 2D SAXS patterns initially recorded were azimuthally averaged to obtain 1D patterns and normalized to the absolute scale using a standard procedure previously reported.[85] To ensure accurate background subtraction the sample holder was a flow-through capillary of 2 mm diameter.

2.6 Cryogenic Transmission Electron Microscopy

Cryogenic transmission electron microscopy (Cryo-TEM) is a powerful technique relying on the interaction of an electron source with matter, particularly suited for the investigation of soft structures such as lipid aggregates dispersed in aqueous environments. Indeed, the possibility to visualize these structures without dehydration that would alter their morphology, but instead operating a rapid freezing that prevents reorganization offers an unparalleled advantage.[79] On the other hand, since the contrast is generated by the difference in electron density between the nanostructures and the vitrified film, these measurements can be challenging since most lipid molecules do not possess many electron-rich atoms. Nevertheless, the imaging upper and lower limits usually span several orders of magnitude in the nano- and micro-range, which is a particularly appropriate scale for the study of soft matter nanosystems.[87] The limitation in the upper value is mostly due to the 3D-size of the objects, since the thickness value of the vitrified specimen is limited by the presence of the surrounding water and its resulting electron scattering. The resolution limit in the order of few nanometers allows to identify many morphological details of lipid supramolecular aggregates, including sometimes the inner organization of nonlamellar mesophase structures, while for lamellar aggregates it is possible to differentiate the bilayer and the aqueous compartment and visualize the uni- or multi-lamellar stacking. Nevertheless, the identification of 3-D structures from 2-D micrographs is not always straightforward, as the correlation is complicated by orientation effects of the scattering objects in the medium and by the thinner or thicker parts of the vitrified film. Still, it is possible to make some considerations on fat-based aggregates depending on their different contrast density and interpretate micrographs with the help of the experience.[87] Clearly, also the film thickness plays a role in the contrast visualization, and the size distribution evaluation is sometimes also affected by the chosen

measurement technique. Thus, these considerations highlight the necessity to complement the visual evidence from cryo-TEM with other structural techniques.

In the present thesis Cryo-TEM experiments for micrographs in Figure 10 (a-d) were carried out on a Glacios (Thermo Fisher Scientific) Cryo-Transmission Electron Microscope equipped with a field emission gun (FEG) operating at 200 kV at the Electron Microscopy Platform of the Institut de Biologie Structurale (IBS, Grenoble). The images were recorded on a Falcon II direct electron detector at calibrated magnifications of 57,000 equivalent to 0.25 nm/pixel in the camera counted mode. For the time of exposure 1.5 s, the number of fractions was equal to the number of frames. Total dose did not exceed 3800 e/nm2 for each acquisition. The samples were frozen using a fully automated Vitrobot Mark IV (Thermo Fisher Scientific) device. A drop (4 μL) of the solution was deposited on a R 0.6/1 holey carbon 400 mesh grid (Quantifoil Micro Tools GmbH, Germany) made hydrophilic by negative glow discharging. After 2 s of blot time with blot force 1, the grid was rapidly plunge frozen in liquid ethane cooled by liquid nitrogen to prevent ice crystals formation. Cryo-TEM experiments for micrographs in Figure 11 (a-d) were performed on a Tecnai G2 Spirit Twin microscope (FEI, Czech Republic) in the Polymer Morphology department of the Institute of Macromolecular Chemistry (Czech Academy of Sciences, Prague). The microscope was equipped with a cryo-attachment (Gatan, CA, USA). The samples for cryogenic microscopy were prepared as follows: 3 μL of the sample solution were dropped to an electron microscopy grid covered with a holey carbon supporting film (Electron Microscopy Sciences/Mir Biotech, Czech Republic), which was hydrophilized just before the experiment by means of glow discharge (Expanded Plasma Cleaner, Harrick Plasma, USA). The excess of the solution was removed by blotting (Whatman no. 1 filter paper) for 1 s, and the grid was plunged into liquid ethane held at -181 °C. The frozen samples were kept at liquid nitrogen temperature (-196°C), inserted in the TEM cryo-holder and transferred into the TEM microscope. The TEM observations were performed at -173 °C using bright field imaging at the accelerating voltage of 120 kV.

2.7 Nuclear Magnetic Resonance

Nuclear Magnetic Resonance spectroscopy is a technique that relies on the magnetic properties of the nuclei of certain atoms and isotopes and their ability to resonate at characteristic frequencies when immersed in an applied magnetic field. Some of the most relevant information in one-dimensional NMR spectra is given by the possibility to identify the electronic structure and the chemical groups

in the environment surrounding the nucleus of interest. Particularly, the study of the structure, connectivity, distances and angles in the molecule is performed thanks to the investigation of the interactions in the chemical environment. These latter depend either on the presence of adjacent chemically bound nuclei, that interact through spin-spin scalar coupling mediated by spatially close electrons, or on the dipolar coupling given by spin-spin interactions taking place between neighboring but not chemically bound atoms. The data extracted from NMR spectra allow to reconstruct the molecular structure both at the connectivity and at the spatial level. Moreover, the study of the dynamics of the system can be obtained from the nuclear relaxation times occurring after the magnetization is induced, when the energy is transferred to the chemical environment through spin-lattice (T_1) relaxation. This transition is caused by the molecular motions that generate fluctuating magnetic fields which in turn provoke spin transitions, thus giving information on the amplitude and timescale of the molecular motions. In addition, information on structural order, e. g. the degree of crystallinity and crystallization kinetics in certain polymers, can be obtain through the investigation of the spin-spin (T_2) relaxation time.[88] Magnetic resonances has given through the years rather valuable data on dispersed lipid nanosystems, even though ^{1}H-NMR spectra of lipid bilayers are often not very informative, since broadening of line width does not allow precise assignments. Moreover, lipid-water systems that form mesophases (e. g. lamellar, cubic, hexagonal assemblies) generally possess a coexistence of long range order with short range disorder.[89] The local structure of these systems was investigated by crystallographic measurements that were only able to detect the disordered aspect but gave no information on its origin. Thus, these systems have been probed by several magnetic resonance techniques which are sensitive to both local environment and to the dynamics, showing that such disorder is in fact of dynamical origin. This finding is particularly relevant for deeper understanding of the liposolubility, polymorphism and thermodynamics of lipid mesophases and it has shown the significance of magnetic resonance application on these aggregates. Later on, these methodologies developed to study lyotropic mesophases were extended to the study of liposomes and other lipid aggregates as well.[90]

In this thesis NMR spectra of cubosomes and liposomes were recorded on Bruker 600 spectrometer (DRX-600 AVANCE), operating at 14.07 T and equipped with an *xyz* gradient unit, at 298 K. Monodimensional ^{1}H experiments were acquired with 128 scans over 64K of data, a spectral width of 6000 Hz and relaxation delay of 5 s was employed. A resolution enhancement function (LB=0.5 Hz) was applied before Fourier transformation. All the spectra were processed using the Bruker TOPSPIN 3.5 Software. All samples were prepared employing D_2O.

Calorimetry

2.8 Isothermal Titration Calorimetry

For a complete study of the interactions of the macromolecules in a system in solution it is of paramount importance the study of the thermodynamic parameters governing these interactions, and thus their favorability and mechanism of action.[91] These properties influence both the structure and functionality of dispersed soft matter systems. Even though historically it was not the technique of choice for the investigation of these systems, Isothermal Titration Calorimetry is recently becoming increasingly popular to study the heat profile of various interactions in soft self-assembly aggregates and related processes. Indeed, ITC is able to provide the global thermodynamic quantities of the system and elucidate the forces and constants associated with e. g. modifications in conformation, protonation states, and molecule-solvent interactions. This methodology is often complemented by other physico-chemical techniques to obtain deeper insight into the mechanism by which these changes occur. Particularly, ITC data have been often complemented with information from other experimental techniques such as light scattering, NMR, UV-vis, surface plasmon resonance and differential scanning calorimetry (DSC), plus computational studies.[92] Even though the experimental procedure is analogous for all measurements, since it consists of a titration of one compound with the other one with both systems immersed in the same solution at constant temperature (i. e. 298 K), the methodology can be adapted to various applications. Several different experiments were reported in the past employing this technique, such as the calculation of the critical aggregation concentration (CAC) for micellization processes and the monitoring of the self-aggregation in polyelectrolyte polymers, to name two for exemplificative purposes.[91,92] Regarding guest-host aggregations, ITC is a pivotal technique to obtain the thermodynamic profile of the complex formation and its stoichiometry, which are rather relevant aspects to achieve the complete thermodynamic picture of drug encapsulation into the aggregates and determine the most favored conditions for host-guest interaction. Moreover, thanks to the high sensitivity of this technique, it is possible to investigate assembly-disassembly processes and rearrangements at the molecular level with high precision, which is particularly useful for soft aggregates in dilute regimes as the ones studied here. On the other hand, such sensitivity must be considered when the experimental protocol is planned, since even dilution, protonation/deprotonation or solvation processes might cause large injection peaks, so no other processes should occur in the meantime.

In this thesis, ITC was employed to assess the onset of thermal events in the two nanocarrier series upon titrations either with water or hydroalcoholic solution (10% v/v EtOH) and study the stability of the nanovectors. ITC measurements were performed using a nano-ITC (TA instruments, New

Castle, DE, USA) at 25 °C. Water or hydroalcoholic solution were injected (syringe volume 50 µl) into the calorimetric vessel (170 µl) containing a lipid dispersion (0.5 mM), in aliquots of 2 µl with 300 s intervals between the individual injections.

Absorption spectroscopy

2.9 Encapsulation efficiency

The encapsulation efficiency (EE %) is a parameter indicating the amount of cargo molecule that the nanocarrier can incorporate and consequently transport, with respect to the theoretical amount loaded when the formulation is prepared. As illustrated by equation (3), it can be expressed as the percentage of actual loaded amount of drug out of the total original amount of drug added during preparation. The encapsulated drug can be detected by employing several analytical techniques e. g. direct or indirect spectrophotometric measurements and chromatographic analysis on the previously disrupted carrier sample, referring to previously obtained calibration curves for the investigated substance.

In this thesis encapsulation efficiency of the loaded compounds in cubosome and liposome samples was quantified by UV–Vis assay. The samples were properly diluted in ethanol to disrupt the lipid nanovectors and release the entrapped molecules, as well as to avoid the scattering background due to large aggregates in solution. Absorption spectra were recorded at room temperature on a Thermo Scientific Evolution 220 UV–Vis spectrophotometer, equipped with a xenon flash lamp and double-beam geometry, using 10 mm path length quartz cuvettes. Absorption maxima at 425 nm, 350 nm, and 270 nm wavelengths were chosen for curcumin, piperine and α-tocopherol, respectively. The quantification was carried out recording the absorbances of standard solutions in the dynamic range of linearity (curcumin 0.92-3.68 mg/L; α-tocopherol, 2.15-8.6 mg/L; and piperine, 0.285-2.85 mg/L) and calibration curves showing correlation factors $R^2 > 0.990$ were accepted for subsequent analyses. All spectra were recorded in triplicate and averaged (n=3). The encapsulation efficiency (EE%) of nanovectors was calculated by the following equation, as above described:

$$Encapsulation\ efficiency\ (\%) = \frac{loaded\ amount}{tot\ amount} * 100$$

(3)

Another relevant parameter is the drug loading (DL %) that defines the mass of loaded drug as a percentage of the total mass of the delivery system as described by equation (4), giving an estimate

of the quantity of encapsulated molecules over the total lipid amount employed for nanocarrier formulation. The drug loading (DL %) was calculated as follows:

$$Drug\ loading\ (\%) = \frac{loaded\ drug\ (mol)}{Tot\ lipid\ (mol)} * 100$$

(4)

These two parameters, EE% and DL%, are complementary in the estimate of the efficiency of the formulation in the incorporation of the drug.

2.10 Stability and release experiments in biorelevant media

As mentioned above (see Introduction and Methods: characterization and analysis sections), the stability of drug delivery dispersed nanosystems and their consequent release properties are rather relevant parameters to be considered for formulation design. In fact, nanocarriers should be able to safely incorporate and preserve their loaded cargo from the external environment that might cause degradation and release it when the target is reached with the appropriate rate. These conditions imply that the nanovector should be resistant to several stress conditions typical of physiological environments, e. g. pH abrupt changes, ionic force variations and dilution, plus the presence of surface-active agents such as surfactants, enzymes, etc. At the same time, the carrier should also be able to degrade or disaggregate to release its cargo at the target site, in suitable rates to grant the optimal distribution and uptake. The stability and release studies should be carefully planned to consider many variables such as the nature and composition of the tested formulation, the stability of the drug and release medium, release mechanisms, sampling interval and duration of the study to select the most appropriate conditions. Increased stress conditions can also be induced to investigate the resistance of the carriers or to accelerate release in months-long studies.[93] In fact, in vitro stability and release should be evaluated until at least 80% or a plateau of drug release is reached, as recommended by the FDA. It is possible to play with several parameters to vary carrier resistance and discharge properties, starting from the experimental setup. The formulations can be directly injected in the release medium as it is done with simulated digestion studies or introduced in a dialysis membrane which is then placed in the medium, that is the most popular method for stability testing of nanodispersions.[94] Then, the choice of the most suitable medium is a significant aspect since many factors must be considered. Indeed, adequate solubility of the released molecule to ensure that sink conditions are maintained throughout the entire duration of the test, stability of the drug in the medium

to prevent degradation and constant conditions of the medium need to be carefully evaluated. To test harsher or accelerating conditions various methods have been reported, e. g. high temperature, extreme pH, using organic solvents (alcohol, acetone, acetonitrile) as co-solvents and adding surfactants to the medium.[95] Such testing conditions were found to correlate well with standard conditions, in that the consequent release profiles were similar using e. g. hydro-alcoholic solutions and extreme pH conditions.[93]

Stability and release experiments for the two nanocarrier series were carried out in a biorelevant Simulated Gastric Fluid (SGF) medium (Biorelevant.com Ltd, UK) containing physiological surfactants and salts at the appropriate pH (around 2.3) and temperature (37 °C), mixed with increasing EtOH concentrations (from 40% to 60% v/v in increments of 10%), to simulate progressively more hostile conditions for nanovectors stability and evaluate the release profile for curcumin in this environment. The samples with chosen standard curcumin concentration (10^{-2}M) (see Tab.2) have been selected for testing to maintain the appropriate range of linearity after dilution for UV-Vis measures. Samples were diluted 1:2.5 and 1 mL was introduced in a previously re-hydrated 6-8 kD RC dialysis membrane (Spectrum™ Spectra/Por™) closed at both extremities, that was then submerged in 200 mL of release medium at 37 °C under magnetic agitation. Then 500 µl aliquots were taken from the external medium every 2 hours in triplicate (n=3) at significative time points and replaced with fresh medium kept in the same state, in order to maintain sink conditions, for a total duration of 48 hours. This time duration was chosen both to be able to monitor the release for a sufficient time (up to plateau) and avoid excessive presence of curcumin in the aqueous release medium, considering its tendency to degrade in such environment.

Absorption spectra were recorded at room temperature on a Thermo Scientific Evolution 220 UV–Vis spectrophotometer, equipped with a xenon flash lamp and double-beam geometry, using 1 cm path length quartz cuvettes. UV-Vis spectroscopy was employed to evaluate both the cumulative release of curcumin from samples subjected to stability tests at various time intervals and the curcumin bioaccessibility at the end of the digestion process (see paragraph 2.11). For stability and release tests in aqueous biorelevant media and ethanol, the samples were analyzed at a final dilution of 1:500, in the linearity range of curcumin and choosing the absorption maxima at 425 nm wavelength.[72] The baseline for UV-Vis measurements at 425 nm was measured with an aqueous control sample mixed with EtOH at the correspondent percentage. The cumulative release values were calculated from a known calibration curve using equation (5) and normalizing samples on the basis of their previously measured encapsulation efficiency (see Table 4).

$$Cumulative\ release\ (\%) = \frac{Abs\ sample}{Abs\ Std} * 100$$

(5)

SAXS measurements were performed as well to study the stability of cubosomes and liposomes and complement the observation of drug release on bulk scale by Visible spectroscopy with the analysis of the structural disassembling of the aggregates at the nanoscale. The same experimental setup and medium conditions (selecting only ethanol 60% v/v medium) were employed to carry out the investigation of the aggregate de-structuring by synchrotron SAXS of both nanovector series in such conditions. Sample aliquots (20 µl) were taken from inside the dialysis bag every 2 hours and diluted accordingly to reach a sufficient volume for SAXS analysis (200 µl), then irradiated in the same conditions mentioned above for SAXS experiments employing 2 mm quartz capillaries. DLS control measurements were carried out as well.

2.11 Stability and release in digestion conditions

Following the testing in non-specific media, stability and release properties of the nanocarriers were assessed in simulated gastrointestinal fluid (or GIT model) with specificity for lipid nanodispersions. Since biorelevant media were firstly employed during the 90s to assess the stability of pharmacological formulations in the gastrointestinal lumen, a variety of testing media with different complexity and specificity have been proposed. Indeed, this was the response to the necessity of a reliable in vitro testing tool to evaluate the stability and bioavailability of drug delivery systems in digestive conditions.[96] Considering the ever-growing popularity of lipid-based nanocarriers, particularly in the pharmaceutical industry to increase the bioavailability of highly lipophilic drugs in the gastrointestinal tract or in the food industry to obtain food-grade systems to improve absorption and administration of fats, fluids simulating human digestive conditions were required. However, depending on the formulation type and encapsulated drug, also the degree of complexity and biorelevance needed for a thorough assessment can vary greatly. In fact, considering the various levels of simulation of gastrointestinal conditions with increasing complexity e. g. going from the simplest where only pH and temperature are adjusted (level 1), then adding buffer capacity (level 2) and bile components with digestion products (level 3), until also enzymes are included in the most complex fluids (level 4), several types of tests can be performed.[96,97] In most investigations of lipid nanocarriers stability, retention and release properties in digestive conditions, simulated gastric fluid (SGF) and intestinal fluid (SIF) that include bile salts with addition of pancreatic enzymes i. e. lipases

are generally employed.[77,97] These components are rather significative in the lipid digestion process and thus need to be included to assess reliably the stability of the nanocarrier and the bioaccessibility of the loaded cargo. Digestive enzymes, particularly those intervening in the small intestine since this is the region where most of the lipid digestion and absorption occur, play a critical role in the disaggregation of the lipid nanosystems. Specifically, pancreatic lipase is responsible for converting TAGs and DAGs into FFAs and MAGs, thus inducing the nanovector to disassembly and free its cargo. The lipid components and their digestion products are solubilized within mixed micelles and vesicles formed by bile salts, that will also incorporate and transport the hydrophobic cargo molecules thus making them accessible for absorption.

Stability and release experiments on the two nanovectors series subjected to digestion conditions in a gastrointestinal (GIT) model simulating the gastric and intestinal environments were carried out in a commercial biorelevant Simulated Gastric Fluid/Simulated Intestinal Fluid (SGF/SIF) medium (Biorelevant.com Ltd), with the addition of digestion enzymes, i. e. pepsin and pancreatin (Sigma-Aldrich) in gastric and intestinal environments, respectively. Briefly, the samples were diluted 1:10 and heated 5-10 minutes at 37 degrees under magnetic agitation, then a 1:1 v/v pre-heated volume of SGF with pepsin 3.2 mg/ml was added. The pH was adjusted to 2.5 and the mixture was incubated for 1 hour at 37 degrees with magnetic agitation. After one hour the digestion was stopped bringing the pH at 7, then an aliquot was taken to analyze curcumin release at time t=1h. The remaining volume was mixed with a 1:1 v/v SIF medium containing 2 mg/ml pancreatin and the pH was adjusted to 7. Then the mixture was kept for 2 hours at 37 degrees with magnetic agitation, and sampling of digesta were taken at 30, 60, 90 and 120 minutes. The digestion was stopped by rapid freezing in dry ice. All samplings were carried out in duplicate.[77]

Regarding the stability and release tests in digestion conditions, UV-Vis spectroscopy measures allowed to evaluate both the release of curcumin in the digesta samples at various time intervals and the curcumin bioaccessibility at the end of the whole digestion process through the GIT model. The digesta aliquots at different times were centrifuged at 5000 rpm for 30 minutes, then the clear supernatant that constitutes the micellar phase where the digested curcumin is solubilized was taken for analysis. Curcumin was extracted by adding EtOH (1:500 final dilution), to obtain absorption intensity at 425 nm in an appropriate range. The cumulative release was then calculated from a known calibration curve, using the equation (5) previously described. The bioaccessibility % of curcumin after the whole digestion process (time t=180 minutes in Figure 25) was calculated according to the equation (6):[81]

$$Bioaccessibility\ (\%) = \frac{C_{Micell}}{C_{Raw\ digesta}} * 100$$

(6)

where C_{Micell} is the curcumin concentration in the micellar phase and $C_{Raw\ digesta}$ is the curcumin retrieved from nanovectors at the end of the digestion process in the raw digesta.[80,81]

2.12 ABTS assay: kinetic of absorbance decrement of $ABTS^{\bullet+}$ radical treated with nanovectors in two different conditions

The ABTS assay is an analytical photometric method employed for the screening of the radical scavenging ability of antioxidant compounds, evaluated through the resultant quenching of the $ABTS^{\bullet+}$ radical cation with respect to reference Trolox standards solutions, also called TEAC (Trolox Equivalent Antioxidant Capacity). Among several methods used for the measurement of the total antioxidant activity of various samples, in particular from natural origin e. g. food extracts, beverages, human body fluids, this conceptually simple decolorization assay is especially useful as it can be applied to both lipophilic and hydrophilic antioxidants. In fact, contrarily to other methods previously used this assay relies on the scavenging by hydrogen- or electron-donation of the pre-formed free radical, the blue/green $ABTS^{\bullet+}$ chromophore, as the marker of antioxidant activity.[98] The antioxidants added to the radical cation solution reduce it to ABTS, hence decolorizing the solution. The measured percentage inhibition or decrement of absorbance of the $ABTS^{\bullet+}$ radical gives the extent of reduction and thus of antioxidant activity of the tested sample compared to the standard Trolox, on a timescale dependent from the concentration of the antioxidant and the rate of the reaction. So, the dose-response curve of decrement of absorbance of the $ABTS^{\bullet+}$ radical cation reacting with known Trolox concentrations as a standard is plotted as a function of concentration, and the capacity of the tested sample to inhibit the radical is calculated relative to Trolox during the specific time range. As reported in the literature, through this method it was possible to quantify the antioxidant capacity of several carotenoids, flavonoids, phenolics, etc., after obtaining the individual dose-response curves for each compound at specific time points. The assay is easily adaptable to different experimental conditions, both in terms of used solvents and reaction times since the $ABTS^{\bullet+}$ radical is stable in solution up to several hours, moreover its reactivity towards an ample variety of natural antioxidants make this assay the technique of choice for this type of evaluations. The percentage of decrement of absorbance of the sample of interest at a selected concentration compared to that obtained with Trolox is indicative of the antioxidant capacity, moreover it is also possible to calculate the TEAC at a designated time

point. Indeed, this value is obtained from the ratio of the plot gradient of the percentage decrement vs concentration of the antioxidant and the gradient of the same plot for Trolox. Nevertheless, for the study of the kinetics of release and antioxidant capacity of guest molecules from formulations, the decrement of absorbance that is given by a selected concentration over a certain time scale is a more relevant parameter.[98]

The ABTS assay was employed to evaluate the kinetics of antioxidant capacity of the two series of lipid nanocarriers both diluted in EtOH (that disrupts the lipid structures) and simply diluted in water, at least for 7 h. The protocol previously described by Bonechi et al.,[99] was used with some modifications. Briefly, $ABTS^{\bullet+}$ free radical cation was prepared by treating a solution of ABTS (7 mM) with a $K_2S_2O_8$ solution (140 mM) and incubating overnight (12–16 h in the darkness at 4 ± 1 °C). Then it was properly diluted in absolute EtOH or MilliQ water before use. A known volume was then treated with Trolox standard solutions (ranging 0–20.00 μM) for calibration. After 30 min of incubation the absorption at 734 nm was recorded with a UV–Vis spectrometer against EtOH or water, as reference. The nanovector samples were initially diluted 1:100 (either in EtOH or in water), to avoid interference from algae material absorbance (matrix effect). Then 20 μL of each sample were added to 1.00 mL of $ABTS^{\bullet+}$ and 80 μL of EtOH or water (final sample dilution 1:5500). Calibration curves were built reporting the relative decreasing in absorbance (Abs_{734}%) of the $ABTS^{\bullet+}$ solution treated with standards (Abs_{Std})or samples (Abs_{Spl}), with respect to the blank solution (Abs_{Blk}), according to equation (7):

$$Abs_{734}\ (\%) = \left[1 - \left(\frac{Abs_{Std/Spl}}{Abs_{Blk}}\right)\right] * 100 \quad \textbf{(7)}$$

Calibration curves were plotted as ΔAbs% *vs* Trolox standard concentration at each chosen time point and the ones showing correlation factors $R^2 > 0.990$ were accepted for analysis. The Trolox-treated samples stability was checked during time. All measurements were recorded in triplicate and averaged (n=3).

In vitro techniques: cytotoxicity and hydrogen peroxide treatment

2.13 Cell cultures and cytotoxicity test

Following the assessment of the efficacy of lipid nanocarriers in simulated environments and their antioxidant properties from a chemical perspective, their biocompatibility and antioxidant capacity were tested in cellular assays. As a preliminary step before further applications, the in vitro cytotoxicity was evaluated to evidence the feasibility of these tests. For this purpose, the direct contact tests, proposed by ISO 10995-5:2009[100] was used. Introduced as a standard, this test is in fact suitable for several types of samples with various shapes, sizes or physical status (i. e. liquid or solid). Indeed, the generic assessment of in vitro acute toxicity is not dependent on the end application for which the sample is intended, so that many cell lines from the American Type Collection are recommended in the ISO 10995-5:2009 document. Among the advised lines, NIH3T3 mouse fibroblasts were chosen to test cytotoxicity for lipid nanocarriers, as previously reported in the literature.[101] Accordingly, the same cell line was selected to evaluate the antioxidant capacity of nanocarriers loaded with guest molecules in a biological context. In both tests, the non-cytotoxicity and the antioxidant effect were evaluated on the basis of the percentage of viable cells after the treatments. This value was calculated by referring to the cell viability of NIH3T3 treated with the control, which is considered equal to 100%.

Fibroblasts NIH3T3 were used for the experiments. Cells were propagated in DMEM at 37 ±1 °C in a humidified atmosphere, containing 5% CO_2. The culture medium was supplemented with 10% foetal calf serum, 1% L-glutamine-penicillin-streptomycin solution, and 1% MEM non-essential amino acid solution. Once at confluence, the cells were washed with PBS 0.1 M, separated with trypsin-EDTA solution and centrifuged (5 min at 1000 rcf). The pellet was re-suspended in complete medium (dilution 1:15) and $1.5 \cdot 10^3$ cells in 1.0 mL of complete medium were seeded in each well of a 24 well round multiwells and incubated at 37 ± 1 °C in humidified atmosphere of 5% CO_2. Once cells reached the 50% of confluence (i. e. after 24 h of culture) the culture medium was discharged and the test compounds, properly diluted in completed medium, were added to each well. All samples were prepared in triplicate. Complete medium was used as negative control. After 24 h of incubation, cell viability was evaluated by Neutral Red uptake (Sigma-Aldrich, Switzerland).

The *in vitro* cytotoxicity assay was performed for both cubosome and liposome series on empty nanovectors and nanovectors loaded with the three antioxidant molecules (C, P and T) at different concentrations (see Tab.4). The tested nanocarriers concentrations were 0.1, .01 and 5.0% v/v, containing different curcumin, piperine and α-tocopherol concentrations depending on the measured

encapsulation efficiency. The *in vitro* cytotoxicity of C, P and T free solutions in ethanol was also determined.

2.14 Hydrogen peroxide treatment

The lipid dispersions that resulted non-cytotoxic towards NIH3T3 fibroblasts (i. e. cubosome series) were selected for subsequent tests to assess their antioxidant and thus protective capability towards cells treated to induce oxidative stress conditions, and consequently cell death. Among the available options to provoke this outcome, a strong oxidant agent was chosen i. e. hydrogen peroxide. Thus, to determine the protective effect of cubosome nanovectors loaded with the three antioxidants, fibroblasts were pre-incubated with different hydrogen peroxide concentrations (1, 5, 10, 25, 30, 50, 75, 100 μM) for 15 min. Then, cells were washed out and cultured in medium with different concentrations of the tested compounds. Cell viability was evaluated after 24 h incubation at 37 ± 1 °C, in 5% CO_2 atmosphere.

2.15 Evaluation of NIH3T3 fibroblasts viability

The NIH3T3 viability was determined as follows. First, the following solutions were prepared to determine the percentage of viable cells: Neutral Red (NR) stock solution (0.33 g NR dye powder in 100 mL sterile H_2O); NR medium (1.0 mL NR stock solution in 99 mL of routine culture medium pre-warmed to 37 ± 1 °C); NR desorb solution (1:50:49 solution of glacial acetic acid: ethanol: H_2O). At the end of incubation, the routine culture medium was removed from each plate and lid. The cells were carefully rinsed with 1 mL pre-warmed D-PBS. Plates and lids were then gently blotted with paper towels. An aliquot of 1.0 mL NR medium was added to each dish and lid and further incubated at 37 ± 1 °C, 95% humidity, 5.0% CO_2 for 3 h. The cells were checked during incubation for NR crystal formation. After incubation, the NR medium was discharged and the cells were carefully rinsed with 1 mL pre-warmed D-PBS. PBS was decanted and blotted from the dishes and lids and exactly 1 mL NR desorb solution was added to each sample. Plates were placed on a shaker for 20-45 min to extract NR from the cells and form a homogeneous solution. During this step the samples were covered to protect them from light. Five min after removal from the shaker, absorbance was read at 540 nm, by using UV/Visible spectrophotometer (Varian Cary 1E).

Chapter 3

3.Results and discussion: Structure, morphology and molecular interactions

3.1 Dynamic Light Scattering

Dynamic Light Scattering measurements were performed as a preliminary structural analysis at the nanoscale, firstly to assess the presence of nano-objects, the size polydispersity of the obtained systems and the reproducibility of the preparation. Subsequently, DLS was employed to verify the stability of the nanosystems, either from ageing or after being subjected to various de-structuring conditions (i. e. dilution, pH, ionic force, solvents, release media). Nanoscale dimensions were confirmed for both types of dispersed systems and for all the associations with cargo molecules, as shown in Figure 3, though some bigger impurities were sometimes identified due to the natural source material. This accounted for a certain degree of polydispersity, nevertheless the reproducibility of the preparations was confirmed by repeated measures.[72] Size distribution analyses evidenced the presence in all samples of two main size populations. Specifically, both series showed a small population with mean hydrodynamic diameter generally below 100 nm for cubosomes and above 100 nm for liposomes; a second population at higher values around 500 nm was identified in all samples, also showing good reproducibility despite polydispersity. Bigger values obtained above the nanometer scale likely accounted for the presence of impurities of the biomass. The diverse types of supramolecular aggregates present in the samples in some cases influenced the hydrodynamic radius, and consequently the shape of the obtained distribution peaks, even though the comparison of the two aggregate types still revealed similar dimensions with an acceptable error range. The samples loaded with guest molecules often presented bigger dimensions, but not dramatically so, with respect to the empty samples. Indeed, as shown in Figure 3 and Table 3, the different combinations of encapsulated guest molecules did not influence greatly the assembly at supramolecular level, as it can be noticed in comparison with the empty control nanosystems, both cubosomes and liposomes. This evidenced the capability of both types of lipid nanocarriers to easily accommodate cargo molecules in the bilayer surface without significatively modifying the supramolecular structure. Moreover, when the technique was employed to verify the stability, it showed that the nanosystems of either symmetry were rather resistant to de-structuring conditions such as dilution and abrupt pH and ionic force changes, on the contrary it revealed the disruption that occurred when the nanocarriers were exposed to aggressive media, i. e. mixed biorelevant aqueous solution and ethanol. Indeed, after such treatment either no scattering intensity was recorded or the collected signal on the detector was not sufficient

to obtain reliable distribution analyses, thus evidencing the absence of nano-scatterers in the samples and confirming the occurred disaggregation.

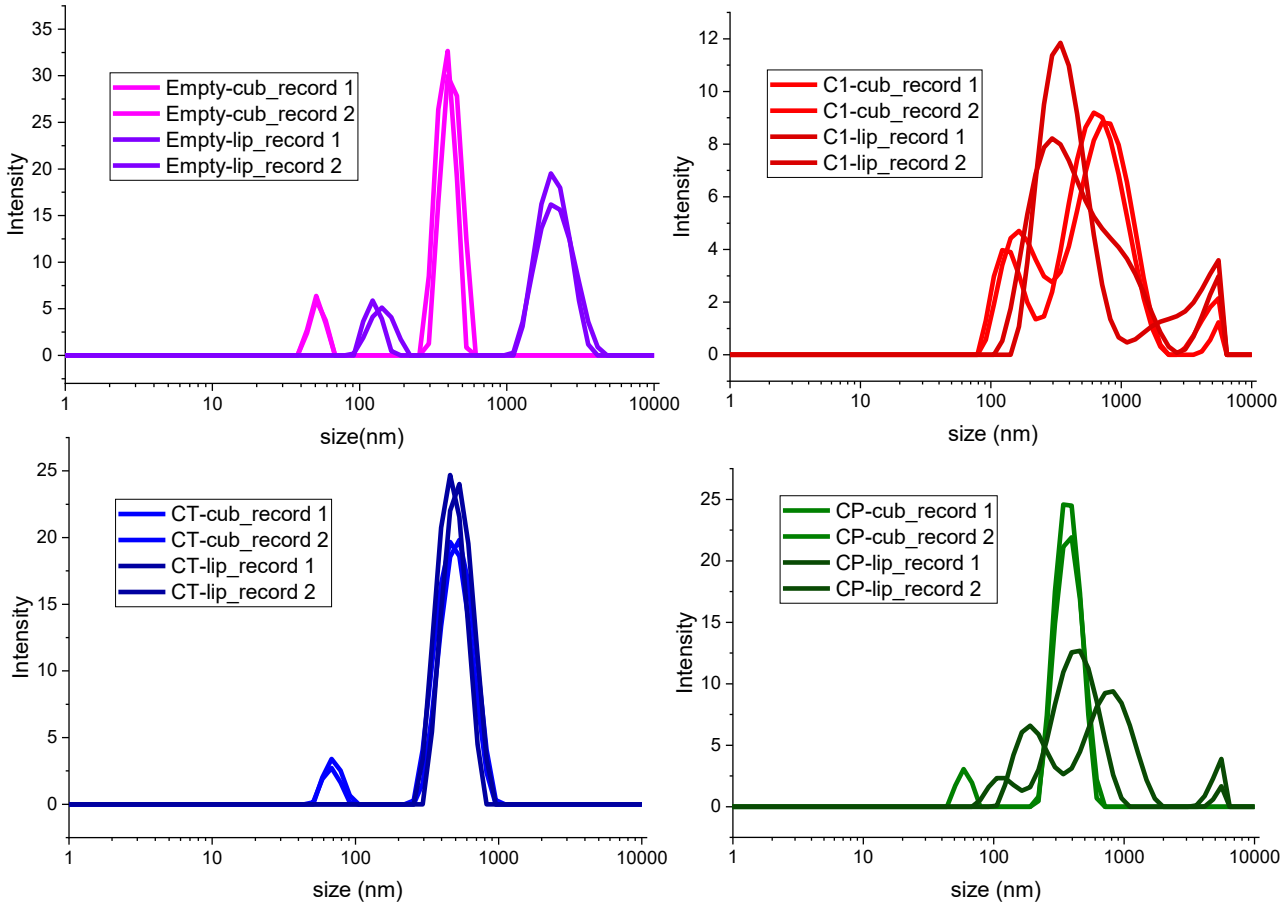

Figure 3. Size distribution analysis for the two nanovector series, compared in couples (color code: light (cubosomes) and dark (liposomes) respectively) on the basis of the encapsulated guest molecules, i. e. Empty (violet), C (red), CT (blue), CP (green).

Sample name	Mean size (nm) Peak 1±SD	Mean size (nm) Peak 2±SD	Polydispersity index (PdI)
Empty-cub	48±3	404±35	0.3
C1-cub	153±15	663±68	0.45
CT-cub	69±8	494±43	0.3
CP-cub	59±2	376±78	0.35
Empty-lip	133±20	2168±68	0.4
C1-lip	318±32	548±50	0.43
CT -lip	495±51	-	0.27
CP -lip	148±37	554±220	0.5

Table 3. Size distribution values ±SD and PdI for all investigated samples

3.2 Small Angle X-Ray Scattering

Advanced structural investigation of the ordering and assembly at supramolecular level over four orders of magnitude was performed through SAXS measurements. The technique was employed firstly to characterize in-depth the structural arrangement. The two nanocarrier series were prepared each in two different concentrations of lipids and encapsulated guest molecules (see Tab.2, Materials and Methods), in order to study the influence of both lipid and antioxidant total concentration on the aggregation and ordering, whereas the lipid/guest molecule ratio was maintained constant. This effect was then investigated both in the same nanovector series and by comparing the two types. The study of the dilute sample series prepared from the triglycerides-rich mixture revealed a complex nonlamellar cubic pattern in the full q-range investigated. The main characteristics were the presence of Bragg peaks in the large q region ascribable to cubic spacing at the unit cell scale, then a q^{-3} slope in the intermediate q-range, typical of globular aggregates and a bump (Figure 4). A large background intensity attributable to the form factor was also evident in all samples. In Figure 4 the complete cubosome series is shown, going from the empty nanocarrier (magenta) to the loaded ones at low and high concentrations (light or dark red, blue and green according to cargo content and low/high concentrations, respectively) following the black arrow. While a similar pattern could be identified on the full intensity plots of all samples, significant differences could be noticed in the large q-range regarding the peak positions and intensities at increasing guest molecules content. In Figure 5 an enlargement is shown at the large q scale, evidencing peak positions and assignments with bars and colored labels. The pattern of two cubic phases could be identified, the Pn3m and the Im3m,[39,78] whose superposed peaks were indicative of coexistence of both arrangements, differently pronounced in each sample according to type and concentration of the guest molecules. Specifically, a visible enhancement in peak intensity and sharpness could be noticed at higher curcumin encapsulation, even though also the presence of one or the other adjuvant played a role in the peak pattern. Indeed, the interactions between adjuvant molecules were found to be able to influence the spacing of Bragg peaks as well, particularly noticeable at the lower concentrations, while at increasing cargo loading curcumin dominated the interactions with the matrix (Figure 5). This indicated a marked influence of curcumin on the overall ordering of cubosome dispersions, which was in accordance with complementary results that evidenced the ability of such molecule to drive tighter bilayer packing and more structured supramolecular aggregation.[72] The Bragg peaks in all the plots were superposed to a background ascribable to the large bumps of form factors, due to the sum of the contributions of coexisting phases to the scattering intensity.

Figure 6 shows the SAXS diagrams of the full liposome series, from the empty nanovector (magenta) to the ones loaded at different concentrations, respectively. The scattering curve profile of liposomes was governed as well by the form factors of coexisting phases, in this case attributable to lipid bilayers, and by a q^{-2} decay in the intermediate q range indicative of liposomal aggregates. At variance with cubosome samples, the liposome series showed the start of a plateau in the Guinier region, though also in this case bigger aggregates and likely some impurities from the natural matrix caused a rise in intensity in the low q range. In the large q range, the only sample showing slightly pronounced peaks in 1:2:3 spacing, characteristic of lamellar organization, was sample C1-lip. This tendence was opposite to that showed by cubosome samples, highlighting a peculiar behavior in the two different mesophase dispersions. Indeed, while the cubosomes series showed visible enhancement of lipid ordering with the appearance of sharper peaks at higher cargo concentration, no marked change or stacking enhancement was found in the lamellar organization with increased guest molecules encapsulation.

Exemplificative comparison between the two nanocarrier series is presented in Figure 7, that shows two representative cubosome samples, Empty-cub and C1-cub (magenta and red) and the correspondent liposome samples (dark red and blue respectively) all four at the lower lipid and guest molecule content, enlarged in the large q region. While the cubic spacing of the two superposed mesophases could be identified in both cubosome samples (red and orange bars and indices), it is worth noting the correspondence of three peaks (green in Figure 7) with the small ones visible only in sample C1-lip in the 1:2:3 spacing. These data suggest the presence of a small percentage of lamellar bilayers, likely non-correlated, in the cubosome samples coexisting with the main two populations of cubic aggregates.

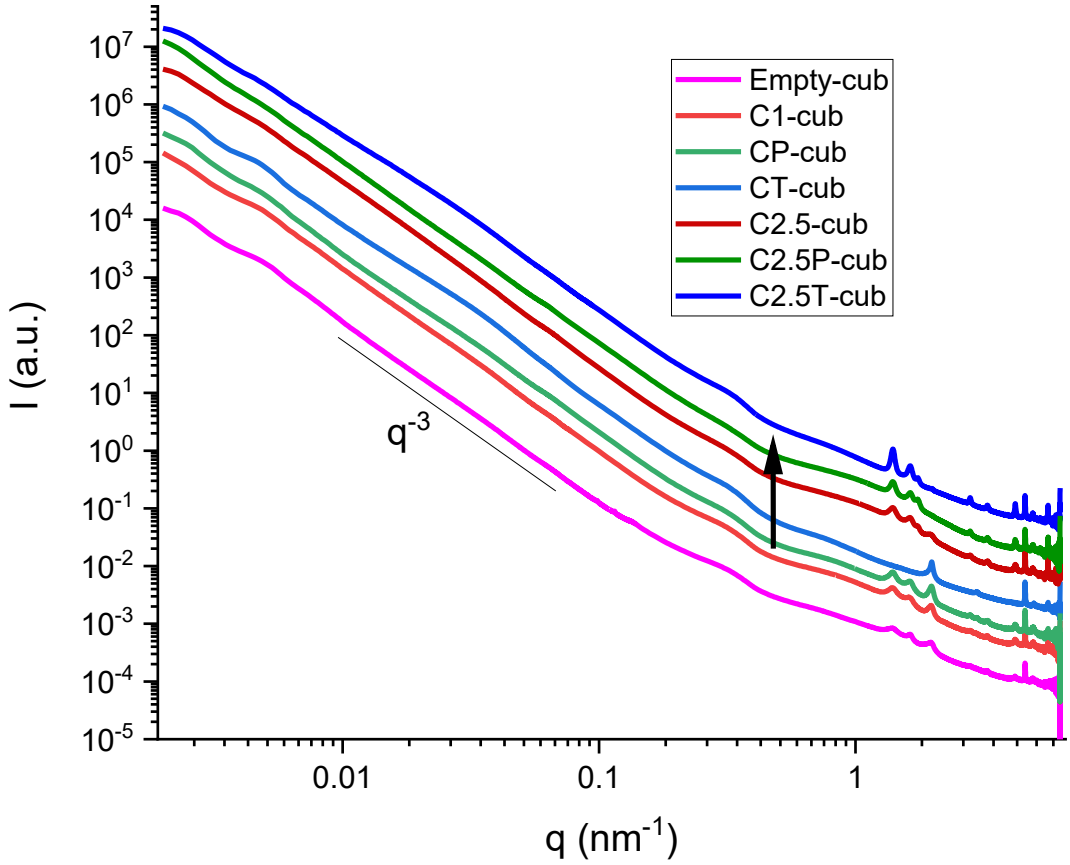

Figure 4. One-dimensional SAXS intensity plot at full instrumental range (3×10^{-3} to 7.5 nm^{-1}) showing the entire cubosome series, at lower (10^{-2}M) and higher ($2.5x10^{-2}$M) curcumin and adjuvant molecules (tocopherol and piperine) concentrations, plus the Empty sample. The black arrow indicates the increasing concentration, the curves were shifted vertically for the sake of clarity.

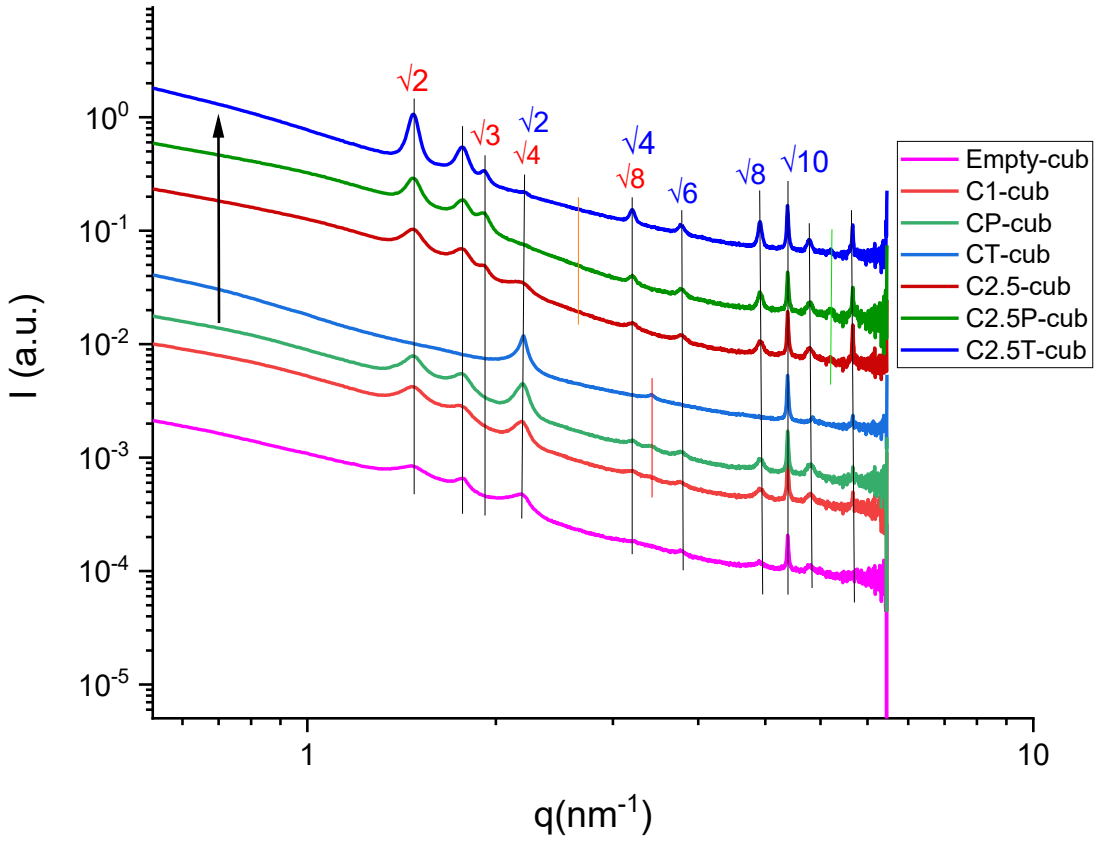

Figure 5. One-dimensional SAXS intensity plot showing the positions of Bragg peaks in the two cubic mesophases (red and blue labels indicating the q-spacing) for cubosome samples at the two lipid and guest molecule concentrations. For the sake of clarity, the lines indicating smaller peaks visible only in one group of samples were colored differently.

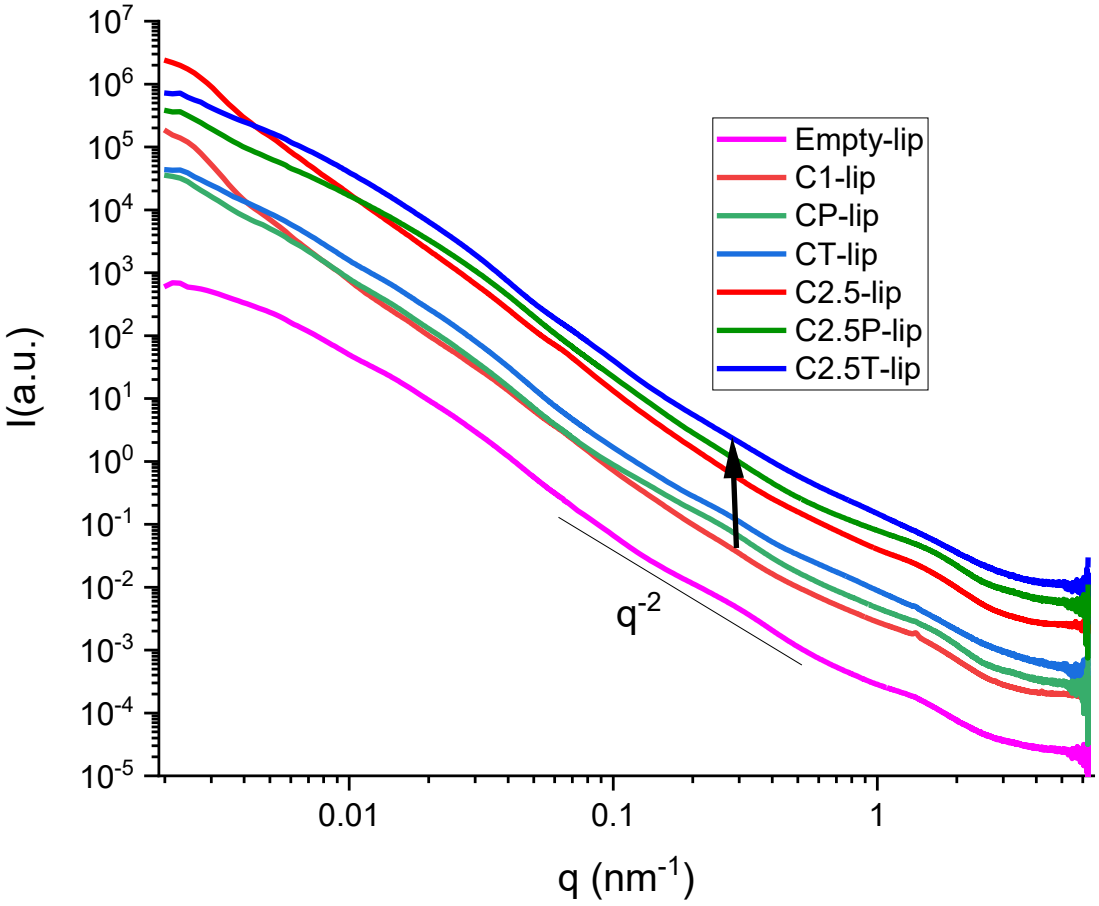

Figure 6. One-dimensional SAXS intensity plot at full instrumental range (3×10^{-3} to 7.5 nm^{-1}) showing the entire liposome series, at lower (10^{-2}M) and higher (2.5×10^{-2}M) curcumin and adjuvant molecules (tocopherol and piperine) concentrations, plus the Empty sample (same color code as cubosome series). The black arrow indicates the increasing concentration, the curves were shifted vertically for the sake of clarity.

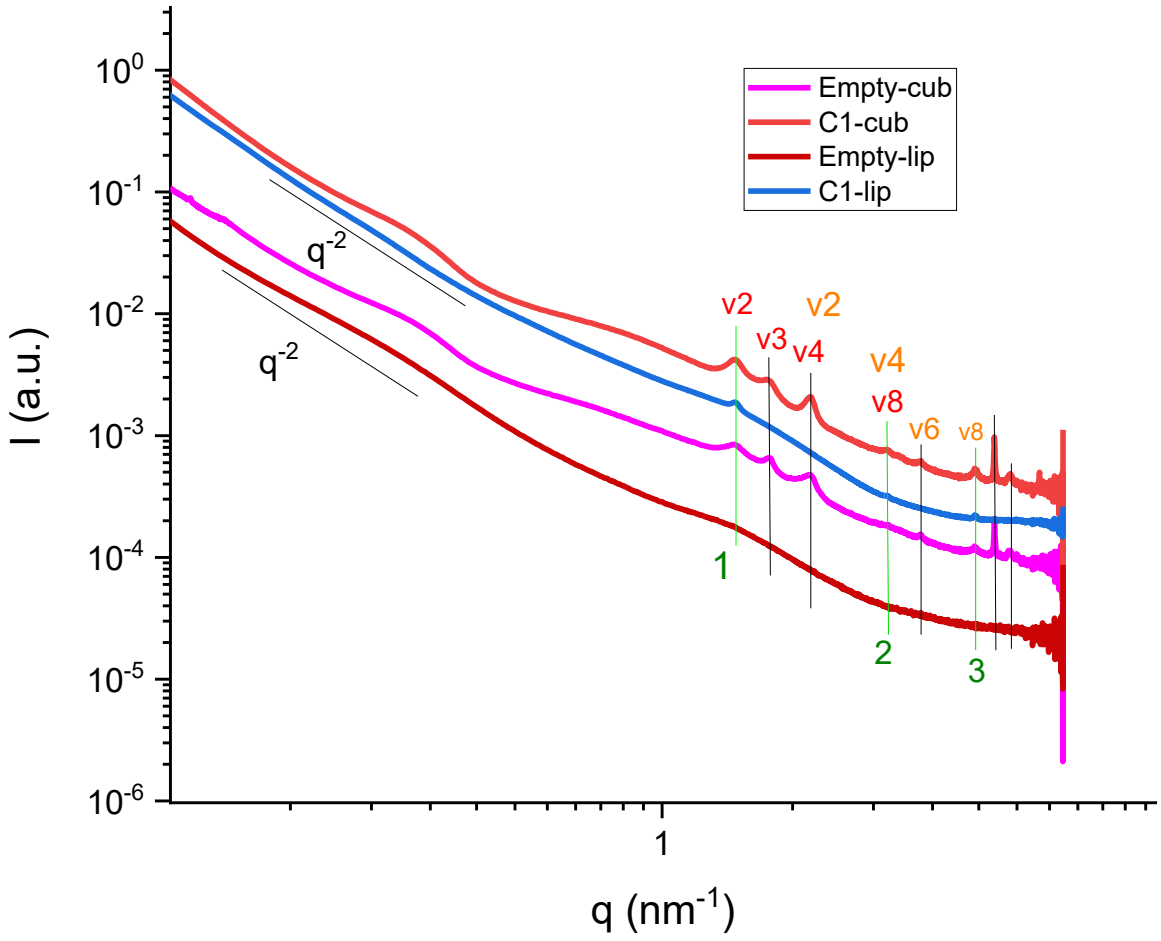

Figure 7. One-dimensional SAXS intensity plot showing the positions of the Bragg peaks in the two cubic mesophases (red and orange labels indicating the q-spacing of scattering maxima) for cubosome samples, and the q-spacing of the lamellar phase (green values) for liposome samples as a guide for the eye.

SAXS measurements were employed also in the context of the investigation of stability properties and resistance to disaggregation of the two nanovector series. The kinetics of de-structuring and loss of supramolecular organization was followed by measuring the samples taken at different time points of the disassembling process. Figure 8 shows the time evolution of the intensity plot for a representative cubosome sample undergoing de-structuring. The main characteristics that could be evidenced were the lowered scattering intensity and the almost complete disappearance of the peaks as the system disassembled and released the cargo (Figure 8). Indeed, the Bragg peaks evidencing the cubic organization disappeared almost completely after two hours, except for a barely visible peak and a small bump of a form factor that could still be seen in the aliquots taken after few hours,

indicating the resistance to disaggregation, or hypothetically the ability to re-arrange in different, less organized aggregates.

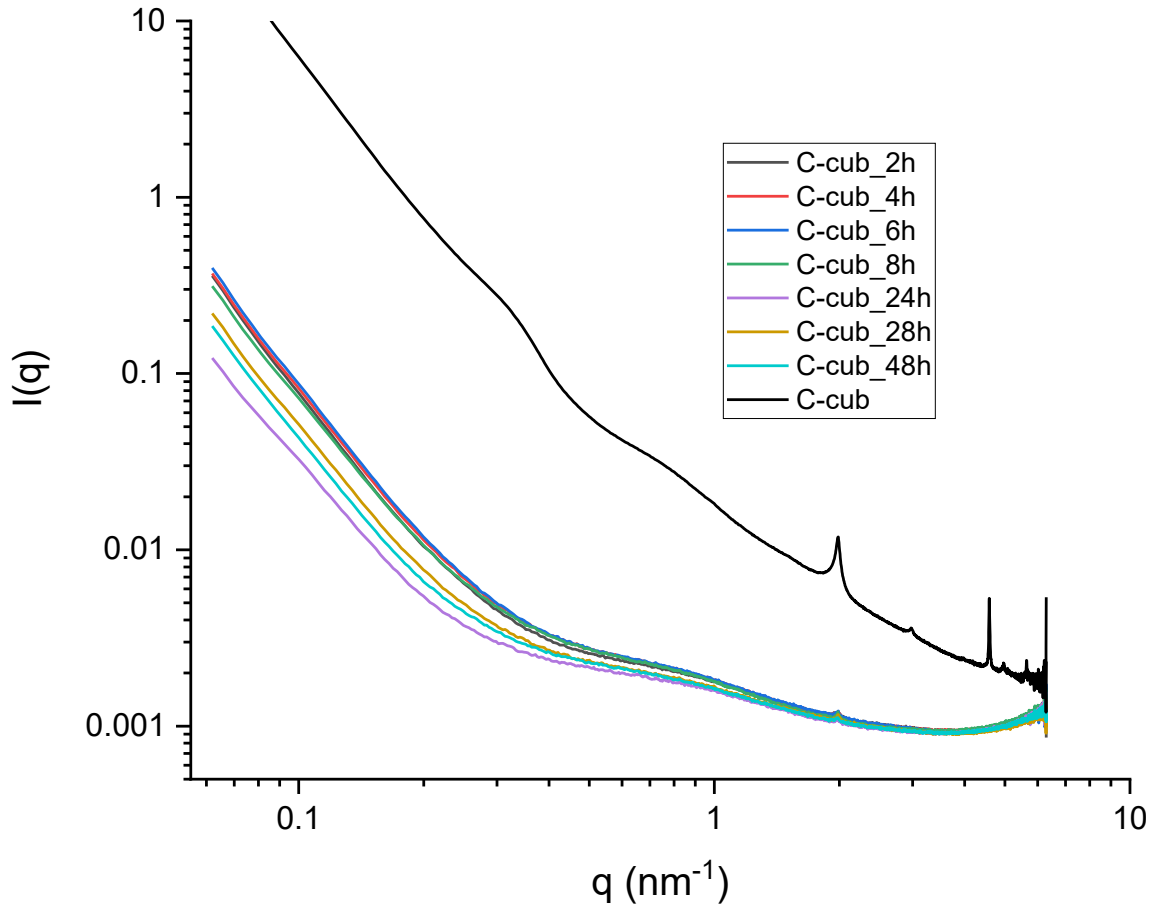

Figure 8. One-dimensional SAXS intensity plot of an exemplificative cubosome system, enlarged in the big q range, showing the progressive loss of supramolecular structuring in sample aliquots taken every two hours from inside the dialysis bag.

Figure 9 shows the intensity plot of a representative liposome sample irradiated during its disassembling. The small peaks indicating the presence of lamellar organization disappeared right away after the first two hours, although the form factor was still visible after few hours. It could be hypothesized the presence of some supramolecular organization, albeit unstable such as uncorrelated bilayers and some resistance to complete de-structuring.

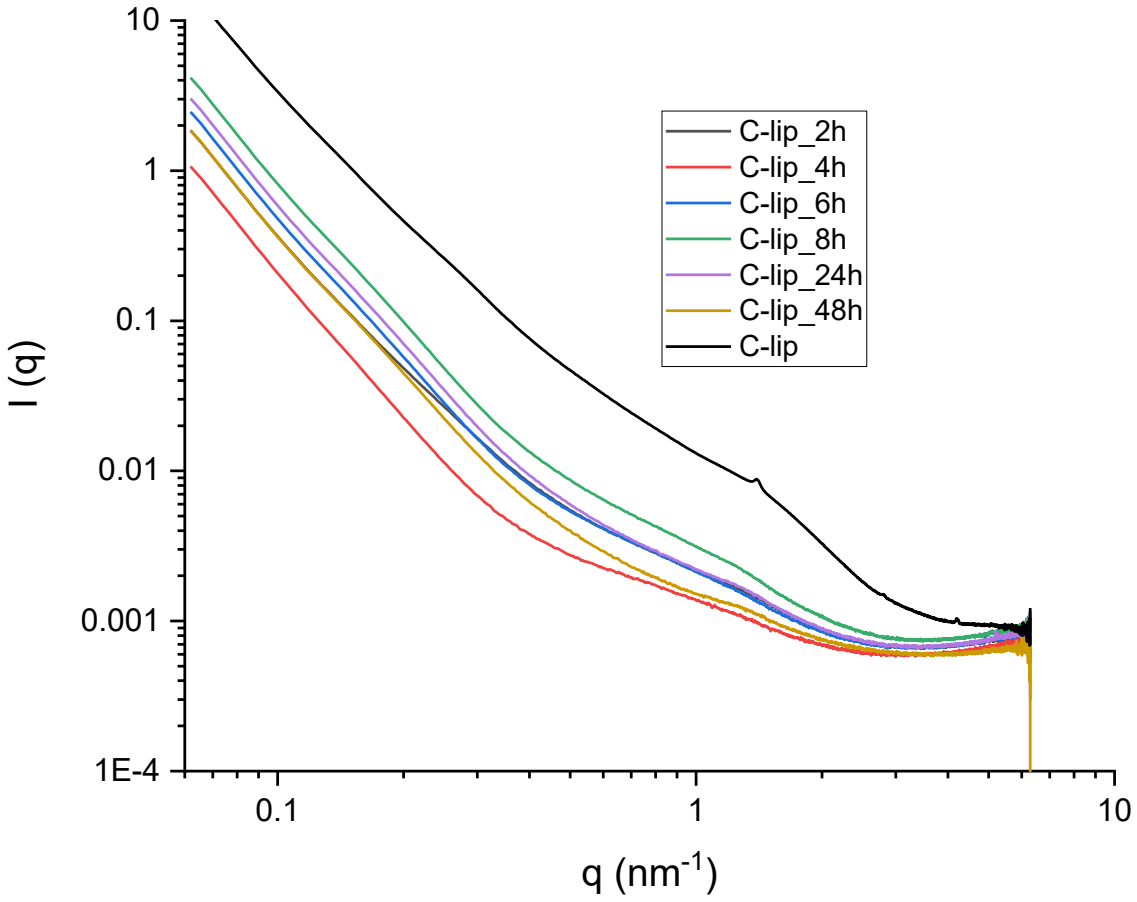

Figure 9. One-dimensional SAXS intensity plot of an exemplificative liposome sample, enlarged in the big q range, showing the progressive loss of supramolecular structuring in aliquots taken every two hours from the dialysis bag.

3.3 Cryogenic Transmission Electron Microscopy

The visualization of the mesophase dispersions with cryo-TEM was carried out over the course of time with two different instruments, after establishing an optimal protocol for the vitrification process of these samples. Indeed, often the vitrified specimens contained rather thick layers that could be attributed to the natural material present in the samples, that enveloped the nanosystems which in turn tended to adhere to each other and form bigger aggregates. Nevertheless, both sets of imaging measurements gave comparable and reproducible results confirming the preliminary size analysis data obtained by DLS (Tab.3), and despite the high number of micrographs showing the large and thick aggregates we could identify isolated particles.

In the set of cryo-TEM micrographs obtained from the first imaging experiment (Figure 10 a-d), it was possible to notice aggregates with inner nonlamellar nanostructures falling into the ranges

identified by DLS, such as a mostly spherical population around 100 nm consistent with DLS results, and non-spherical types of aggregates, i.e. tubular and square-shaped nanostructures with similar dimensions, all of them showing dense internal organization (Figure 10).[39] While it was not possible to identify precisely the spacings of the inner structure due to the low content of electron-rich molecules in the triglyceride matrix (low TEM contrast), a nonlamellar organization could be plainly seen which confirmed SAXS results. Moreover, unilamellar structures in the range 350–500 nm could be visualized as well, as seen with light scattering experiments (Figure 10b). Even though the size polydispersity obtained by DLS could be justified by the presence of two populations, it was observed that the broadening of the distributions could also be due to the sometimes-uncommon morphologies present in such samples (Figure 10 a-d).

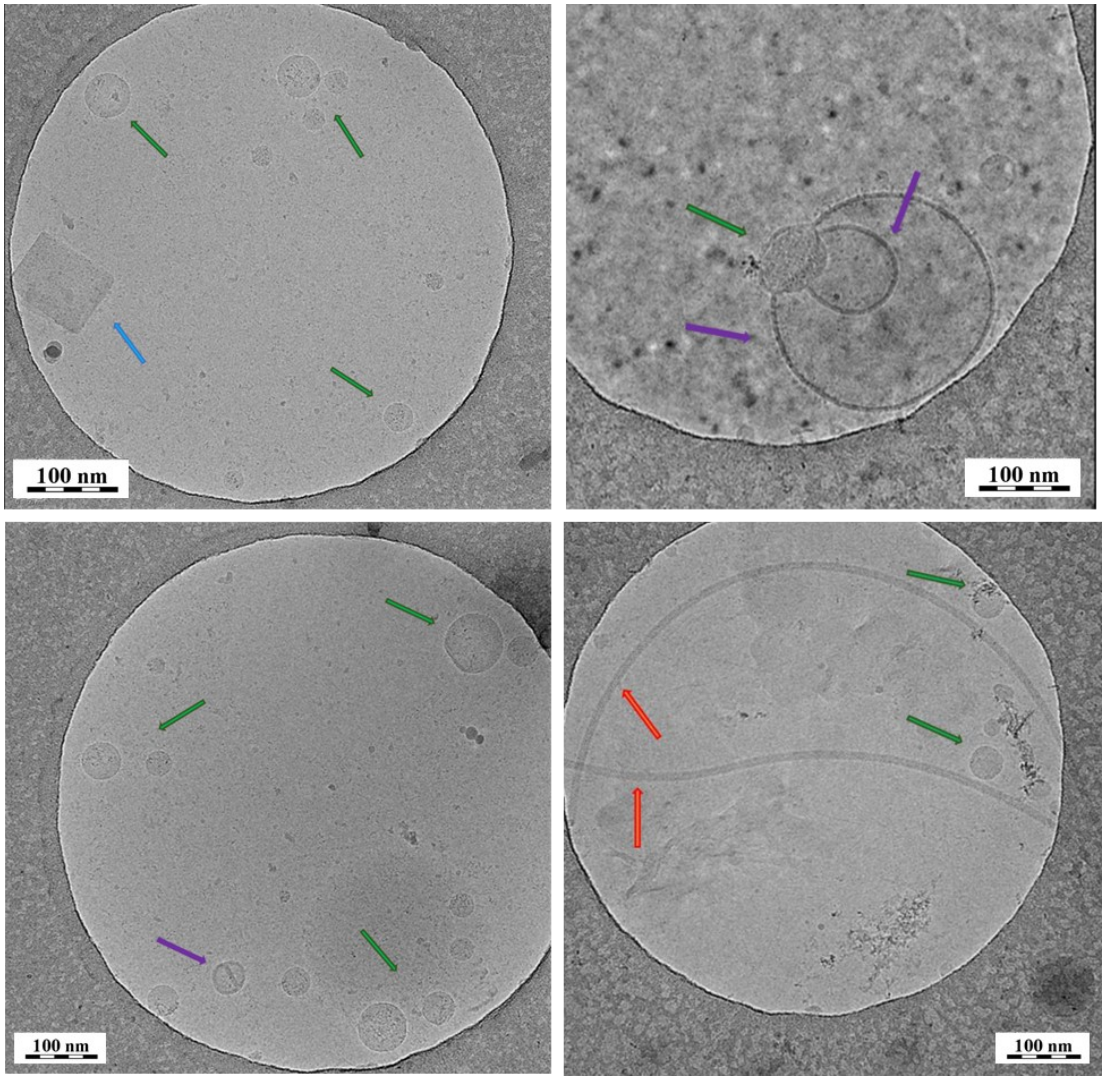

Figure 10 (a-d). From a) to d) left to right and top to bottom respectively, spherical aggregates with inner dense structures (green arrows), rectangular aggregate (blue arrow), unilamellar structures

(violet arrows), uncommon shapes (red arrows). The undefined objects visible in d) are attributed to layers of the natural material present in the samples.

Typical cryo-TEM micrographs obtained from the second imaging experiment of cubosome and liposome systems are displayed in Figure 11 a-d. Despite some micrographs showing large and thick aggregates, we could identify isolated particles in samples belonging to both nanocarrier series in the dimension ranges previously identified by DLS measurements. In the cubosome systems (Fig. 11a, 11c) the particles were denser and more compact, showing higher contrast in cryo-TEM micrographs, slightly smaller than 100 nm and irregular in shape. On the other hand, in the liposome systems (Fig. 11b, 11d) the particles were larger (mostly above 100 nm) and almost spherical; as previously observed in the first set of measurements, sometimes they also exhibited onion-like structures (Figs. 10b and 11b two-shell onion nanoaggregate). It is worth noticing that no apparent morphological differences between individual samples within the same nanovector series (i. e. within the cubosome set and liposome set of samples, respectively) could be detected. We could then conclude that the encapsulation of the guest molecules did not change dramatically the inner organization and both types of nanocarriers were able to re-arrange easily to accommodate the loaded cargo. The fact that the average size of cubosome particles was smaller than the average size of the liposomal particles was in accordance with DLS results (cf. Figure 11a-b and Table 2), even though both techniques showed that the dimensions were still in a comparable range. Even though with the present technique the most frequently detected nanostructures were the ones falling in the smaller size population around 100 nm, likely due to experimental criticalities (i. e. sample vitrification), also some bigger aggregates could be visualized (Figures 10b and 11b). Furthermore, both sets of cryo-TEM experiments evidenced that occasionally, the cubosome samples also contained few lamellar vesicles (Fig. 10 b-c) or complex meta-stable nanoaggregates (Fig. 10 d). This finding was in agreement with the speculation suggested by SAXS data regarding the likely presence in cubosome samples of a small percentage of lamellar structures.

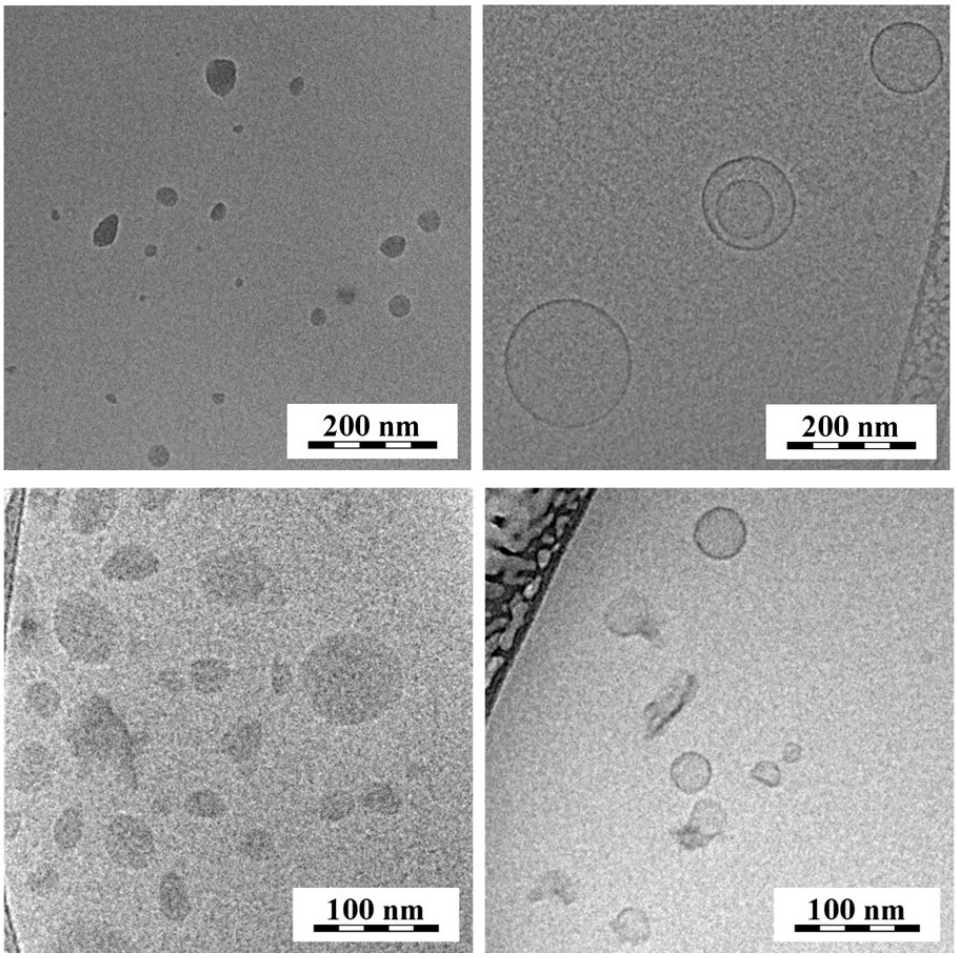

Figure 11. Representative cryo-TEM micrographs from a) to d) left to right and top to bottom respectively showing nanoaggregates in cubosome (left, a and c) and liposome (right, b and d) samples.

3.4 Nuclear Magnetic Resonance

The identification of a different structural arrangement in the two lipid nanocarrier series was carried out as well by NMR. Indeed, even though such technique is somewhat less popular in recent times for such purpose, various experiments were carried out in the past that were able to differentiate dispersed lipid mesophases from their resonance spectra.

In lyotropic systems molecules experience motions and averaging of anisotropic interactions according to the different long range symmetries present in the aggregate at the supramolecular level.[102] Nonlamellar lipid nanostructures in dilute regimes can be differentiated from liposomes on the basis of their magnetic resonance spectra by performing various types of experiments.[89] Through the years proton, phosphorus and deuterium lineshape NMR, and relaxation time measurements have

been performed on these dispersed nanosystems, together with spin labeling EPR, and these techniques were able to distinguish optically birefringent systems such as lamellar, cubic, inverted hexagonal and monolayered interdigitated phases. Typically, while nonlamellar structures in dilute regime are characterized by narrow NMR signals, liposomal and analogous aggregates commonly show marked line broadening. Indeed, the lateral diffusion in onion-like lamellar systems generally does not modify the molecular angle with the applied magnetic field and only fast rotations along the axes are present, whereas in nonlamellar phases the translational diffusion on the curved surface of the supramolecular aggregate is able to generate averaging of dipolar interactions and relaxation over both short and long distances, thus driving to line narrowing.[90] In fact, the fast translational diffusion in the isotropic structure of nonlamellar systems modulates all inter- and intramolecular interactions, contrarily to lamellar phases where these latter are not affected by diffusion along planes and show instead relaxation by slower motions. Thus, cubic phases which possess pronounced isotropy are characterized by narrow, micellar-like, NMR peaks.

The NMR investigation of our dispersed nanosystems (liposomes and cubosomes) reflected the above-described peculiarities of lamellar and nonlamellar structures regarding the arrangement of the lipid matrix, confirming SAXS and cryo-TEM results. Figure 12 shows the comparison of the ^{1}H spectra of Empty-cub (black curve) and Empty-lip (red curve) samples where the different packing and aggregation of the two nanosystems types was clearly evidenced. As expected, the proton signals of the lipid matrix in the liposome sample were quite broad in the range 5-5.5 ppm, which accounts for protons experiencing intermediate de-shielding (e. g. protons close to the polar heads or bound to unsaturated carbons), indicating tight molecular packing and hindered motions of the chains. Such tendency could be identified also in the range at 3-4 ppm, accounting for the terminal $-CH_3$ and $-CH_2$ groups in the alkyl chains, where the liposome sample presented rather broadened signals, contrarily to the cubosome system that in both spectral areas showed narrower peaks. These data evidenced that the cubic dispersions possessed faster dynamics of lipid chains due to higher mobility in the short-range interactions with respect to the liposomes and such property at the molecular level was extended to the whole aggregate, evidencing faster translational diffusion at the supramolecular scale.

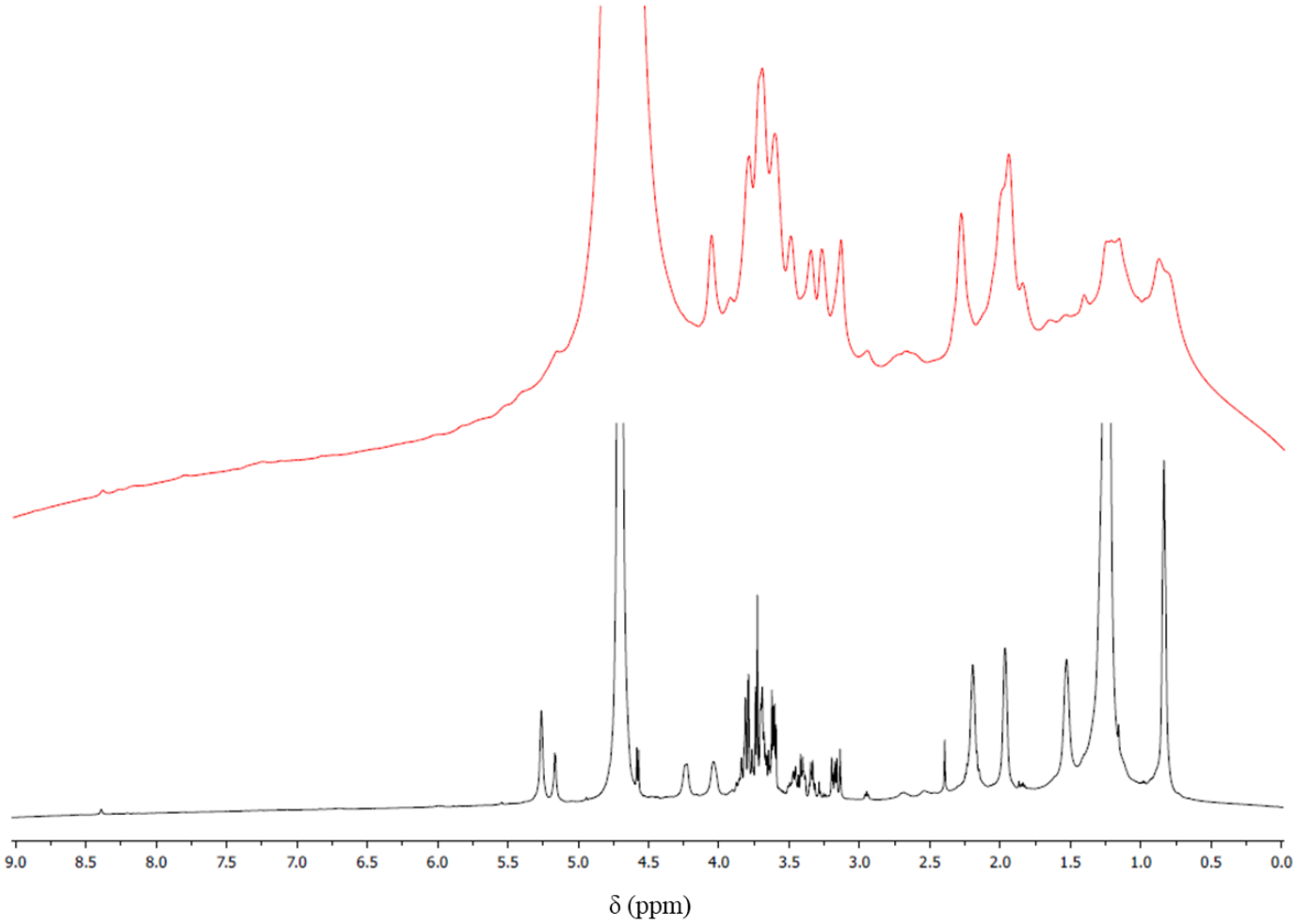

Figure 12. ^{1}H spectrum in the 0-9.0 ppm range recorded at 600 MHz and 298 K for: Empty-cub (black), Empty-lip (red)

The peculiarities of the two nanovector types emerged also during the study of the loaded cargo and its localization. Indeed, the main purpose of NMR experiments was the investigation of host- guest interactions between the encapsulated molecules and the lipid matrix, and the effects of guest molecule incorporation at different concentrations. Particularly, the most relevant results were observed in only-curcumin loaded samples, as previously seen in SAXS experiments. Different concentrations and molar ratios were analyzed to assess the localization and influence of such molecule on the lipid inner organization.

In Figure 13 the ^{1}H spectra recorded at 600 MHz of empty and curcumin loaded cubosome samples, namely Empty-cub, C1-cub and CT-cub is reported. The typical resonances of lipid alkyl chains in the range 2.0-0.8 ppm could be seen in the NMR spectrum of the Empty-cub nanovectors (black curve). Despite the higher molecular mobility of cubosome samples with respect to liposomes, these

lipid aggregate systems generally presented wide peaks. Such broadened resonances are in fact typical of amphiphiles forming aggregates or molecules that are associated with large structures.[102,103] As expected, the proton signals of the lipid matrix in the most packed nanosystems, that had longer diffusion rates and hindered reorientation of the molecules, were enlarged beyond detection due to short relaxation times. Moreover, no proton signals of curcumin in the 9.0-5.0 ppm region where the aromatic signals are localized were visible either in C-cub or in CT-cub samples, both loaded with curcumin at 10^{-2} M (Fig. 13 red and green spectra, respectively). However, when the curcumin content was progressively decreased as shown in Figure 14 (all three cubosome samples loaded with only curcumin at 10^{-3} M black, 5.10^{-4} M red and 10^{-4} M green), small proton signals of curcumin in the aromatic region became visible even when the concentration was lowered of only one order of magnitude (10^{-3} M, black in Figure 14, spectra and inset with magnification).[72]

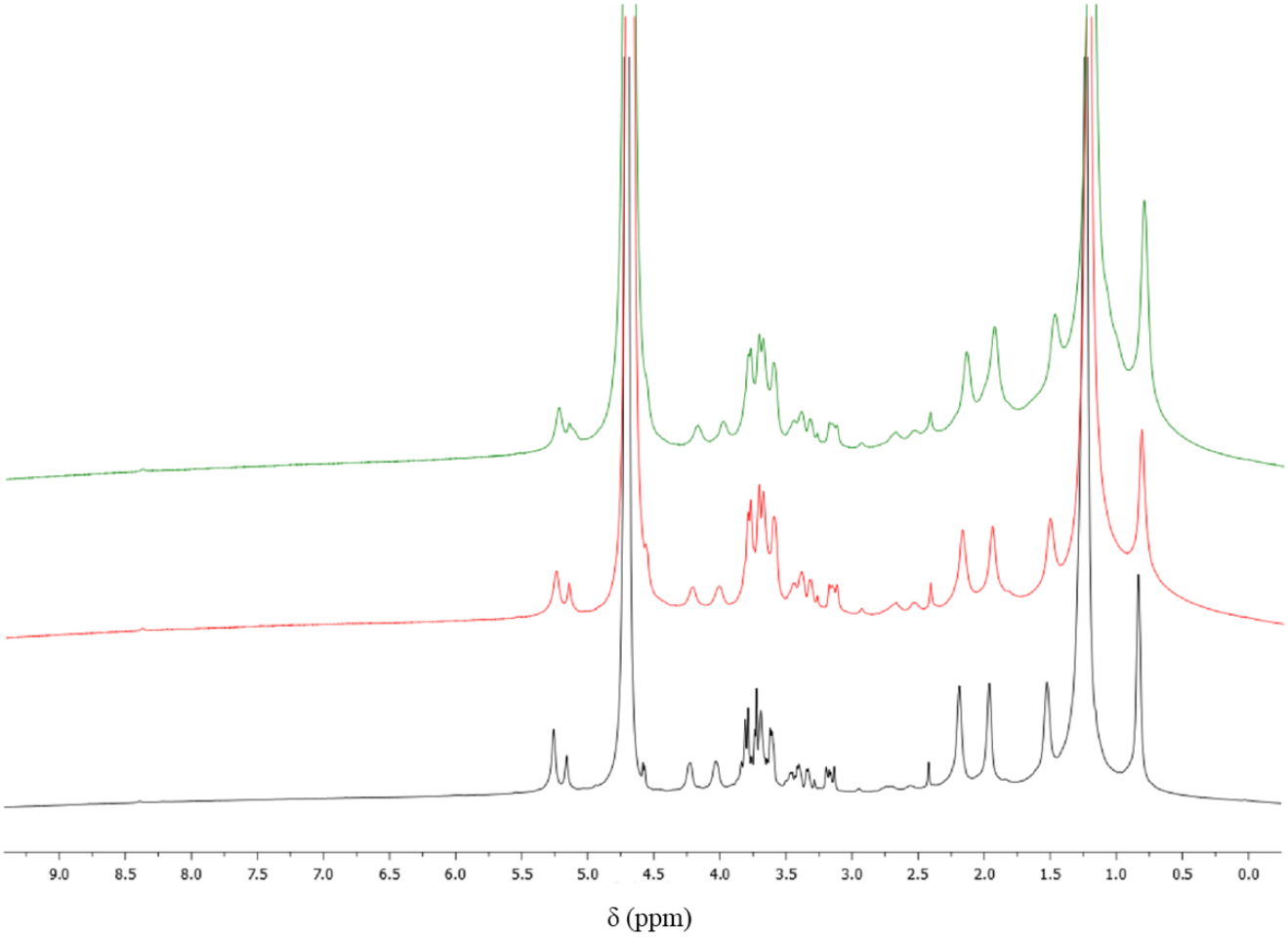

Figure 13. ^{1}H spectrum in the 0-9.5 ppm range recorded at 600 MHz and 298 K for: Empty-cub (black); C1-cub (red); CT-cub (green).

This evidence proved that curcumin encapsulated at our chosen standard concentration (10^{-2} M) in the cubosome systems was strongly associated by molecular interactions to the lipid aggregates, i. e. likely intercalated within the lipid matrix in a region of restricted molecular mobility, due to the close packing of the cubic inner structure and concurred to the strengthening of lipid intercorrelation. This hypothesis was previously suggested by studies reported in the literature, that highlighted also in phospholipid nanocarriers the presence of curcumin localized in such regions, e. g. close to the polar heads, according to DSC experiments[104] and molecular modeling[105]. Moreover, it was observed that also the signals of the lipid matrix were influenced by curcumin concentration, as they became markedly narrower when the curcumin content was gradually decreased. Such effect was particularly evident in the region where alkyl chains resonate at 2.0-0.8 ppm (Figure 14). The dynamics of the systems was considered to clarify this finding that might appear counterintuitive. Indeed, at lower curcumin concentration faster molecular motions of the lipid matrix were allowed, which is consistent with the presence of smaller aggregates or with less tightly packed structures. Thus, these data were in agreement with the evidence obtained from SAXS measurements, which showed that higher concentration of curcumin was able to impose stronger correlation and ordering in lipid cubic aggregates.[72]

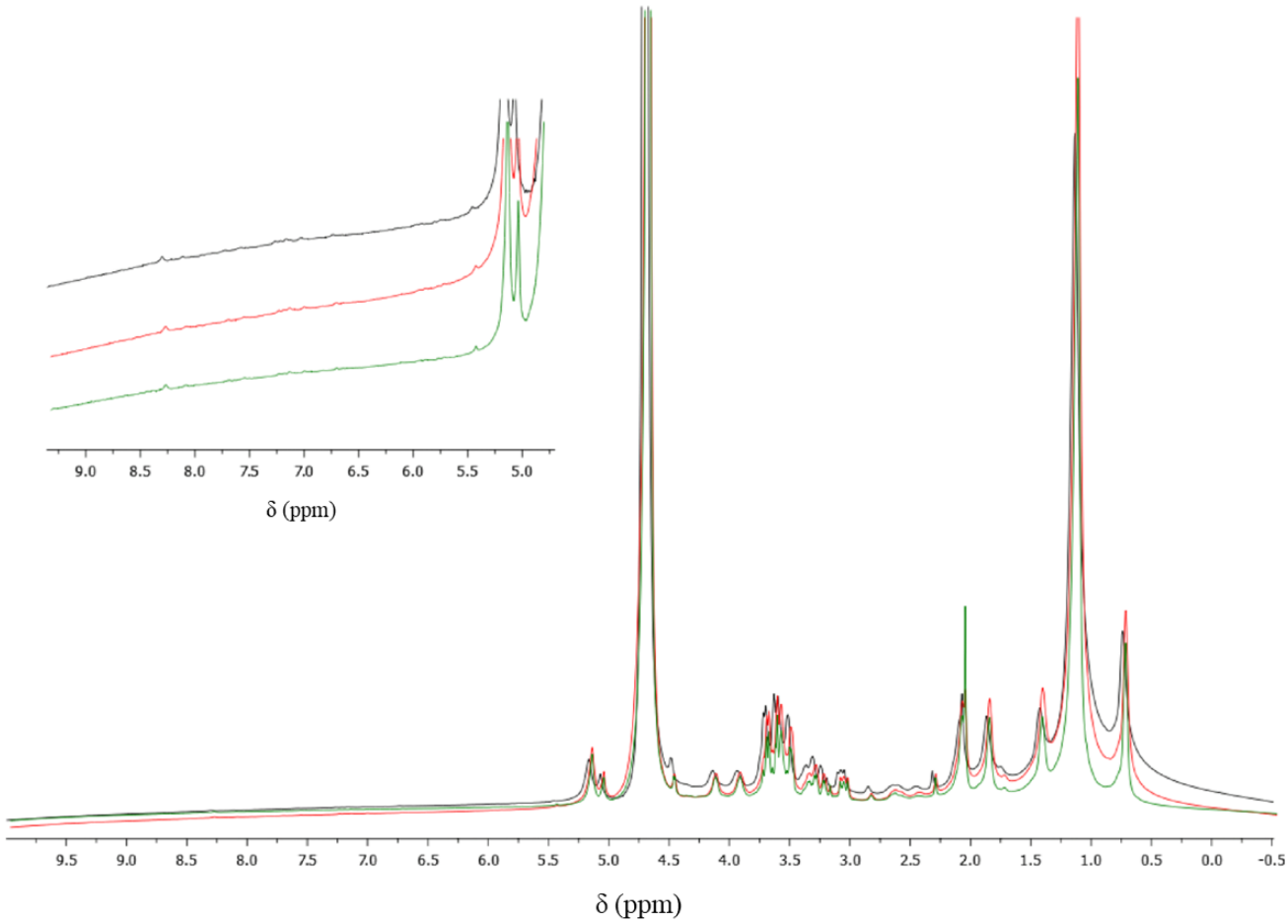

Figure 14. ^{1}H NMR spectrum (600 MHz) in the -0.5-10.5 ppm range of cubic nanoaggregates with three different curcumin concentration: 10^{-3} M (black), 5.10^{-4} M (red) and 10^{-4} M (green). Magnification of the 9.0-5.0 ppm region, highlighting the aromatic proton signals of curcumin.

Moreover, as shown in the ^{1}H spectra in Figure 15, when varied curcumin concentrations were encapsulated in the liposome systems (10^{-3} M (black), $5x10^{-4}$ M (red) and 10^{-4} M (green) respectively), no detectable change of peak width was evident in the spectra, as opposed to the peak narrowing in the cubic nanovectors. These data were also in agreement with SAXS spectra, clearly showing that structural differences between the two nanovector series had a deep impact on the motions exerted by the lipid matrix, also in the presence of interacting guest molecules, and confirming a different mobility and dynamics in the two series of nanovectors (Figures 4 and 6).

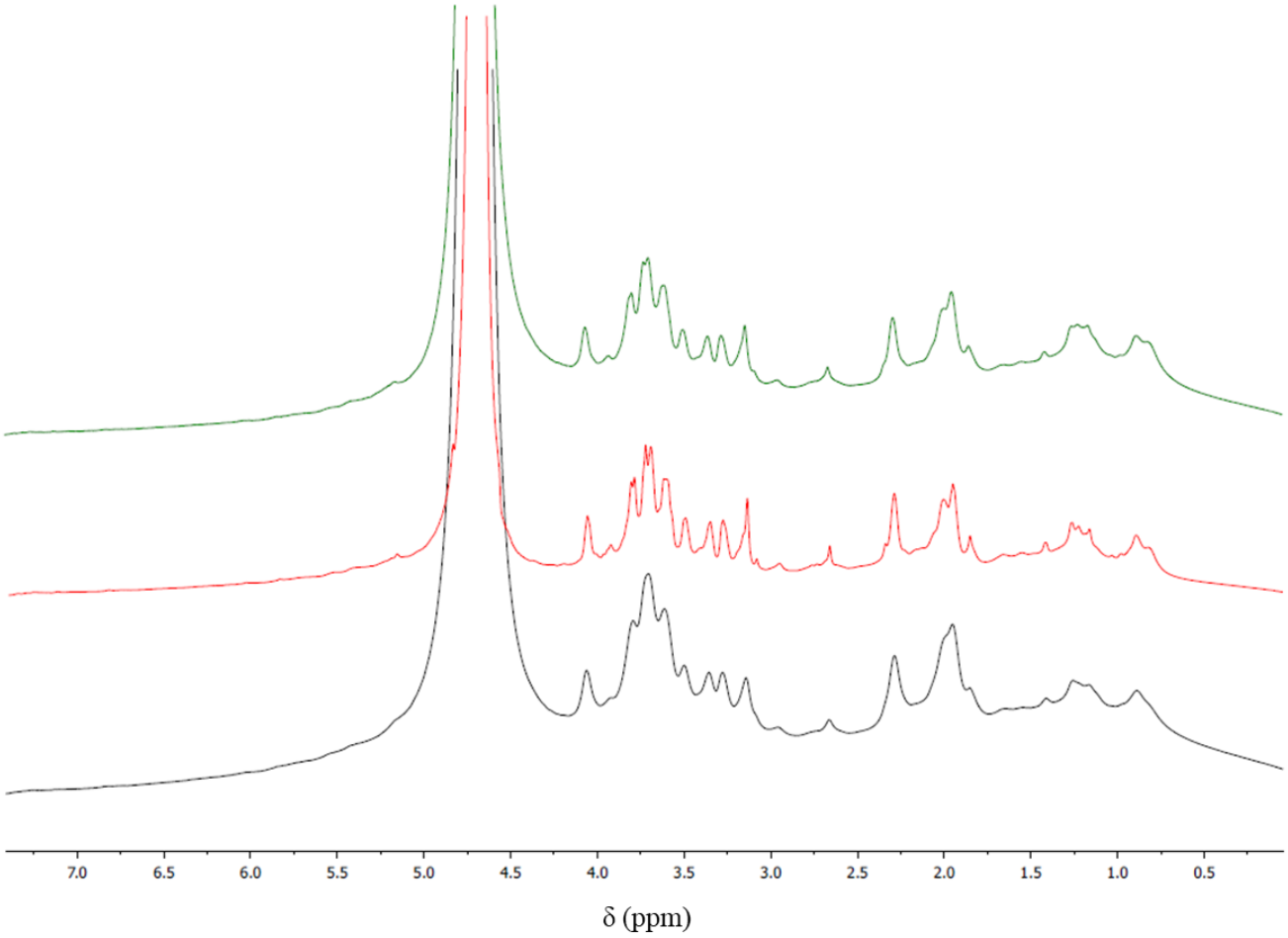

Figure 15. NMR spectra of liposome samples at different curcumin concentration, 10^{-3} M (black curve), $5x10^{-4}$ M (red curve) and 10^{-4} M (green curve).

3.5 Isothermal Titration Calorimetry

The investigation of the interactions and stability of the two nanocarrier series was performed by preliminary ITC measurements to complement structural knowledge with a thermodynamic approach. Indeed, the above described data at the molecular scale from SAXS and NMR supported the hypothesis of a different influence exerted by guest molecules-lipid matrix interactions, depending both on the cargo molecule and on the supramolecular arrangement. Considering the high sensitivity of microcalorimetry, titration experiments were carried out either in water or hydroalcoholic solution (EtOH 10% v/v) to evidence nanocarrier stability variations and thus probe the strength of intra-aggregate interactions. The first results obtained both in water or ethanol 10% v/v gave different thermal profiles according to nanocarrier series and encapsulated guest molecules. Figure 16 shows the heat profiles upon titration with water of Empty-cub and Empty-lip (top, from left to right) and of C-cub and C-lip (bottom, from left to right). Though all samples showed low intensity, molecular

fluctuations and intra-bilayer rearrangements were hypothesized for sample C-cub that presented a markedly different profile with respect to the others, evidencing that a thermal event occurred upon dilution with water.

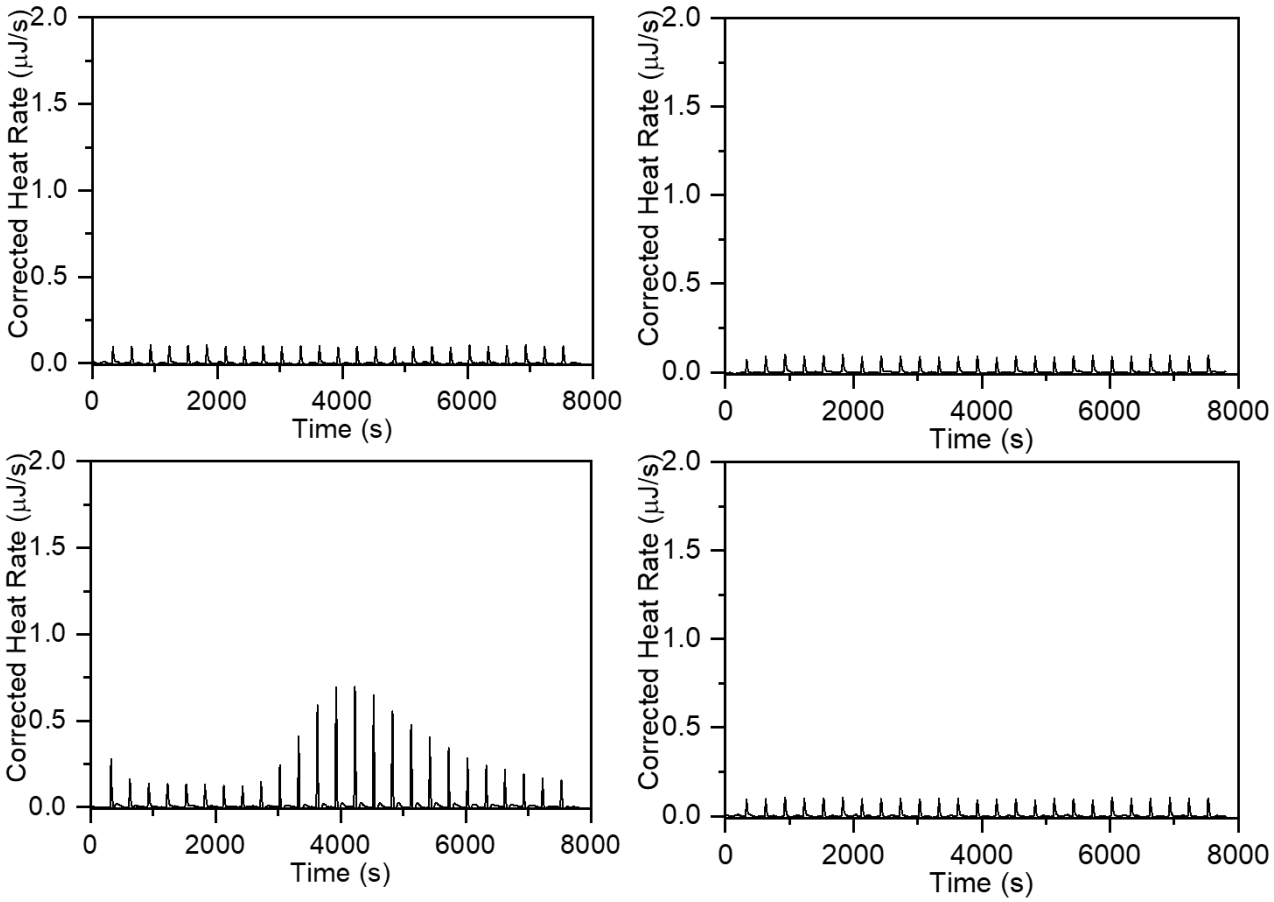

Figure 16. Heat profiles of cubosome (Empty-cub and C-cub, left column, top to bottom) and liposome samples (Empty-lip and C-lip, right column, top to bottom) upon titration with water.

Experiments carried out by titration with ethanol 10% (v/v) showed more complex profiles, also in this case differing both on the nanocarrier type and guest molecules. Figure 17 shows the thermal profiles of samples Empty-cub and Empty-lip (top, from left to right) and samples C-cub and C-lip (bottom, from left to right) upon hydroalcoholic dilution. In this case it could be evidenced that the Empty samples showed thermal events as well, likely undergoing small rearrangements at the bilayer level, while both C-cub and C-lip showed different profiles. It can be hypothesized that the curcumin loaded nanocarriers experienced more marked rearrangements due to the presence of the guest molecule, that impacted differently on the lipid matrix structure with respect to the empty aggregates. On the other hand, it is reasonable to expect that the ethanol molecules should exert a dramatically disrupting effect on the bilayer packing with respect to water molecules, because of deeper

intercalation below the polar heads. This results in a more active role of ethanol in the disassembly of the supramolecular structure, tough higher percentages are needed to observe this effect at the macroscopic level, as discussed below (see section 3.7).

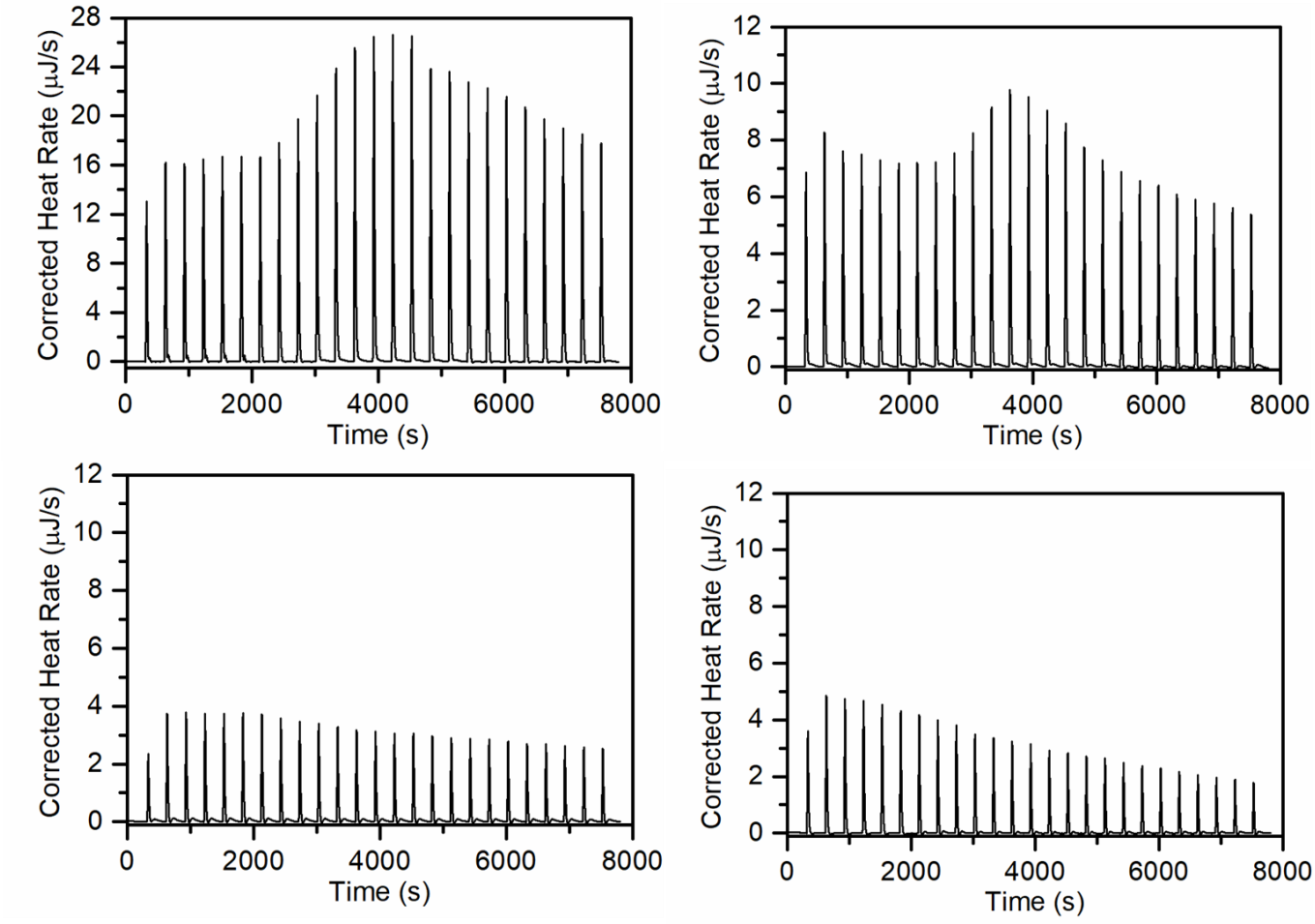

Figure 17. Heat profiles of cubosome (Empty-cub and C-cub, left column, top to bottom) and liposome samples (Empty-lip and C-lip, right column, top to bottom) upon titration with ethanol.

Results and discussion: Encapsulation, stability and functionality

3.6 Encapsulation efficiency (%)

The efficiency of guest molecule encapsulation of the two nanosystems series was assessed spectrophotometrically to obtain information on loading capacity, evaluate the encapsulation limit and test stability and release properties. The two aggregate types were compared to evidence the different encapsulation capability based on their structural arrangement in a structure-function perspective. As shown in Table 4, an opposite tendency could be identified regarding curcumin incorporation. Indeed, in cubosome samples higher values of encapsulation efficiency (EE%) were observed when tocopherol or piperine were loaded together with curcumin, as both adjuvants likely favored curcumin insertion thanks to interactions in the confined space of the lipid bilayer. On the contrary, the liposome series showed the opposite trend, as samples CT-lip and CP-lip had lower efficiency for curcumin loading than sample C1-lip (Tab. 4). Moreover, samples CT-cub and CP-cub showed higher EE% percentages for curcumin than CT-lip and CP-lip (Tab. 4). This could be explained considering the supramolecular arrangement, as the liposomal bilayer likely had a lower encapsulation limit and could not adapt as easily as the cubic arrangement to accommodate the two molecules. Nevertheless, as previously evidenced by DLS from the dimensional point of view, both series of nanocarriers showed good encapsulation capability. On the other hand, when samples were loaded only with one of the two adjuvants to be tested for comparison purposes in functionality tests (see section 3.9), they generally showed lower values of EE% than those seen for curcumin alone, likely indicating lower host-guest compatibility. The calibration curves reported below for the three antioxidants were employed for quantification (Figures 18-20) (see Materials & Methods).

Sample name	**Loaded concentration**	**Encapsulation efficiency %±SD**	**RSD %**	**DL % cargo/ lipid ratio (mol/mol)**
C1-cub	10^{-2}M	59±6.06	11.39	19.7
CT-cub	C at 10^{-2}M; T at $5x10^{-3}$M	(C) 70.1±2.5 (T) 94.8±15.17	(C) 3.5 (T) 15.43	(C) 23.4 (T) 15.7
CP-cub	C at 10^{-2}M; P at $5x10^{-3}$M	(C) 80.7±1.08 P 78±4	(C) 1.34 (P) 5.27	(C) 26.9 (P) 13
T-cub	$5x10^{-3}$M	52.3±5	7.3	8.6
P-cub	$5x10^{-3}$M	26.8±0.36	1.35	4.5
C1-lip	10^{-2}M	76.2±2.68	3.5	25.4
CT-lip	C at 10^{-2}M; T at $5x10^{-3}$M	(C) 65.7±4.3 (T) 75±6	(C) 6.58 (T) 8.2	(C) 22 (T) 12.5
CP-lip	C at 10^{-2}M; P at $5x10^{-3}$M	(C) 66.7±2.3 (P) 90±3	(C) 3.47 (P) 5.3	(C) 22.3 (P) 15

T-lip	5x10^{-3}M	54±4.2	7.8	9
P-lip	5x10^{-3}M	88±4.3	4.9	14.7

Table 4. Encapsulation efficiency (EE%) of curcumin (C), tocopherol (T) and piperine (P) expressed as mean ± standard deviation (SD) of measurements in triplicate (n=3), relative standard deviation (RSD%) and drug loading (DL%), determined by UV–Vis for all the samples employed in these experiments.

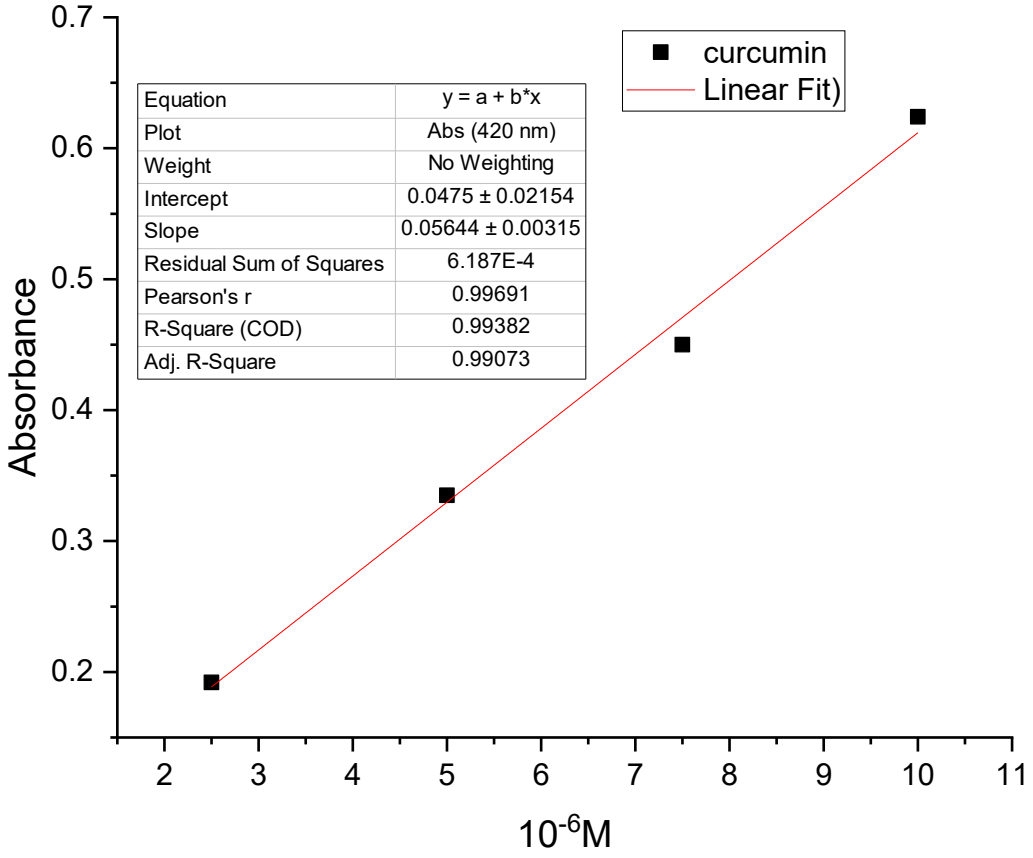

Figure 18. Calibration curve for curcumin in the range 2.5x10^{-6}M -10^{-5}M (0.92-3.68 µg/mL)

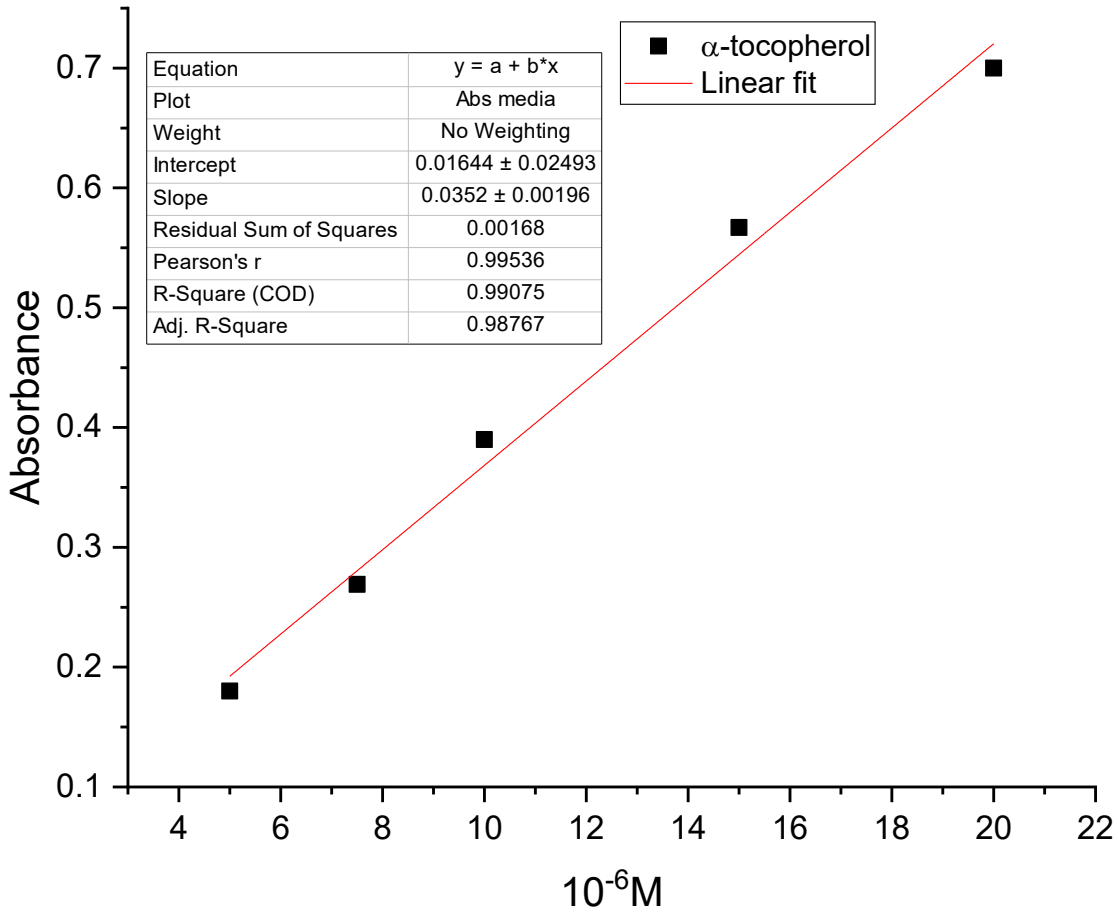

Figure 19. Calibration curve for tocopherol in the range 5x10-^{6}M -2x10-^{5}M (2.15-8.6 µg/mL)

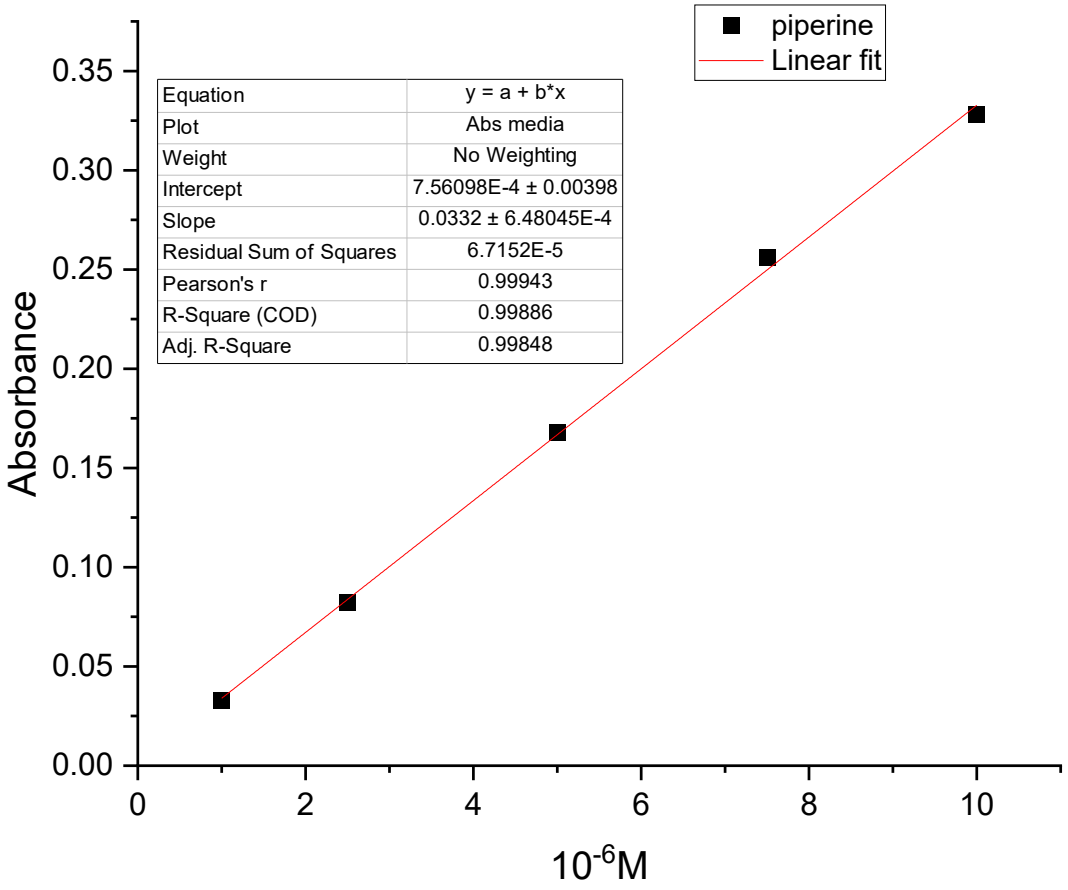

Figure 20. Calibration curve for piperine in the range 5x10-^{6}M -2x10-^{5}M (0.285-2.85 µg/mL)

3.7 Stability and release experiments in biorelevant media/ethanol

The stability of cubosome and liposome dispersions as nanocarriers was tested by using different methods to disrupt the vector-cargo association. Firstly, non-specific tests were employed for a preliminary assessment, such as dilution in water and abrupt pH or ionic force variations with samples in a dialysis bag in biorelevant medium. These experiments revealed high resistance of all the samples to commonly used destructuring techniques, since no curcumin release was detected in the medium. Moreover, control DLS measurements performed after these tests confirmed that the aggregates maintained their overall size in the nano range. For both series of liposome and cubosome samples the evaluation of stability and the release profile under progressively harsher conditions was carried out by gradual ethanol addition (10% step) and mixing with the biorelevant aqueous solution, to mimic a generic aggressive media (see Materials & Methods). As mentioned above, the complementary structural study at different time intervals in the destabilization at the supramolecular scale was performed by SAXS, while the curcumin release at the bulk scale could be evidenced and followed by Visible spectroscopy. The tests at different ethanol percentages were performed starting

from an initial addition of 30% v/v of ethanol, incrementing each time by 10% until finally reaching 70%. This allowed to identify the lower and upper stability limits, as we generally observed almost no curcumin release at 30% of ethanol then a gradual increase until 60%. The release profile at 70% v/v was almost superposed to this latter, indicating that the resistance limit to disassembling was reached at 60% and the aggregates had completely released their cargo. This trend was generally confirmed for both cubosomes and liposomes, as the comparison of the two nanocarrier series on the basis of their supramolecular structures did not present peculiar differences. Indeed, spectroscopic results showed that the variations in the curcumin release profiles depended mostly on the encapsulated molecules rather than the nanovectors structure. Figure 21 shows an exemplificative cumulative release plot, where samples C-cub and C-lip in the same conditions (i. e. 40%, 50% and 60% v/v of ethanol) underwent a similar fate. In general, all systems showed a three-steps pattern of destabilization and de-structuring, that eventually led to cargo release. Specifically, an initial burst followed by a linear trend and, finally, by a plateau was invariably observed. Such pattern was more or less pronounced depending on the ethanol content and thus on the extent of the destabilization. Indeed, regarding the different ethanol percentages (Figure 21a and 21b), there was a general tendency showing a slow and sustained release at 40% ethanol content that reached a stability value around the range of 10-20% cumulative release. This indicated that the samples went partially through a disassembling process but likely, they were able to maintain some arrangement. Similar considerations could be made observing the curves at 50% ethanol content, that showed more linearity in the first points but still reached a plateau release value around 60-70%, suggesting that the nanovectors were still able to partially re-arrange in metastable structures or keep some guest-host association. Finally, a linear increase and plateau in a range of values of almost complete cargo release (90-95%) were reached with 60% ethanol content, indicating the upper limit of stability and resistance to disaggregation for these nanosystems. These analogous results for both cubosomes and liposomes, independently from the aggregates structure, could be explained considering the nonspecific type of disruption conditions and the high resistance and self-assembly ability previously shown by the two series.

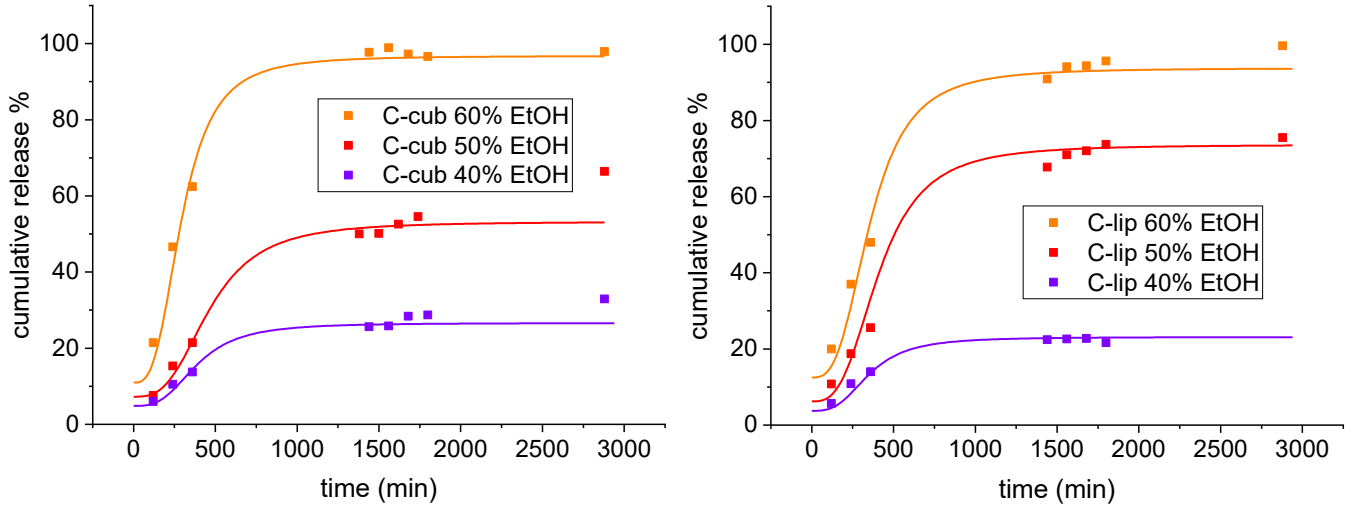

Figures 21a-b. Cumulative release profiles of C1-cub (a, left) and C1-lip (b, right) treated with percentages going from 40% to 60% v/v of EtOH (color code: violet 40%, red 50%, orange 60%, respectively).

On the other hand, the most noticeable difference was found by comparing samples of the same series, i. e. only cubosomes or liposomes, according to the encapsulated molecules. Figure 22 shows the curcumin release profile for both series at the chosen ethanol percentage of 60%. While the overall pattern is comparable for all samples, it can be evidenced the peculiar behavior of both samples CT-cub and CT-lip, that contrarily to the others did not reach complete release of the loaded cargo (plateau values around 80%) (Figure 22). It could be suggested that the concomitant presence of tocopherol as adjuvant for curcumin contributed to better stabilize the aggregates during the destructuring, possibly slowing down the release of curcumin by favoring the guest-host interaction.

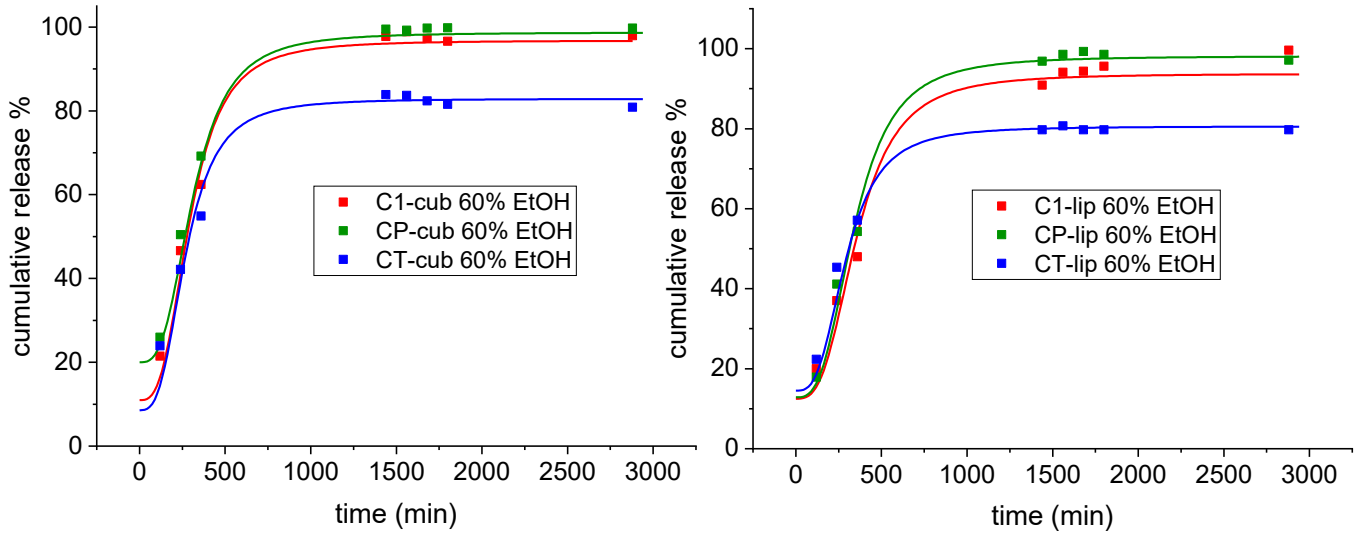

Figure 22a-b. Cumulative release profiles comparison of cubosome (a, left) and liposome (b, right) series treated with 60% v/v EtOH (color code: C red, CP green, CT blue respectively).

Figure 23a-b shows the curcumin release profile of CT-cub and CT-lip at varied ethanol v/v content going from 40% to 70%. It can be noticed that both samples reached particularly low values of cumulative release when treated with 40% v/v ethanol in the medium, showing pronounced stability and resistance to disruption. This evidence suggested that the lower limit for these samples was higher with respect to the others in both series, due to the interplay of the loaded molecules. On the other hand, differences were noticed in the cumulative release values at the higher ethanol percentage (70%) between the cubosome and liposome samples. Indeed, the profile of CT-cub undergoing this treatment showed a fast burst release in the first few hours followed by linear and plateau patterns achieving complete cargo release. On the contrary, CT-lip had faster release at first but then the 70% curve was superposed to the 60%, indicating that the upper limit was already reached in the previous condition.

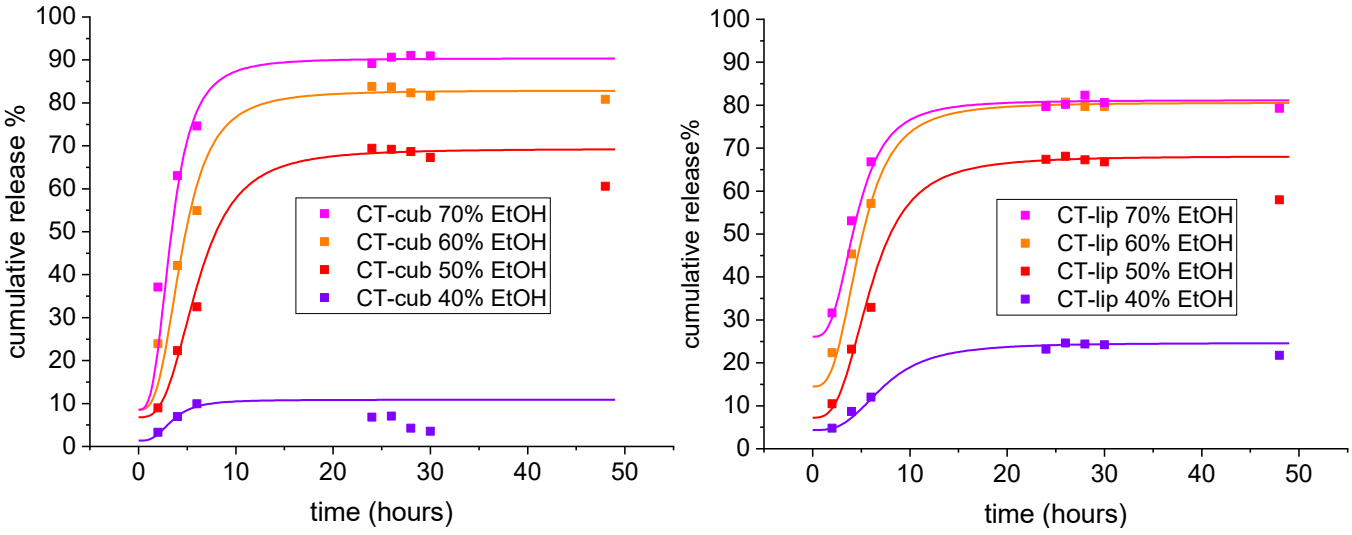

Figure 23a-b. Cumulative release profiles of CT-cub (a) and CT-lip (b) treated with percentages going from 40% to 70% v/v of EtOH (color code: violet 40%, red 50%, orange 60%, magenta 70% respectively).

These results were able to evidence the different role of the loaded molecules and their combined effect in the intercorrelation and structuring properties of the nanovectors. This finding was in agreement with SAXS, NMR and ITC results, once again highlighting the role played by the guest

molecules in the structuring and consequent stability of the nanocarriers. On the other hand, it also showed that these properties are not exclusively dependent on one parameter, e. g. the lipid aggregate type or the guest molecules, but they actually derive from their concomitant action. Finally, in general both cubosome and liposome series showed significant stability and resistance to macroscopic disruption even in rather aggressive conditions, i. e. ethanol content in the medium up to 60-70% v/v.

3.8 Simulated gastrointestinal digestion and release

Following the stability and release experiments in a nonspecific medium such as aqueous biorelevant solution/ethanol (v/v) mixture at increasing percentages, that mimicked the presence of a non-specific more hydrophobic environment, the stability of the nanovectors was tested in a simple simulated digestive medium (GIT model, see Materials & Methods). This testing method was chosen to assess both the resistance to (lipid) carrier-specific attacks such as lipolytic enzymes, and the bioaccessibility of the loaded curcumin at the end of the process as well. Moreover, as in previous experiments, the contribution of various parameters, i. e. the lipid composition and aggregate structure and loaded cargo was considered.

Figure 24 shows the curves of cumulative curcumin release from the nanosystems subjected to digestion through simulated stomach and intestine environments. Noticeably, all samples from both series showed no curcumin release during the first 30 minutes in the gastric environment, revealing marked resistance to acidic pH and pepsin. Release percentages remained rather low after 60 minutes as well (Figure 24), which corresponded to the whole duration of the passage through the gastric tract, indicating low levels of digestion and curcumin bioavailability in the stomach. This evidence confirmed that both types of nanocarriers were highly stable and resistant to simulated gastric fluid (SGF) pH conditions and enzymes, as pepsin could only metabolize the small protein content from the algal biomasses. Even though all samples showed cumulative release percentages in the range 5-10%, it can be evidenced that after 60 minutes the two aggregate types started to differentiate their profiles (Figure 24), in that the liposomes showed a linear slope whereas the cubosomes tended to lower values. This trend was even more accentuated after the first 30 minutes in the intestinal environment (t=90 min in Figure 24), where an at least twofold increment in the profile of released curcumin was observed for all samples. Particularly, for the liposome samples a steeper profile was registered with respect to cubosomes, more than doubling their release values. This showed that all samples and especially liposomes were subjected to high digestive activity in the simulated intestinal fluid (SIF), where most of the digestion and consequent release happened, mainly due to the attack of the mixture of pancreatic enzymes. Nevertheless, all samples preserved some stability and

aggregate structure, keeping up cargo release until the end of the process (t=180 min) even if in smaller increments and evidencing a different behavior in the two aggregate types. Specifically, the liposome series showed more pronounced release up to one hour and half (t=160 min) in the SIF and finally going to plateau at t=180 minutes, whereas the cubosome series showed a profile approximating a plateau starting after one hour (t=120 min in Figure 24) in the intestinal tract. Generally, samples of the liposome series showed higher percentages of cumulative release and bioaccessibility at the end of the digestion process, while cubosome samples showed a slower and sustained release after the attack of digestive enzymes. This could be due to the different lipid composition (triglycerides vs phospholipids) and/or by the lipid accessibility to enzyme attack which depended on the supramolecular arrangement. The bioaccessibility at the end of the whole digestion process is compared for the two aggregates series in Figure 25. Liposomal nanovectors generally showed higher percentages, around 30%, whereas cubosomes reached values around 20%, likely due to easiness of attack of the former systems from enzymes and lower ability in rearranging their structure upon disassembling. These tests confirmed the evidence observed in the stability and release tests in nonspecific medium regarding the marked tendency of these systems to maintain a stable aggregation and preserve the loaded cargo. On the other hand, contrarily to the results from these latter tests here the main differences were not much dependent on the loaded cargo. Indeed, in that case the guest molecules had a significant role in the release properties, at variance with digestion which relies on enzyme specificity and easiness of lipid accessibility.

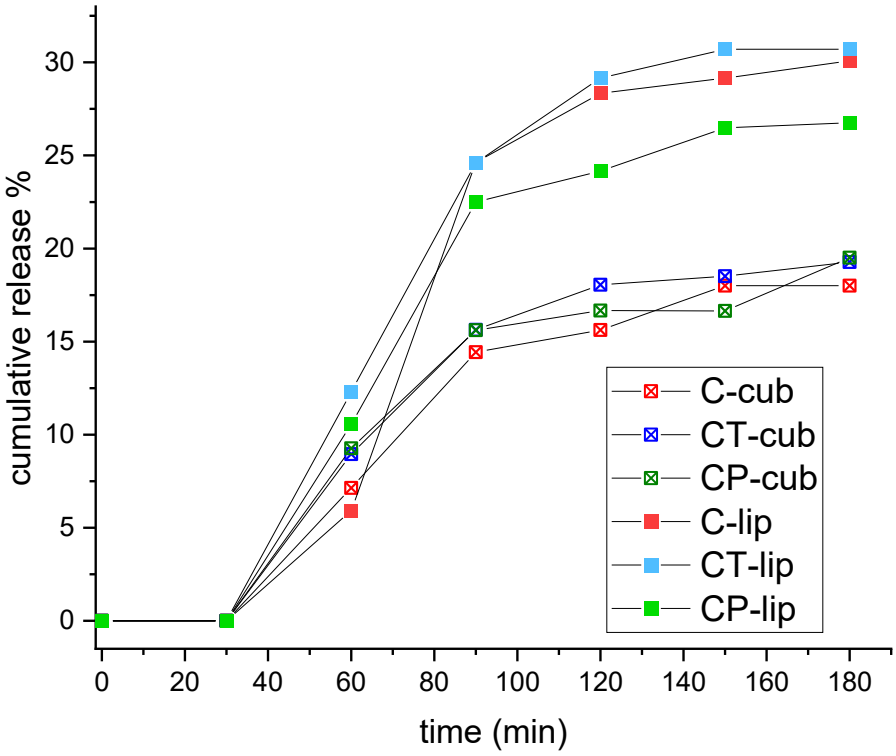

Figure 24. Curcumin cumulative release % curves for liposome and cubosome series throughout 3 hours total SGF/SIF digestion time.

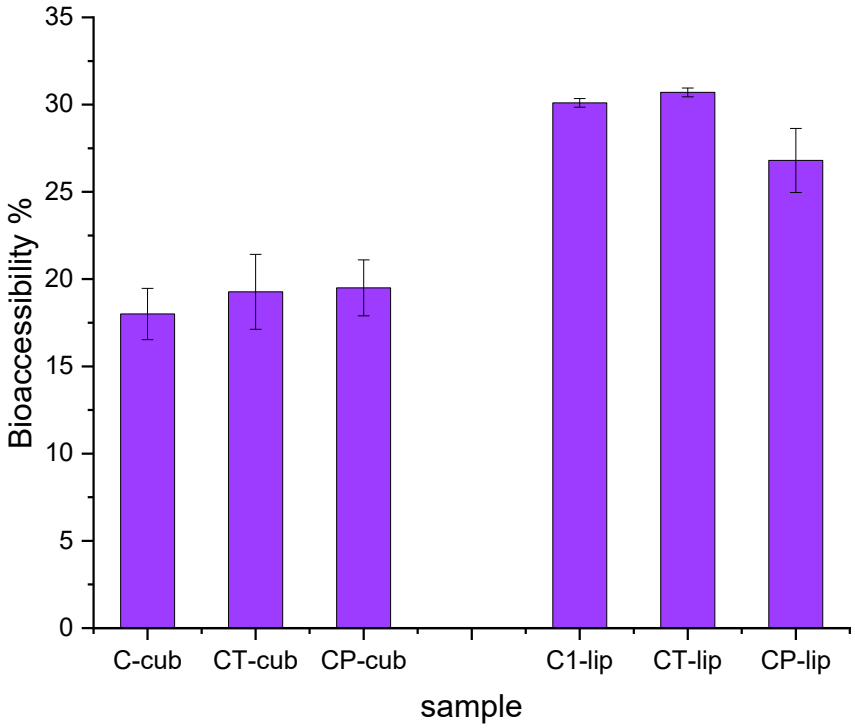

Figure 25. Bioaccessibility% of curcumin at the end of the whole digestion process for cubosomes and liposomes.

3.9 Kinetics of decrement of absorbance of $ABTS^{\bullet+}$ treated with regular and disrupted nanovectors

After the assessment of the stability and release properties of the two nanovector series, we studied their efficacy as drug delivery carriers to preserve the functionality of the encapsulated molecules, and possibly, even enhance their antioxidant properties. The $ABTS^{\bullet+}$ assay was employed to test the antioxidant capacity of the loaded cargo combined with the potential effect of the natural lipid matrix. This assay was performed as a kinetics throughout several hours (7-8h), since we observed that both cubosomes and liposomes exhibited slow release profiles in different conditions.

Considering that ethanol was previously tested as a disruptive agent, but the nanovectors were still able to keep some meta-stability for many hours, two different approaches were chosen to study the antioxidant power of these formulations. Cubosomes and liposomes were tested both in their standard conditions, i. e. diluted aggregates in water, and during a disassembling process induced by dilution in ethanol. In the former case the kinetics of radical insertion in the bilayer, a necessary process to interact with the guest molecules, was investigated together with the spatial localization and consequent accessibility of the cargo molecules in the lipid environment. In the latter case, the kinetics of antioxidant release in the solvent and interaction with the radical was studied, during triggered disruption of the carrier. For this experiment, also cubosome and liposome samples loaded only with either tocopherol or piperine (i. e. T and P -cub or -lip, see Tab. 4) were tested for comparison, to evaluate their individual antioxidant power while encapsulated in the nanocarriers. All samples were administered to the $ABTS^{\bullet+}$ radical cation solution, as described in the Materials and Methods section, and their antioxidant capacity was assessed following the obtained decrement of absorbance (Decr. Abs %) of $ABTS^{\bullet+}$with respect to the administration of Trolox standards.

Figure 26 shows the curves for the Decr. Abs % of $ABTS^{\bullet+}$ for cubosomes and liposomes administered in standard (i. e. unbroken) conditions. In these samples a slower and sustained increment was expected, since the antioxidants remained encapsulated in the carriers. Indeed, for the first few measurements until 30 minutes all the samples showed almost no decrement of absorbance, except for CT-cub and CP-cub for the cubosome series and the three curcumin-loaded samples (C-lip, CT-lip and CP-lip) for the liposome series (Table 5, Figure 26). These were also the samples that performed better along the whole duration of the kinetics, showing steeper curves and higher final decrement values (Table 5). Generally, both series showed higher decrement values for samples loaded with curcumin, either in combination with one of the two adjuvants or alone. In particular, the difference was markedly noticeable for cubosome samples, where the samples T-cub and P-cub showed very low increments and curves almost superposed to the control Empty-cub sample. On the

other hand, the corresponding samples in the liposome series (i. e. T-lip, C-lip and Empty-lip) had a decrement of absorbance effect comparable, even if slightly lower, with the C-cub sample (Figure 26, Table 5). This finding evidenced the role played by the lipid matrix and its composition, indeed it could be suggested that the biomass used as source of lipids for the liposome series contained some active antioxidant agents, contrarily to the one used for the cubosome series. Anyhow also for the liposome series the curcumin loaded samples showed higher antioxidant capacity, whereas the curves of the adjuvants-loaded samples were almost superposed to the Empty-lip control (Figure 26, Table 5). Thus, for these samples the decrement effect was mainly due to the lipid matrix. Regarding the samples that showed higher antioxidant activity in both series, i. e. the curcumin loaded ones, several considerations can be made according to the aggregate type and adjuvants. For the cubosome series, CT-cub and CP-cub showed the highest values of Decr. Abs % (Table 5, Figure 26), particularly CT-cub that was also the best performing of all tested samples. In both cases it could be evinced a synergistic or cooperative effect between either of the two antioxidants (T and P) and curcumin, that was also encapsulated in these samples with higher EE% with respect to C-cub (Tab. 4), so likely both parameters concurred to enhance the antioxidant capacity. Moreover, for this series the synergy between curcumin and α-tocopherol prompted a greater antioxidant effect than that with piperine, indeed even though CP-cub showed higher EE% for curcumin, the decrement curve for CT-cub always had higher percentages (Figure 26). For this approach where the nanovectors were administered in standard conditions, this outcome could be also influenced by the different spatial localization and mobility of the loaded molecules in the confined lipid layer, varying their accessibility and susceptibility to interact with the radical.

On the other hand, the opposite tendency was observed in the case of liposomes. Indeed, for this series the sample C-lip was the one showing greater decrements for the entire duration of the assay, while also having better EE% than either CT-lip or CP- lip (Table 4, Figure 26). These latter samples showed comparable values, even though in this case the higher antioxidant effect and likely synergy was observed for CP-lip (Table 5, Figure 26). However, in liposome samples loaded with curcumin and one of the two adjuvants, the two molecules experienced apparently lower synergy than in the cubosomal structure, since their combination did not result in enhanced antioxidant power with respect to C-lip. This could be traced back to lower accessibility of the molecules enveloped in the bilayer, both to each other or to the radical. In any case, for the entire liposome series the combination of all parameters including the biomass composition, resulted in generally higher values of Decr. Abs % with respect to the corresponding samples in the cubosome series, except for CT-cub (Table 5, Figure 26).

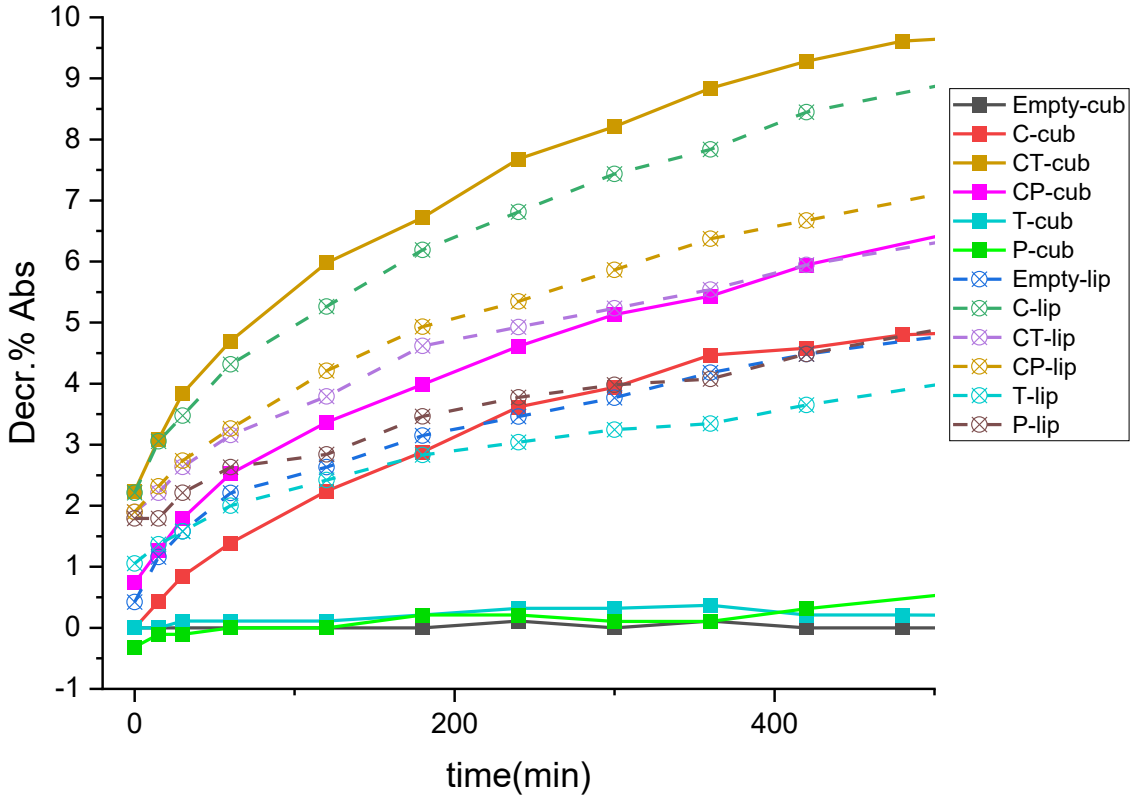

Figure 26. Kinetics of decrement of absorbance for samples in standard (i.e. unbroken) conditions, solid squares for cubosome samples curves, empty circles for liposome samples curves.

Sample	Final Decr.% Abs	Stdev (decr.%)	RSD%
Empty-cub	-	-	-
C-cub	4.58	0.4	8.82
CT-cub	9.28	0.12	1.33
CP-cub	5.94	1.33	22.35
T-cub	0.21	0.06	29.31
P-cub	0.31	0.06	19.25
Empty-lip	4.48	0.27	6.15
C-lip	8.45	0.27	3.27
CT -lip	5.94	0.21	3.51
CP-lip	6.67	0.1	1.56
T-lip	3.65	0.73	20
P-lip	4.48	0.12	2.68

Table 5. Decr. % Abs values, standard deviation and relative standard deviation (RSD) for all tested samples in standard condition. The values are the average of triplicate measures (n=3).

The same protocol was applied to follow the kinetics of antioxidant effect of disassembling nanovectors in presence of ethanol. Figure 27 shows the curves for the Decr. Abs % of $ABTS^{\bullet+}$ for cubosomes and liposomes administered in disrupted conditions. In these samples, as expected, the

decrement of absorbance was already detectable at the first measurement (t=0), right after the administration. Indeed, for this approach the interaction with the radical took place in the solvent, where the guest molecules were gradually released from the disassembling carriers.

In both cubosome and liposome series it was noticeable a progressive increase of values of decr. % Abs, that started higher with respect to those in standard conditions right away from t=0 (Figure 27), predictably more pronounced for samples loaded either with curcumin or curcumin in combination with one of the two adjuvants. For the cubosome series, as already observed in standard conditions, the samples CT-cub and CP-cub showed higher antioxidant power than C-cub, which was expected considering the synergy of the combined guest molecules. Also in these conditions and despite the higher EE% of CP-cub, the two samples showed superposed curves of Decr. Abs % (Figure 27), confirming a stronger synergy and thus antioxidant effect for curcumin and tocopherol in the cubic structures. The T-cub and P-cub samples did not show high values of decrement in these conditions as well, confirming the poor antioxidant activity of tocopherol and piperine when encapsulated alone (Figure 27, Table 6). It could be also suggested that curcumin acts as an enhancer of the functionality for these molecules, and not vice versa only. In these conditions, cubosome curcumin-loaded samples showed generally higher decrement values than liposomes, likely due to their higher curcumin EE% (Figure 27, Tab. 4).

Contrarily to what observed above for standard conditions, the liposome series showed similar behavior to the cubosomes, as both CT-lip and CP-lip displayed cooperative effects of the two entrapped molecules (Figure 27, Tab. 6). Indeed, even if both had lower values of curcumin EE% than C-lip, their curves were at higher decrement percentages or superposed to this latter. Likely the molecules released in the solvent, not being enveloped in the lamellar bilayer like in standard conditions, could interact with each other and enhance reciprocally their functionality toward the radical more easily. As observed above, for the liposome nanocarriers the cooperation between curcumin and piperine to enhance the formers antioxidant power seemed to have more efficacy also in disrupted conditions (Figure 27, Tab. 6), likely also due to high piperine EE%. It could also be hypothesized that the tendency shown by CT-lip in the stability tests to slow down the release when treated with ethanol, played a role also in this context thus resulting in lower antioxidant action. The T-lip and P-lip samples confirmed more pronounced antioxidant activity than the corresponding cubosome samples, even though also in this case they showed curves superposed to Empty-lip, so this effect is likely ascribable to the properties of the lipid matrix.

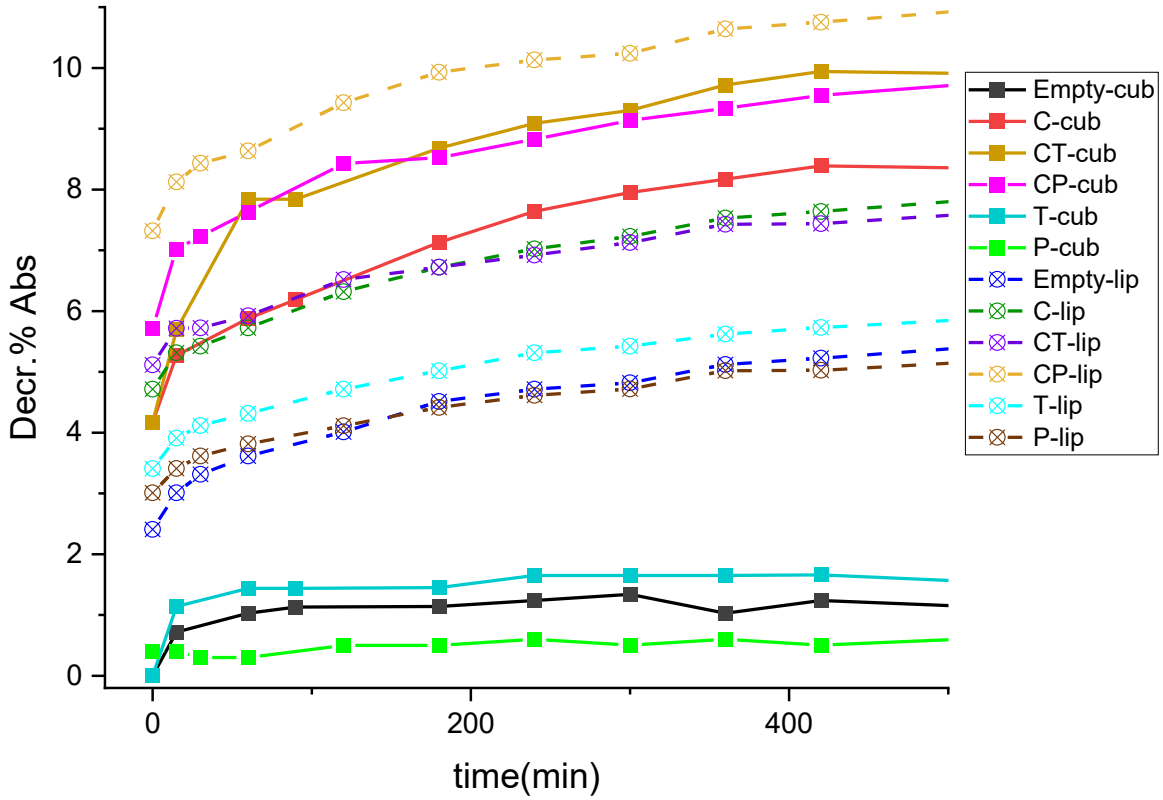

Figure 27. Kinetics of decrement of absorbance % for samples in disrupted conditions, solid squares for cubosome samples curves, empty circles for liposome samples curves.

Sample	Final Decr.% Abs	Stdev (Decr.%)	RSD%
Empty-cub	1.24	0.18	14.46
C-cub	8.39	0.37	4.45
CT-cub	9.94	0.33	3.35
CP-cub	9.56	0.76	7.97
T-cub	1.66	0.06	3.6
P-cub	0.5	0.12	23.09
Empty-lip	5.2	0.31	5.87
C-lip	7.64	1.12	14.65
CT -lip	7.44	0.1	1.35
CP-lip	10.75	0.15	1.43
T-lip	5.73	0.15	2.68
P-lip	5.03	0.5	10.07

Table 6. Decr. % Abs values, standard deviation and relative standard deviation (RSD) for all tested samples in disrupted condition. The values are the average of triplicate measures (n=3).

Some considerations can be made on the two nanovectors series from the data obtained on the antioxidant capacity when administered to the radical solution in either standard or disrupted

conditions, plotted against the EE% for curcumin of each sample (bar plot in Figure 28, only most relevant samples are shown). The samples loaded only with tocopherol or piperine were not taken into account in this comparison, since their antioxidant power was evaluated as a control and they did not show significant activity when encapsulated alone, whereas they were able to enhance curcumin properties when incorporated together. Concerning the cubosome series, CT-cub was the sample that showed highest antioxidant power in both types of administration conditions (Figure 28). This could depend on enhanced synergy of curcumin with tocopherol rather than with piperine in the cubic structures, or on the observed higher encapsulation of tocopherol in the nanocarriers when combined with curcumin, or finally on the different availability of the guest molecules when they are enveloped in the lipid layer or released from it. On the other hand, for liposome samples the contrary seemed to hold in disrupted conditions, since CP-lip showed a better performance (Figure 28) likely due to more efficient piperine encapsulation and synergic action with curcumin once released in the solution. In standard conditions instead the C-lip sample had a greater effect attributed to guest molecule accessibility (Figure 28), as discussed above. In general, all samples showed comparable levels of antioxidant power which were reasonably good considering the extensive final dilution in these experimental conditions (see Materials and Methods), resulting in antioxidant concentrations around five times lower than the Trolox standard. Moreover, these results confirmed once again that the functionality of these nanocarriers is always the product of many parameters and their concurrent influence.

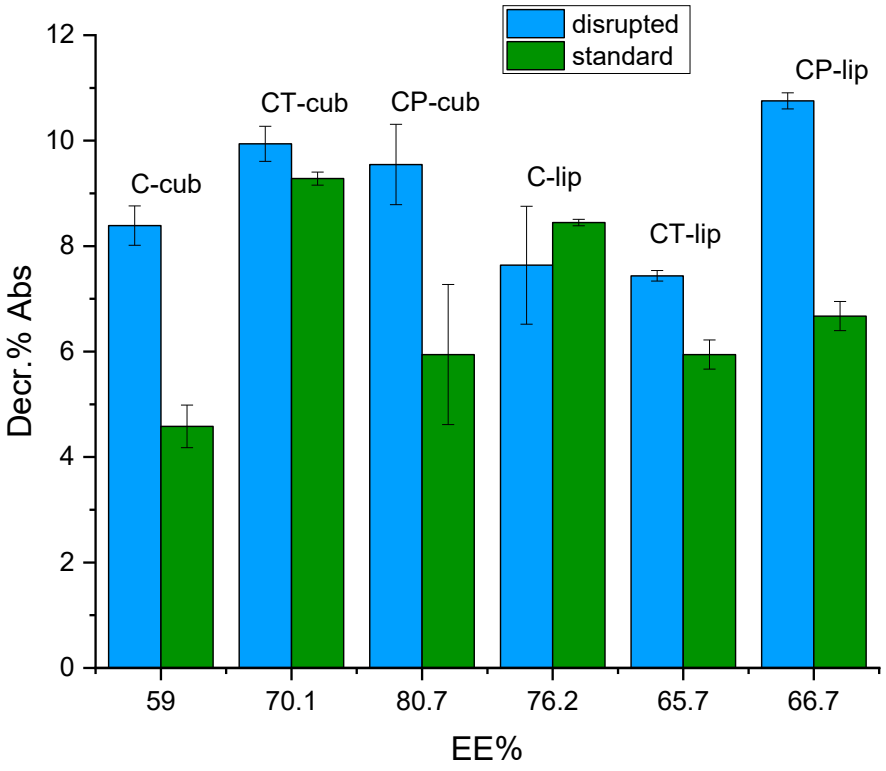

Figure 28. Bar plot showing the Decr. % Abs of relevant samples in either regular or disrupted state against EE%.

In vitro techniques on cell cultures: cytotoxicity and cell viability after hydrogen peroxide treatment

3.10 Cytotoxicity

After the evaluation of the antioxidant capacity of cubosome and liposome formulations using a chemical approach of radical reduction, this property was tested from the biological point of view assessing the antioxidant power on cell cultures. These experiments were meant to complement each other in an integrated perspective, considering also in this case the influence of lipid matrix composition and structural organization together with the loaded cargo. Firstly, the eventual cytotoxic effect of the nanocarriers on cell cultures was evaluated, to assess the feasibility of sample administration and testing in these conditions. The samples tested for this experiment were the same used for the kinetics of decrement of absorbance (see Tabs 5, 6), to maintain equal experimental conditions and test the adjuvants properties individually also for the biological approach. The Empty cubosome and liposome samples were tested as well, to assess the eventual cytotoxic effect given

either by the composition of the lipid matrix or its structure. The samples cytotoxicity was compared to standard solutions of curcumin and the two adjuvants as controls.

The assessment of the cytotoxicity was based on the amount of neutral red incorporation by fibroblasts NIH3T3 after 24 h of contact with different concentrations of free C, P, T in solution. Figure R shows the effect of increasing concentrations of standard solutions of C, T and P towards NIH3T3 viability with respect to the 100% viability of untreated control samples. Cells in contact with curcumin (Figure 29a) showed a strong decrease in viability for concentrations higher than 20 µM, the value corresponding to 50% cell viability reduction respectively. This same effect was observed for tocopherol at 21 µM (Figure 29b), indicating similar cytotoxicity for tocopherol and curcumin, whereas on the contrary piperine in solution showed this effect at more than twofold concentration, i. e. 56 µM (Figure 29c), evidencing less cytotoxic activity of this adjuvant with respect to the other two.

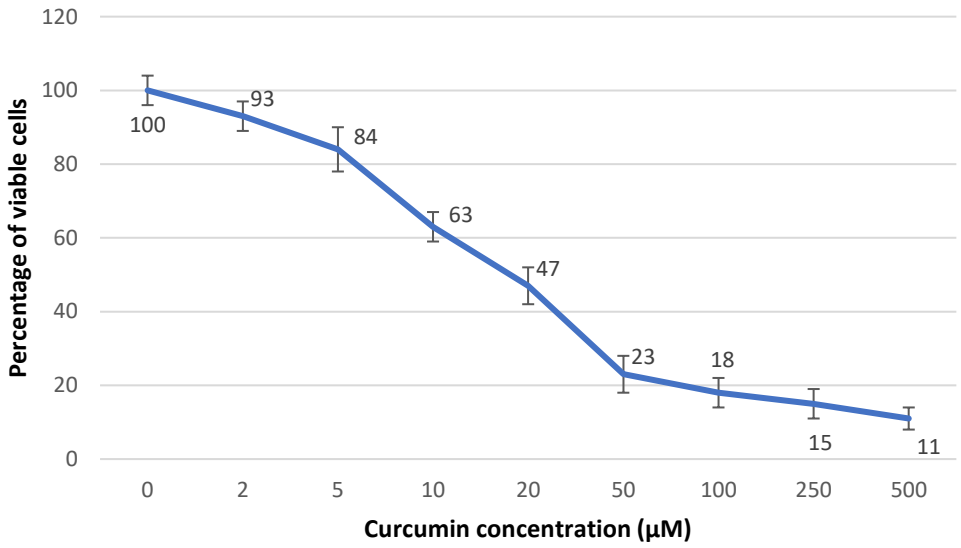

a)

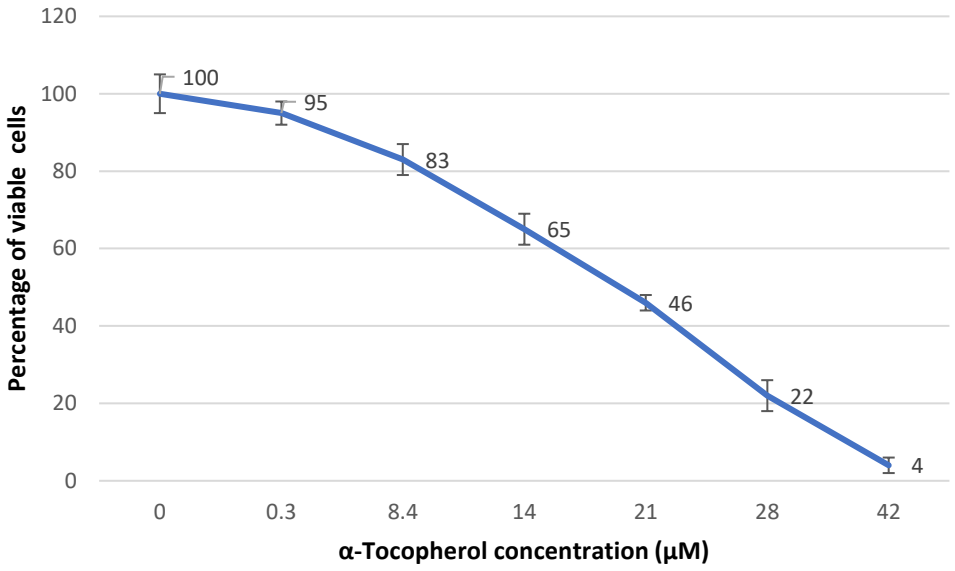

b)

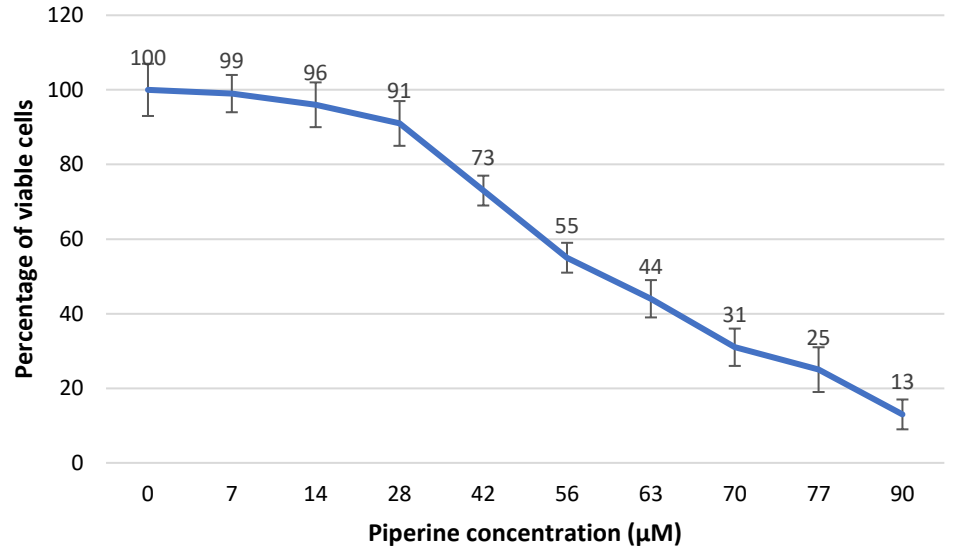

c)

Figure 29 a-c. Fibroblasts viability percentage after 24 h of contact with different concentrations of a) curcumin; b) α-tocopherol; c) piperine standard solutions.

Then the cytotoxicity of the two nanovector series, cubosomes and liposomes, administered to cells at three different concentration values (0.1, 1.0 and 5.0% v/v) was evaluated against a negative control constituted by the complete culture medium. Figure 30 shows the obtained results. The two nanocarrier series showed opposite behaviour likely ascribable to their supramolecular arrangement and different mechanical properties stemming from this fact. Indeed, all liposome samples showed significant cytotoxicity towards NIH3T3, noticeably reducing the percentage of viable cells with increasing concentration administered (Empty-lip in Figure 30, from 0.1 to 5%). Only Empty-lip was shown as a representative sample, to highlight the fact that such effect is not dependent on the loaded

cargo molecules. In fact, from optical microscopy observation of the treated cells, it could be evidenced that the liposome nanovectors at the intermediate and highest tested concentration, i. e. 1.0 and 5.0%, likely caused cell death by adhering to the cells and completely covering their surface (Figure 31 a-d). Thus, exchange processes with the surrounding medium were hindered by this lipid patina, as shown in Figure 31 which compares cells treated with negative control and cubosome samples (a and b respectively) and cells treated with liposomes (c and d). Indeed, cells in contact with complete medium (Fig. 31a) as well as those in presence of cubosome nanocarriers (Fig. 31b) showed the normal fibroblastic morphology. When liposome nanocarriers were added to the culture, the cells resulted completely covered by them (Fig. 31c), due to enhanced adhesion and lamellar stacking effect on the cell surface upon administration of liposome samples. Such mechanic effect relied on the capability of the unilamellar bilayers to flatten their structure and adhere to cell membranes, even at the lowest tested concentration (Fig. 31c). After removing the nanocarriers (Fig. 31d) the cells resulted decreased in number and with altered morphology.

On the contrary, cubosome systems showed no cytotoxic effect towards NIH3T3 at any of the three tested concentrations and independently from the loaded guest molecules (Figure 30). Indeed, the cubosomal arrangement did not exert mechanical adhesion effects nor the presence of the antioxidant molecules imparted any cytotoxicity. Thus, cubosome samples loaded with either one of the three antioxidant or curcumin combined with one of the two adjuvants were chosen for further cell cultures experiments on the in vitro antioxidant activity of the formulations, to compare with the $ABTS^{\bullet+}$ assay. The liposome series was excluded from additional tests since two out of three tested concentrations resulted toxic towards fibroblasts.

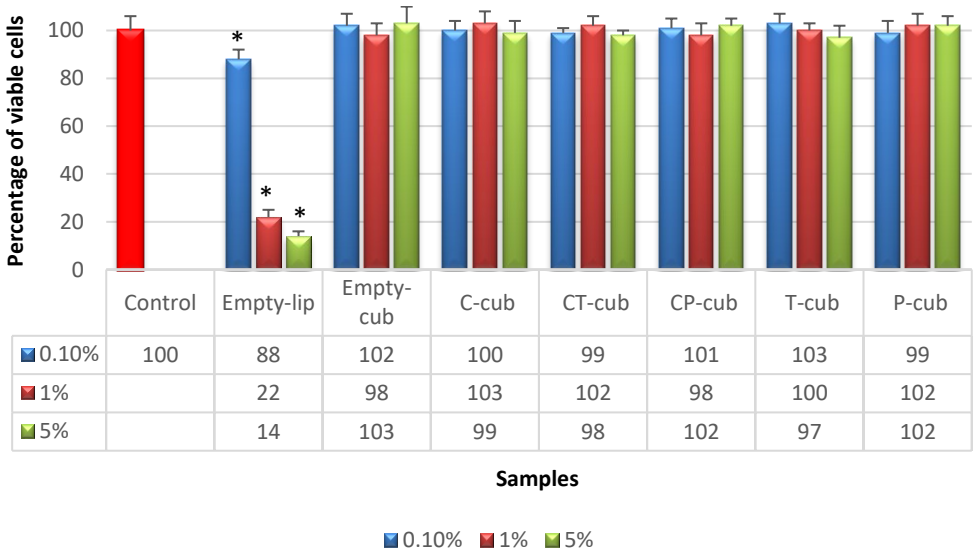

	Control	Empty-lip	Empty-cub	C-cub	CT-cub	CP-cub	T-cub	P-cub
0.10%	100	88	102	100	99	101	103	99
1%		22	98	103	102	98	100	102
5%		14	103	99	98	102	97	102

Figure 30. Fibroblasts viability after 24 h of contact with different concentrations of Empty-lip sample and cubosome samples, both empty and loaded with the guest molecules. * Data are statistically different in comparison to negative control (complete culture medium) $p < 0.01$.

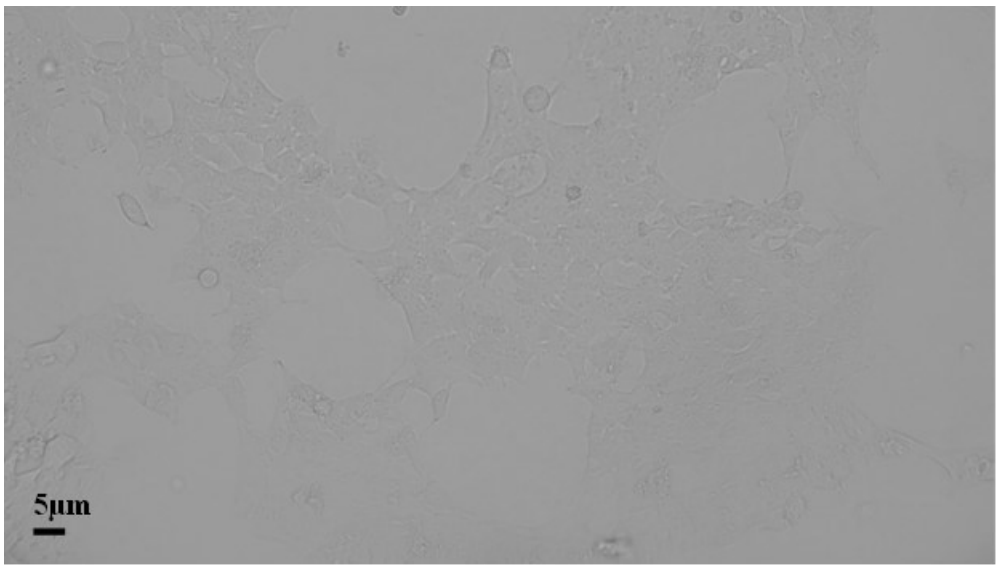

a)

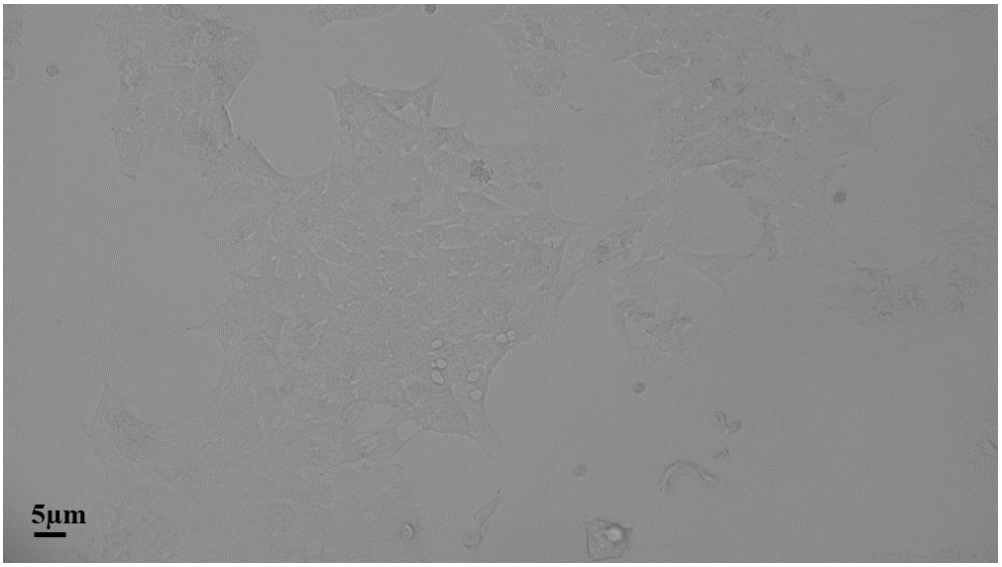

b)

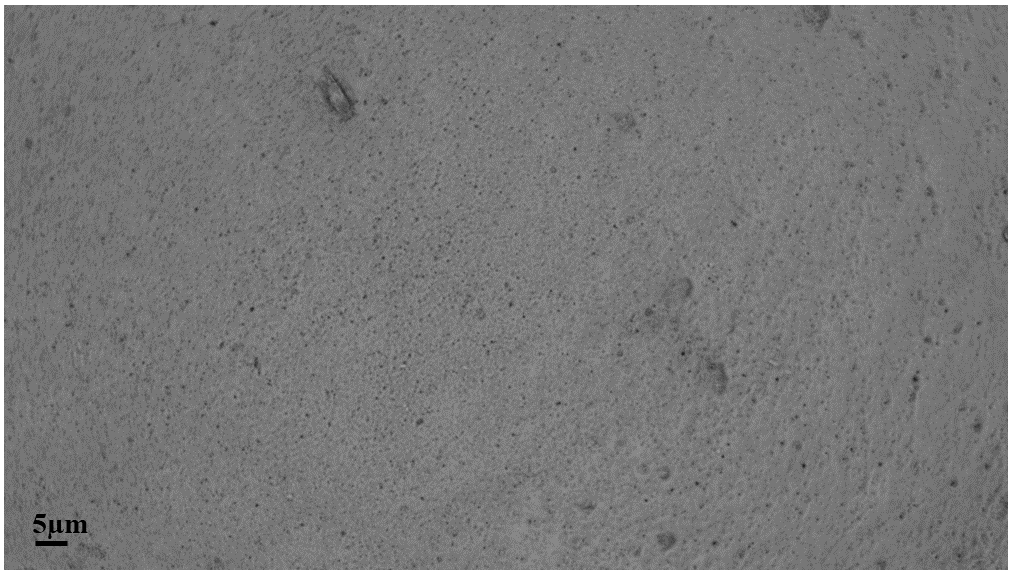

c)

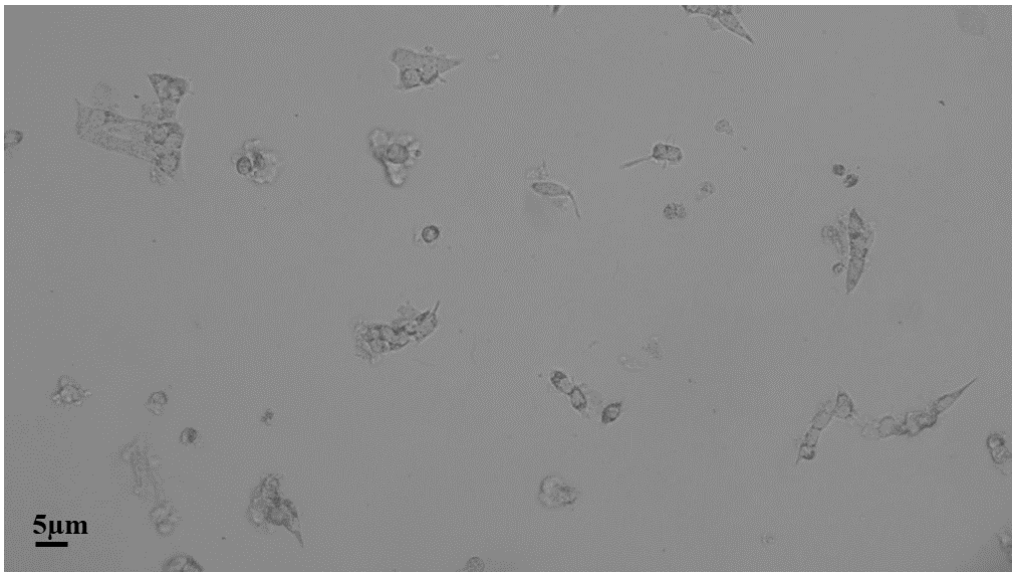

d)

Figure 31 a-d. Optical microscope images of NIH3T3 mouse fibroblasts after 24 hours of contact with: a) negative control (complete medium); b) 0.1% v/v cubosome nanocarriers; c) 0.1% v/v liposome nanocarriers; d) after removing the liposome nanocarrier.

3.11 Cell viability after hydrogen peroxide treatment

Following the administration of cubosomes and liposomes to cells treated with complete medium, the antioxidant capacity of the formulations chosen for further investigation, i. e. the cubosome nanocarriers, was tested on NIH3T3 fibroblasts appropriately pre-treated to induce a condition of oxidative stress. A solution at varied concentrations of a strong oxidant agent, i. e. hydrogen peroxide was administered to the cells thus provoking a cytotoxic effect, then the ability of cubosome samples to reverse such condition and increase the percentage of viable cells was estimated. Specifically, the

concentration-effect relationship for the cytotoxic effects of H_2O_2 on NIH3T3 fibroblasts was obtained by testing solutions of hydrogen peroxide ranging in concentration from 1 to 100 μM (Figure 32, blue curve) and measuring the correspondent decreasing percentages of cell viability with increasing H_2O_2. Firstly, after the treatment, two different types of controls were tested, i. e. administration of either standard solutions of the three antioxidants alone or the Empty-cub nanovectors, to determine the antioxidant capability of the guest molecules free in solution and of the lipid carrier separately. This allowed to evaluate the individual influence of these parameters in the ability of cubosomes samples to reverse the cytotoxic effect, revealed by the decrement of cell viability after treatment with H_2O_2. Then following these control tests, the cubosome samples loaded with only one of the three antioxidants and with curcumin together with one of the two adjuvants were administered. As said above, the liposome samples were not tested, since cytotoxicity tests showed cytotoxicity at two of the tested concentrations, i. e. 1 and 5% (v/v).

Figure 32a and 32b shows the two control tests. Cell viability decreased by increasing hydrogen peroxide concentration and the administration of Empty-cub nanovectors at any of the tested concentrations, i.e. 0.1%, 1% and 5%, could not significantly improve cell viability after the oxidant treatment (Fig. 32a). Thus, the Empty cubosomes were not capable of antioxidant effect on these cells. To compare the two different approaches, biological and chemical, it could be noticed that this sample did not give significant antioxidant capability performance neither in the $ABTS^{\bullet+}$ radical assay. The same trend was observed for solutions of free curcumin at 1 μM, and α-tocopherol at 0.3 μM (Figure 32b). On the contrary, piperine at 28 μM was able to significatively increase cell viability when fibroblasts were treated with H_2O_2 concentrations of 5, 10, 25 and 30 μM but not at higher values, revealing a good ability to protect cells and to reduce cell death. The three concentrations of the antioxidant solutions were chosen on the basis of their previously known non-cytotoxicity at such values.

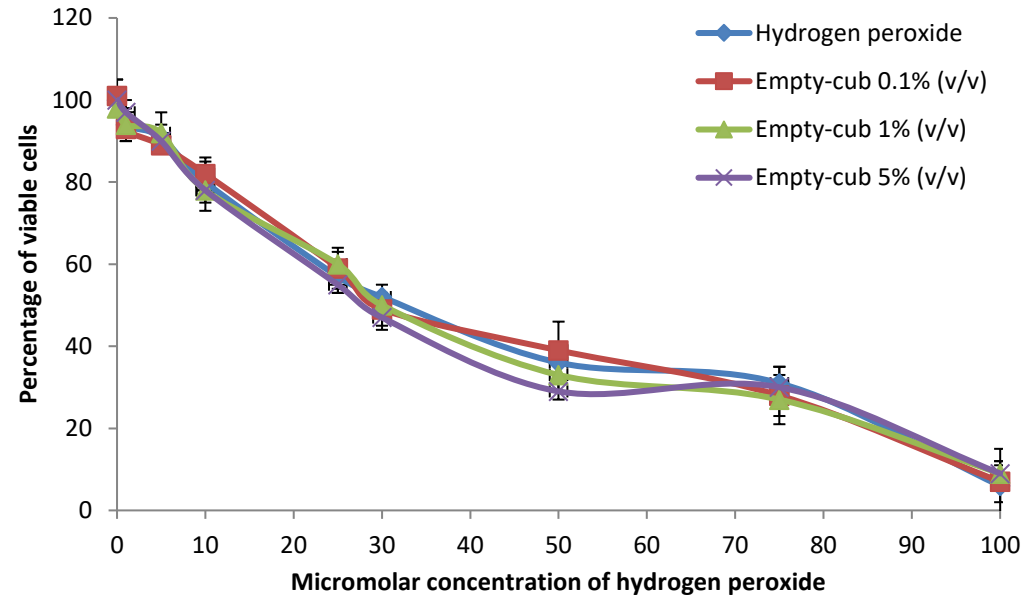

a)

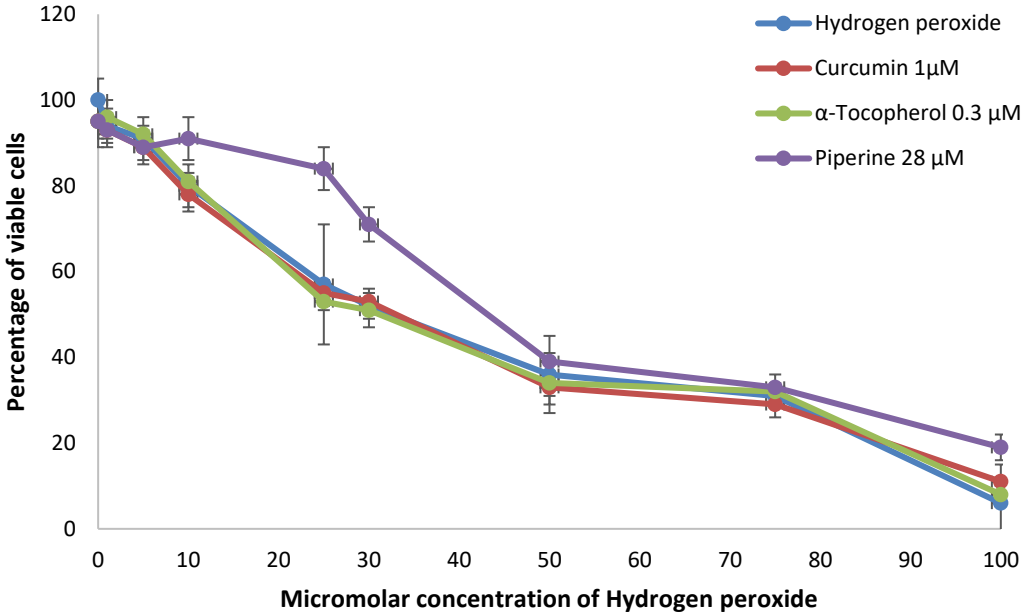

b)

Figure 32 a-b. a) Antioxidant activity of Empty-cub nanocarriers. The nanocarriers did not have any antioxidant effect towards hydrogen peroxide at the tested concentrations. b) Antioxidant activity of non-cytotoxic concentrations of solutions of curcumin, α-tocopherol and piperine.

Figure 33 a-c shows the curves of viability percentages for cubosomes loaded with only one of the three antioxidants, i. e. C-cub, T-cub and P-cub. Each sample was tested at three different concentrations of the cargo, i. e. $5.0 \cdot 10^{-1}$ µM, $1.0 \cdot 10^{-1}$ µM and $1.0 \cdot 10^{-2}$ µM, taking into account both the original concentrations loaded and their EE% (see Tab.4).

Figure 33a displays the cell viability for C-cub nanovectors at the highest curcumin concentration ($5.0 \cdot 10^{-1}$ µM), that showed antioxidant activity towards hydrogen peroxide concentration of 1, 5, 10 and 25 µM ($p < 0.01$; ANOVA), thus demonstrating good antioxidant power toward cells. Particularly, it gave a better performance than the curcumin solution control. Similarly, Figure 33b shows that the presence of loaded α-tocopherol gave to T-cub nanovectors significant antioxidant activity at the molecule concentration of $1.1 \cdot 10^{-1}$ and $5.2 \cdot 10^{-1}$ µM towards hydrogen peroxide concentration of 1, 5, 10, 25 and 30 µM ($p < 0.01$). Just like curcumin, the encapsulation in the nanocarriers was able to enhance their antioxidant activity towards fibroblasts while attenuating potential cytotoxic effects.

Finally, Figure 33c shows that P-cub nanocarriers at all the concentration values tested were able to increase the percentage of cell viability, exhibiting antioxidant activity towards hydrogen peroxide concentration of 1, 5, 10, 25, 30 and 50 µM ($p < 0.01$) and for the highest piperine concentrations, i. e. $5.0 \cdot 10^{-1}$ µM, $1.0 \cdot 10^{-1}$ µM, also for hydrogen peroxide higher up to 100 µM, that was the highest tested. These results confirmed that, indeed, the encapsulated molecules had preserved and even enhanced their antioxidant capability thanks to the loading in the cubosome nanovectors. Noticeably, the T-cub and P-cub samples showed better performances in the evaluation of antioxidant properties through this biological approach than what was seen with the chemical approach towards the radical. Thus, their administration to the cells highlighted this property complementing the $ABTS^{\bullet+}$ assay.

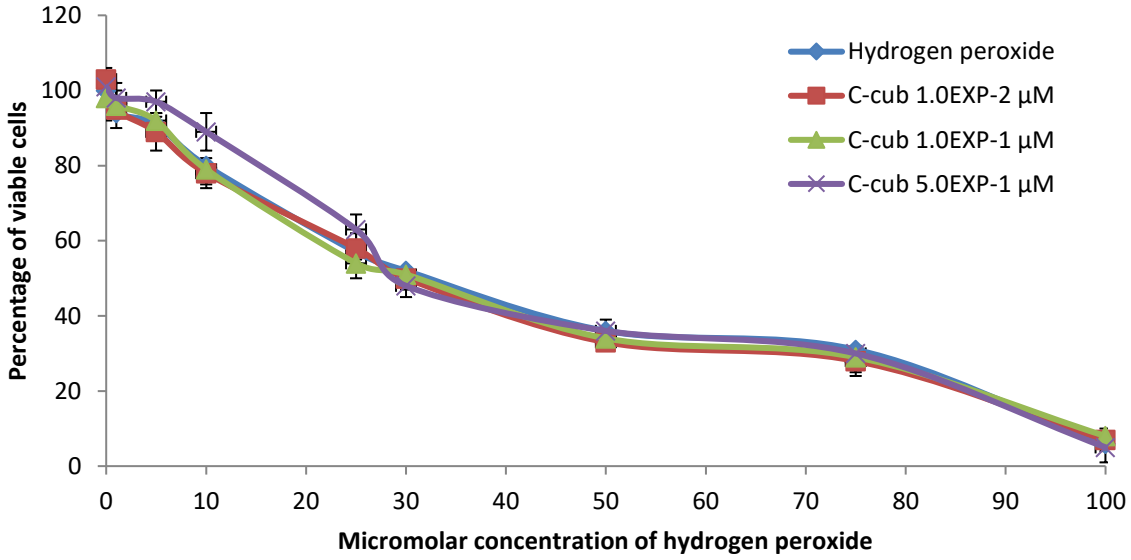

a)

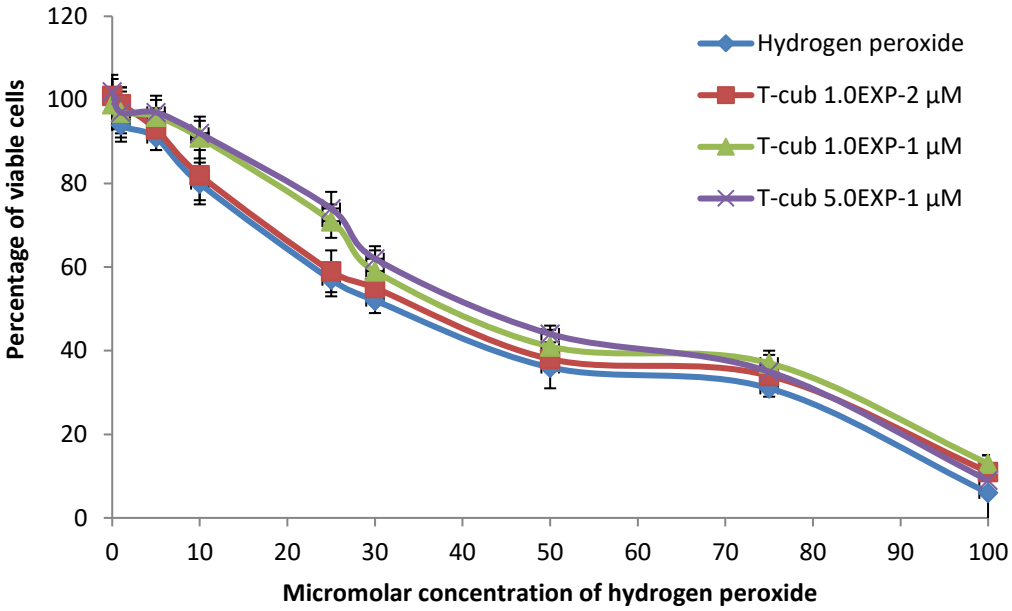

b)

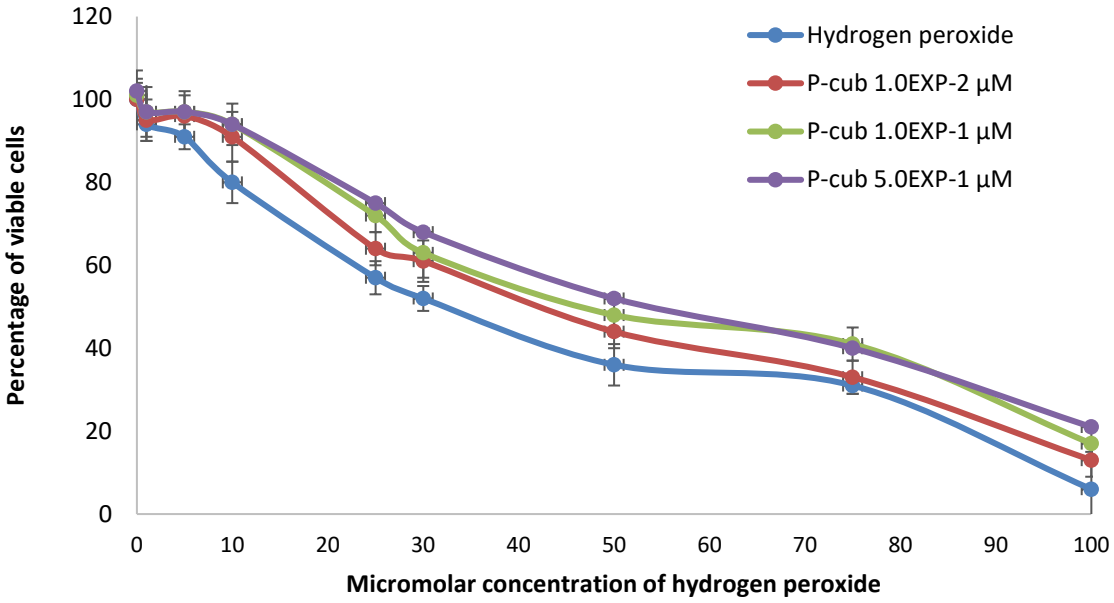

c)

Figure 33 a-c. Antioxidant activity of a) cubosomes loaded with curcumin $1.0 \cdot 10^{-2}$ M b) cubosomes loaded with tocopherol $5.0 \cdot 10^{-3}$ M c) cubosomes loaded with piperine $5.0 \cdot 10^{-3}$ M.

Figure 34a-b shows the cell viability obtained for CT-cub and CP-cub samples, both administered at three different curcumin/adjuvant concentrations, i. e. C at $5.0 \cdot 10^{-1}$ µM, $1.0 \cdot 10^{-1}$ µM and $1.0 \cdot 10^{-2}$ µM and T or P at $2.5 \cdot 10^{-1}$ µM, $5.0 \cdot 10^{-2}$ µM and $5.0 \cdot 10^{-3}$ µM, respectively. The loading of cubic nanovectors with both curcumin/α-tocopherol (CT-cub) or curcumin/piperine (CP-cub) increased the ability of the nanosystems to protect cells from hydrogen peroxide pre-treatment as shown in Figure

34a-b. In both nanosystems, the lowest concentration tested of the molecules (i. e. curcumin $1.0 \cdot 10^{-2}$ µM/α-tocopherol $5.0 \cdot 10^{-3}$ µM and curcumin $1.0 \cdot 10^{-2}$ µM/piperine $5.0 \cdot 10^{-3}$ µM) did not show any protective effect (red curves) towards fibroblasts. On the contrary both CT-cub at curcumin $1.0 \cdot 10^{-1}$ µM/α-tocopherol $5.0 \cdot 10^{-2}$ µM and CP-cub at curcumin $1.0 \cdot 10^{-1}$ µM/piperine $5.0 \cdot 10^{-2}$ µM were able to protect cells from the toxic effect of hydrogen peroxide pre-treatment at concentrations of 10, 25 and 30 µM, showing greater antioxidant effect than the antioxidants encapsulated alone, particularly in the case of CT-cub. Finally, both samples at the highest antioxidant molecules concentrations tested, i.e. curcumin 5.0^{-1} µM/α-tocopherol $2.5 \cdot 10^{-1}$ µM and curcumin $5.0 \cdot 10^{-1}$ µM/piperine $2.5 \cdot 10^{-1}$ µM were able to exercise a protective effect also against H_2O_2 concentration value of 50 µM, enhancing the antioxidant capabilities observed both by the free solutions of the molecules and the antioxidants encapsulated alone. These results confirmed that the loading of nanocarriers with two molecules, i. e. curcumin plus one adjuvant improved their antioxidant activity towards cell systems thanks to a synergistic effect. Moreover, comparing the results of the chemical and biological methods to assess the antioxidant capacity of these samples, it can be noticed that in this case the CP-cub sample performed, even if slightly, better than CT-cub contrarily to the radical decrement of absorbance assay. This could be explained considering the different administration and interaction modalities with the targets, which influenced the resulting functionality of the tested samples. Indeed, this combination of varied approaches from different perspectives offered valuable evidence on the functionality of these complex nanosystems in various conditions.

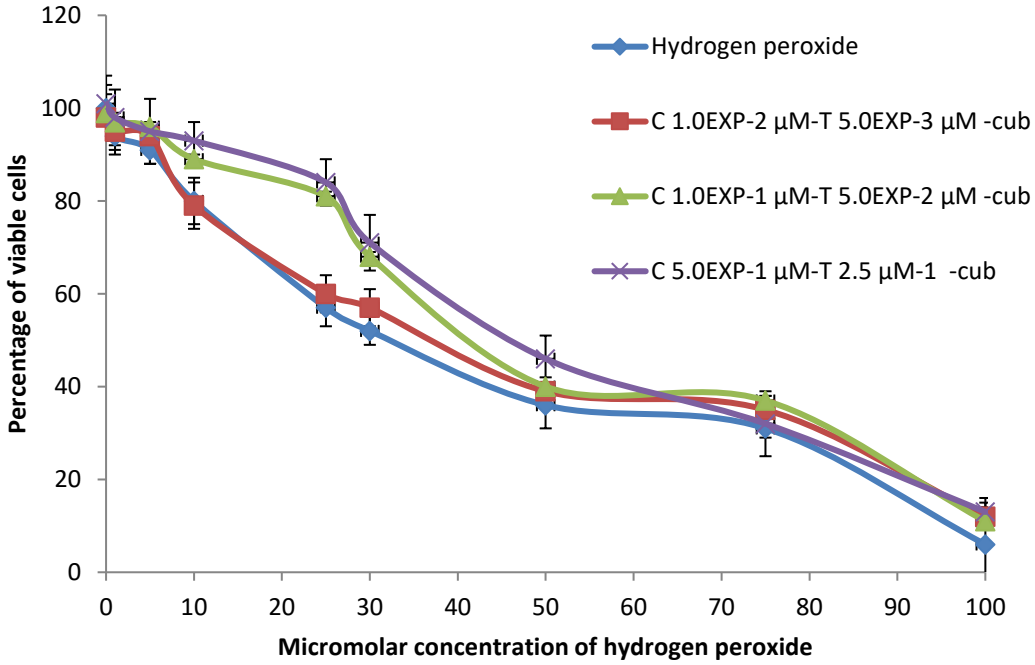

a)

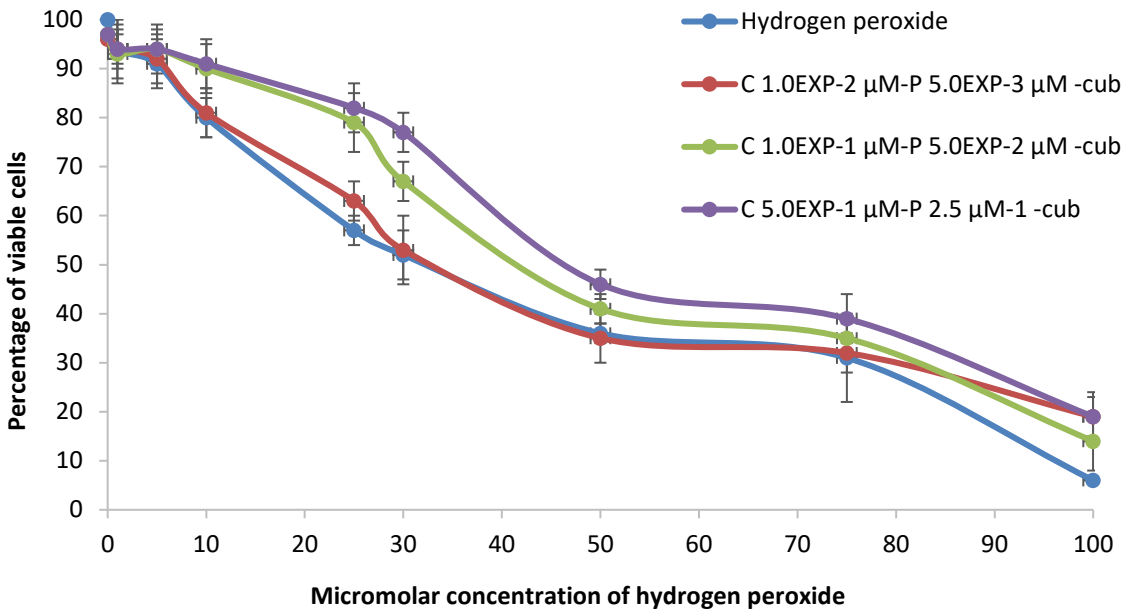

b)

Figure 34a-b. Antioxidant activity of a) cubosome nanocarriers loaded with curcumin $1.0 \cdot 10^{-2}$ M and tocopherol $5.0 \cdot 10^{-3}$ M b) cubosome nanocarriers loaded with curcumin $1.0 \cdot 10^{-2}$ M and piperine $5.0 \cdot 10^{-3}$ M.

Chapter 4

4.Conclusions and perspectives

The poor water solubility of most bioactive drugs is one of the major challenges in pharmaceutics. In particular, hydrophobic natural molecules with antioxidant, anti-inflammatory and nutritive properties have yet to find large market applicability due to their scarce bioavailability and stability in vivo. Several formulation strategies have been devised through the years to improve solubilization and prolong systemic circulation and uptake of these bioactives. Encapsulation and vehiculation techniques represent the most versatile and used approaches since many available engineering and targeting options have proved to be successful to reach the market and clinical approval. Particularly, the interest for the development of encapsulating agents for orally delivered drugs and dietary supplements has driven the development of biocompatible and biodegradable carriers from biological macromolecules, e. g. lipids, used as building blocks. The polymorphism of these amphiphilic molecules are fundamental attributes to obtain nanocarriers with various supramolecular arrangements according to the desired application and target. The presence of hydrophobic and hydrophilic moieties ensures the affinity with several drug candidates and their successful solubilization in aqueous environments. Moreover, the membrane mimetic structure of their aggregates in water and their nontoxic character grant safety for human and animal use, particularly when the lipid building blocks are obtained from natural sources. These natural-derived lipid nanocarriers thus find large applicability for drugs to be delivered and absorbed in different tissues and organs, such as the gastrointestinal tract through digestion.

In this thesis, novel lipid nanocarriers were formulated and prepared from natural sources, i. e. algal biomasses, to obtain biocompatible and biodegradable vectors for industrially attractive hydrophobic antioxidants. Particularly, curcumin was selected as the antioxidant of choice to be encapsulated and two others, i. e. α-tocopherol and piperine were employed as adjuvants to exploit the synergistic effect in combination with curcumin. The use of natural-derived lipids was preferred to increase both guest molecule-carrier and carrier-target compatibility and favor their combined biofunctionality. Moreover, algal biomasses have already been deemed as safe and food-grade material, and are employed as food ingredients and dietary supplements. Two biomasses were selected from *Nannochloropsis oceanica* sp., a genus of microalgae known for its high intrinsic lipid content, after treatment in two different growth conditions, which resulted in accumulated lipid classes either mostly polar or nonpolar respectively. These diverse compositions generated two distinct series of lipid nanoaggregates in dilute regime with supramolecular liposomal organization from the biomass

containing mainly polar lipids, and nanosystems with cubic internal arrangement from the one containing neutral lipids. Both series of nanovectors were loaded with high efficiency with curcumin, alone or associated with one of the two adjuvants, thanks to the high surface-to-volume ratio available and good flexibility of the host assemblies with either architecture. The obtained loaded formulations were thus characterized following an integrated approach which included structural and physico-chemical characterization and the assessment of their functional/bioanalytical properties, to achieve a comprehensive knowledge of these delivery nanosystems. Specifically, the two series were compared on the basis of their supramolecular organization and guest molecules interactions, and the impact of these features on their applicative potential was evaluated in various testing environments. The concomitant use of different techniques with complementary specificity was necessary to obtain in-depth knowledge of the investigated formulations.

Firstly, the structural and morphological properties of the two nanovector series were investigated and compared combining scattering and imaging techniques to obtain complementary information, then these data were integrated with magnetic resonance investigation. Regarding the size distribution and morphology, DLS experiments gave insights on the presence of two polydisperse yet controlled populations of aggregates at the nanoscale and cryo-TEM imaging visually confirmed this result, showing in both liposome and cubosomes samples smaller structures around 100-200 nm and bigger ones in the 500 nm range. Electron microscopy analysis showed the presence of slightly bigger aggregates in the liposomal systems with respect to cubosomes while still being in a comparable range, which again correlated well with dynamic light scattering results. This can be due to the different arrangement and spacing allowed in a certain size range in the two architectures. Both techniques evidenced that there was no noticeable size difference in the same nanovector series, indeed the comparison of loaded systems with empty ones showed that these latter were only slightly smaller. This signified that all nanocarrier structures were flexible and dynamical enough to adjust at the bilayer level to guest molecules insertion while maintaining their supramolecular architecture. The imaging data were able to show the presence of different nanostructures in the two series and displayed the occasional coexistence of lamellar vesicles or other small meta-stable structures in cubosome samples, justifying some detected polydispersity. These morphological analyses complemented well the data obtained by SAXS, that was the main technique to investigate the supramolecular structure of the two nanovector types. In fact, SAXS measurements identified the predominance of two cubic symmetries, the Pn3m and the Im3m, in the formulations constituted mostly of neutral lipids and the presence of liposomal vesicles in the ones made mainly from polar lipids. Moreover, SAXS data suggested the presence of a small population of uncorrelated lamellar bilayers in cubosome samples, which was then confirmed by imaging. These experiments were also

able to evidence the role exerted by curcumin on the structure and intercorrelation at the bilayer scale, thus influencing the spacing and the peak pattern in the cubosome series. Indeed, higher curcumin concentration was found to influence the inner bilayer organization due to the interactions with the matrix, imparting more pronounced lipid ordering that resulted in enhanced and sharper Bragg peaks indicative of the cubic symmetries. Some differences in the peak pattern were also observed according to the loaded adjuvants, particularly in the samples loaded at lower concentrations, evidencing that also the interactions between guest molecules played a role on the inner structuring of cubosomes. On the contrary, the structural organization of liposome samples was not evidently affected by the concentration and interactions of cargo molecules. All these findings were confirmed by proton NMR, that supported both the structural identification of the two series and the hypothesis on guest molecule-lipid matrix interactions. Indeed, NMR spectra were consistent with scattering and imaging data on the supramolecular arrangement and bilayer packing, showing typical narrow or broad peak shapes for cubosomes and liposomes respectively. Moreover, the experiments with decreasing curcumin concentrations showed that curcumin at the selected loading amount was able to impose tighter bilayer intercorrelation and packing, while lower concentrations resulted in faster lipid motions due to looser inner organization. As already noticed in SAXS plots, this effect was only detected for cubosome samples whereas liposomes were not apparently influenced by cargo concentration. This evidence highlighted how the supramolecular peculiarities of the two nanocarrier series influenced the interactions and dynamics of the nanosystems at the molecular level, which in turn impacted on the structure and packing at the bilayer level as well.

The analysis of the interactions and their strength at the molecular scale was carried out from a thermodynamic perspective by preliminary calorimetric experiments. The data obtained with ITC gave an interesting view on how the guest molecule-lipid matrix interactions impact differently on the nanovectors stability according to their structural arrangement. Molecular fluctuations and intra-bilayer rearrangements were evidenced as a result of thermal peak profiles observed upon titration, with different intensity and shape depending both on the series and loaded cargo. The sensitivity of this technique allowed to identify small but significant stability variations upon either water or ethanol dilution that could not be revealed by stability tests assessed with UV-Vis measurements, thus offering a different perspective on molecular and supramolecular stability. In fact, as seen in bulk stability tests, the supramolecular arrangement was maintained up to 60% v/v of ethanol, whereas the bilayer arrangement experienced fluctuations already at 10% v/v ethanol addition. Moreover, the calorimetric profile upon water or ethanol titration differed from cubosomes to liposome samples, which was likely due to different heats of rearrangement depending on the bilayer assembly in the two structures. ITC experiments confirmed the role of curcumin in these local rearrangements, in

agreement with SAXS and NMR results, confirming the influence of this molecule on bilayer structure and stability from a thermal perspective. Furthermore, calorimetry gave additional insights to the results obtained from the stability tests carried out with a bulk perspective, where the larger variations could be seen mainly depending on the guest molecules. In fact, in this assessment carried out by UV-Vis to evaluate the release of curcumin upon carrier disaggregation, consequently to the addition of varied ethanol percentages, the sample release profiles at a chosen percentage were quite similar between the two series. Moreover, also the structural destabilization followed by SAXS showed comparable intensity curves, in either case likely because the disaggregating conditions were nonspecific. The most significant differences in UV-Vis measures were observed according to the cargo, since the samples loaded with combined curcumin and tocopherol in both series showed a slower release profile and did not reach complete release, contrarily to the other cubosome and liposome samples. This peculiar behavior could be explained with stronger stabilization of the carrier in these two samples likely induced by the adjuvant action of tocopherol towards curcumin, favoring guest-matrix interactions and thus slowing down the release. All these results were in line with SAXS and NMR observations regarding the different role played by guest molecules in the lipid matrix packing and stability, while at the same time evidencing that these latter properties are not influenced exclusively by cargo or carrier structure, but by the interplay of many parameters. In addition, release tests showed that both nanocarrier series possess significant resistance and stability at the supramolecular level, maintaining their architecture even in disruptive conditions with high upper limits, while at the same time showing flexibility to allow intra-bilayer rearrangements during cargo release. It can also be hypothesized that this latter property contributed to favor the overall stability and capacity to maintain some type of aggregation even in the harshest conditions.

This concurring role of guest molecules and carrier structure in the functional properties could be noticed also considering the encapsulation efficiency in the two series. Indeed, cubosomes and liposomes showed opposite trends in the influence of adjuvant addition on the EE% of curcumin, in that the interactions with tocopherol or piperine favored higher curcumin encapsulation in cubosome samples and lower encapsulation in liposomes. Thus, the cubosomal bilayer adapted more easily to fit two molecules in the confined space whereas liposomes showed lower flexibility, even though both nanovector series possessed good encapsulation efficiency without altering dramatically their size, as shown by DLS.

The predominant impact of carrier composition and assembly on functionality was evidenced in the simulated digestion tests performed in biorelevant environment with the lipid-specific action of gastrointestinal lipolytic enzymes. This assessment evidenced the resistance toward disruption of the

two series in gastric conditions and their capacity to maintain curcumin bioaccessible for absorption until the end of the whole digestion. In fact, both cubosome and liposome samples showed total resistance to gastric conditions and ability to preserve their cargo until the absorption site i. e. the intestinal tract was reached. The impact of carrier type on the digestion profile was noticeable during the passage through the intestinal environment, since liposomal aggregates showed a twofold increment in the release profile of curcumin from the digested carriers. On the contrary, cubosomes showed lower release values corresponding to lower digestion rate, even though the fraction of curcumin available for absorption at the end of the process still represented a good percentage. Even though both series displayed some resistance to disassembly, these results evidenced high digestive activity in the simulated intestinal tract influenced mostly by the supramolecular arrangement. The main reasons of different carrier impact in this test lie both on the enzymes specificity to lipid composition and on the accessibility of lipids to enzyme attack according to arrangement and positioning.

The interplay between guest molecules and carrier structure influencing functionality was also evidenced by antioxidant capability tests using chemical or biological approach, i. e. the $ABTS^{\bullet+}$ radical assay and in vivo hydrogen peroxide tests. Regarding the kinetics of decrement of absorbance of the radical interacting with the loaded antioxidants in standard and disruptive conditions, cubosomes and liposomes showed some peculiarities related both to carrier type and to the guest molecules. Since the kinetics in standard conditions was related to the process of insertion of the radical in the bilayer and the accessibility of guest molecules according to their localization, whereas in disaggregating conditions it was related to the release of the antioxidants and their synergistic interactions, the influence of either carrier, cargo or both had a different impact on the outcome. In fact, cubosome samples loaded with curcumin and tocopherol showed higher antioxidant activity in both testing conditions, which evidenced that the synergy between the two molecules was favored in the cubic bilayer or the localization and accessibility were improved when encapsulated together. On the other hand, the curcumin-piperine combination was more effective for liposomes in disassembled state, while the aggregates loaded with curcumin alone performed better in the standard state, depending on effective interactions in the former case and accessibility in the latter. These findings evidenced that the resulting antioxidant power of the two formulation series was generally contingent to the contribution of different parameters, depending on the testing conditions, even though all curcumin loaded samples in the two series showed comparable functionality. Also, as already seen in digestion experiments, the carrier composition influenced the antioxidant efficacy since the biomass components of liposome carriers themselves showed some antioxidant effect. The guest molecule-matrix interactions and the guest-guest interactions played a major role both in the encapsulation

capability and in the antioxidant power towards $ABTS^{\bullet+}$ radical, evidencing that the synergy between curcumin-adjuvant favored by loading in the confined bilayer space had a relevant impact on both properties. This finding is particularly interesting since it showed that host-guest interactions are able to influence the structure, dynamics/stability and inner packing at the bilayer level as indicated by SAXS, NMR, ITC and stability tests, and at the same time this property affects the functionality, as seen with these cargo-related efficiency activities.

Moreover, different mechanical properties dependent on carrier matrix composition and structure were evidenced also by cytotoxicity tests, where liposome samples resulted toxic to fibroblasts due to adhesion to cell membrane likely due to lamellar stacking on the surface, which covered the cell surface and decreased viability. On the contrary, cubosome samples resulted nontoxic and could be evaluated to assess their ability to preserve guest molecules in vitro and their antioxidant capacity towards cells, treated by inducing oxidative stress with hydrogen peroxide. These experiments were a biological complement to the results obtained from the radical decrement of absorbance assay. Interestingly, the antioxidants loaded in the nanocarriers were able to give better performance than the free solutions showing enhanced antioxidant capacity even at lower concentrations, while also mitigating their own cytotoxicity with respect to these latter. Also in this assay the cubosome samples loaded with curcumin and adjuvant gave better performance, showing enhanced properties both with respect to the free solutions and the single encapsulated antioxidants. This finding was in accordance with the $ABTS^{\bullet+}$ assay, thus integrating the chemical perspective with the biological one. On the other hand, cubosomes loaded with only tocopherol and piperine showed improved capabilities in hydrogen peroxide test with respect to the radical assay, showing that the in vitro performance of these molecules was boosted by cubosome encapsulation. So, most cubosome samples showed protective ability towards cells against oxidative stress and increased the percentage of viable cells, particularly in the case of samples loaded with curcumin and an adjuvant. As already seen in the $ABTS^{\bullet+}$ assay, the simultaneous loading of two molecules produced a combined synergistic effect on functionality, assessed from different perspectives. Even though the administration approach and interaction with the target were dependent on the assay type, the complementing results confirmed the assumptions on the higher efficacy of the use of adjuvants combined with curcumin.

Future perspectives on this work involve deeper investigation of some aspects yet to be clarified, though several physico-chemical and functional properties of these nanocarriers have been enlightened. In fact, the complexity of nanosystems derived from natural matrices include the presence of various classes of lipid building blocks, so that the overall properties of the resulting aggregates usually stem from an average of the properties of the starting molecules. Even though the

assessment of these properties is generally complicated by this fact, it is particularly relevant considering the interest and attractivity for large applicability of systems obtained from natural sources.

Specifically, one the most relevant aspects that could be further investigated concerns calorimetric experiments. The preliminary analyses by Isothermal Titration Calorimetry included in the present thesis gave interesting insights on structural and interaction properties from a thermodynamical perspective. In fact, these measurements allowed to identify the presence of thermal events at molecular level upon dilution. This led to hypothesize that small molecular rearrangements and fluctuations occur which depend on guest-lipid matrix interactions, even though it was not possible yet to extract parameter calculations that would allow to make thermodynamical considerations. Indeed, the investigation of these interactions, their favorability and impact on the nanosystems from the energetical perspective would offer additional physico-chemical understanding of the two carrier series. Moreover, complementary experiments carried out with Differential Scanning Calorimetry would allow to study phase transitions and heats of rearrangement for the lipid aggregates, thus extracting the thermal behavior according to carrier structure and stability. Regarding additional studies of guest molecule interactions and influence on nanosystem assembly, two-dimensional and deuterium NMR analyses could be employed to expand previous results.

Further studies could involve changes of the encapsulated molecules to explore different adjuvant combinations and exploit the effect on functionality of their interactions with the carriers. Moreover, different biomasses could be selected as starting material or specific lipid classes could be separated and chosen for carrier assembly from the ones here employed, opening the possibility to further engineering and manipulations.

5.Acknowledgements

This doctoral thesis is the scientific outcome of the collaboration of my two co-tutoring research groups in the Universities of Siena and Florence (CSGI), and it involved work and effort from myself and several people that gave their precious contribution.

Prof. Mario Tredici and Prof. Liliana Rodolfi from the Department of Agriculture, Food, Environment and Forestry (DAGRI), University of Florence are gratefully acknowledged for cultivation and analysis of the algal biomasses.

Dr. Felicia Menicucci from the CNR, Florence Unit and Prof. Luca Calamai from the Department of Agriculture, Food, Environment and Forestry (DAGRI), University of Florence are thanked as well for additional work and Mass spectroscopy analyses on the biomass materials.

The European Synchrotron Radiation Facility (ESRF, Grenoble) and the ID02 beamline staff are thanked for beamtime allocation and scientific and technical support.

This work used the EM facilities at the Grenoble Instruct-ERIC Center (ISBG ; UMS 3518 CNRS CEA-UGA-EMBL) with support from the French Infrastructure for Integrated Structural Biology (FRISBI ; ANR-10-INSB-05-02) and GRAL, a project of the University Grenoble Alpes graduate school (Ecoles Universitaires de Recherche) CBH-EUR-GS (ANR-17-EURE-0003) within the Grenoble Partnership for Structural Biology. The IBS Electron Microscope facility is supported by the Auvergne Rhône-Alpes Region, the Fonds Feder, the Fondation pour la Recherche Médicale and GIS-IBiSA. Dr. Guy Schoehn as the main platform developer and manager, and Dr. Maria Bacia-Verloop are gratefully acknowledged.

Dr. Miroslav Slouf, Dr. Ewa Pavlova and the entire Polymer Morphology Department of the Institute of Macromolecular Chemistry (IMC) of the Czech Academy of Sciences are gratefully acknowledged for welcoming me in the group for my period abroad as visiting PhD student, for scientific and technical support and for use of the Electron Microscopy platform.

Prof. Concetta Giancola and Dr. Federica D'Aria from the Department of Pharmacy of the University of Napoli Federico II are gratefully thanked for Isothermal Titration Calorimetry analyses and scientific and technical support and discussion.

Mesofarma S.r.l. (Reggio Calabria, Italy) is especially acknowledged for funding my PhD project and stimulating discussion.

Last but not least, my amazing colleagues from my group in Florence are thanked for support (scientific and particularly not scientific), laughter and friendship during the course of these challenging and intense years for all of us.

All my loved ones are thanked for their helpful presence and support during this time.

6.References

[1] Allen T. M. and Cullis P. R., Drug Delivery Systems: Entering the Mainstream, *Science*, **2004**, 303, 1818-22.
[2] LaVan DA, McGuire T, Langer R. Small-scale systems for in vivo drug delivery. *Nature Biotechnology*. **2003**, 21, 1184-91.
[3] Park K. Controlled drug delivery systems: Past forward and future back. *J Contr Rel* **2014**, 190, 3-8.
[4] Yun HY, Lee BK, Park K. Controlled Drug Delivery: Historical perspective for the next generation *J Contr Rel* **2015**, 219, 2-7.
[5] Rodrigues, T., Reker, D., Schneider, P. *et al.* Counting on natural products for drug design. *Nature Chem*, **2016**, 8, 531–541
[6] Watkins R, Wu L, Zhang C, Davis RM, Xu B. Natural product-based nanomedicine: recent advances and issues. *Int J Nanomedicine*. **2015**, 28, 6055-74
[7] Thomford NE, Senthebane DA, Rowe A, Munro D, Seele P, Maroyi A, Dzobo K. Natural Products for Drug Discovery in the 21st Century: Innovations for Novel Drug Discovery. *Int J Mol Sci.* **2018**,19,1578.
[8] Blanco E., Shen H., Ferrari, M. Principles of nanoparticle design for overcoming biological barriers to drug delivery. *Nat Biotechnol*, **2015**, 33**,** 941–951
[9] Wong, H.L., Bendayan, R., Rauth, A.M. & Wu, X.Y. Simultaneous delivery of doxorubicin and GG918 (Elacridar) by new polymer-lipid hybrid nanoparticles (PLN) for enhanced treatment of multidrug-resistant breast cancer. *J. Control. Release,* **2006**, 116, 275–284
[10] Xiong, X.B. & Lavasanifar, A. Traceable multifunctional micellar nanocarriers for cancer-targeted co-delivery of MDR-1 siRNA and doxorubicin. *ACS Nano* **2011**, 5, 5202–5213
[11] Patel, N.R., Rathi, A., Mongayt, D. & Torchilin, V.P. Reversal of multidrug resistance by co-delivery of tariquidar (XR9576) and paclitaxel using long-circulating liposomes. *Int. J. Pharm.* **2011**, 416, 296–299.
[12] Bergström C. A. S., Wassvik C. M., Johansson K., Hubatsch I. Poorly Soluble Marketed Drugs Display Solvation Limited Solubility. *J. Med. Chem.* **2007**, 50, 5858–5862
[13] Lipinski C. A., Lombardo F., Dominy B. W., Feeny P. J. Experimental and computational approaches to estimate solubility and permeability in drug discovery and development settings. *Adv. Drug Delivery Rev*. **1997**, 23, 3-25.
[14] Bergstrom C. A. S., Norinder U., Luthman K., Artursson P. Experimental and computational screening models for prediction of aqueous drug solubility. *Pharm. Res*. **2002**, 19,182-188.
[15] Wassvik C. M., Holmen A. G., Bergstrom C. A. S., Zamora I., Artursson P. Contribution of solid-state properties to the aqueous solubility of drugs. *Eur. J. Pharm. Sci*. **2006**, 29, 294-305.
[16] Csicsák D, Borbás E, Kádár S. *et al.* Towards more accurate solubility measurements with real time monitoring: a carvedilol case study. *New Journal of Chemistry* **2021,** 45,11618-11625.
[17] Avdeef A. Absorption and Drug Development: Solubility, Permeability, and Charge State, **2012**, John Wiley & Sons, Inc.
[18] Jakubiak P, Wagner B, Grimm HP, Petrig-Schaffland J., Schuler F., Alvarez-Sanchez R. Development of a unified dissolution and precipitation model and its use for the prediction of oral drug absorption. *Mol Pharmaceutics* **2015**, 13, 2, 586–598.
[19] Grant D.J.W., Brittain H.G., In H.G. Brittain (Ed.), Physical Characterization of Pharmaceutical Solids, Marcel Dekker, New York (1995), pp. 321-386
[20] Baka E, Comer J E.A., Takács-Novák K. Study of equilibrium solubility measurement by saturation shake-flask method using hydrochlorothiazide as model compound J *Pharm Bio Anal* **2008**, 46, 335-341

[21] Avdeef A. Solubility of sparingly-soluble ionizable drugs, *Adv Drug Deliv Rev* **2007**, 59, 568–590.
[22] Lipinski C.A. Drug-like properties and the causes of poor solubility and poor permeability *J Pharmacol Toxicol Methods* **2000**, 44, 235-249
[23] Avdeef A., Bendels S., Tsinman O. *et al.* Solubility-Excipient Classification Gradient Maps. *Pharm Res,* **2007**, 24, 530–545.
[24] Cooper ER. Nanoparticles: A personal experience for formulating poorly water soluble drugs. *J Control Release*. **2010**,141,300-2.
[25] McClements D.J. Nanoparticle- and microparticle-based delivery systems: Encapsulation, protection and release of active components. **2014**, CRC Press, Boca Raton, FL
[26] Torchilin VP. Nanocarriers. *Pharm Res*. **2007**, 24,2333-4.
[27] Zaki N.M., Artursson P., Bergström C. A. S. A Modified Physiological BCS for Prediction of Intestinal Absorption in Drug Discovery *Mol. Pharmaceutics* **2010**, 7, 1478–1487.
[28] Joye I. J., Davidov-Pardo G, McClements DJ. Nanotechnology for increased micronutrient bioavailability. *Trends Food Sci Technol* **2014**,40,168-182
[29] Patra, J.K., Das, G., Fraceto, L.F. *et al.* Nano based drug delivery systems: recent developments and future prospects. *J Nanobiotechnol* **2018**, 16, 71.
[30] Jiang W, Kim BY, Rutka JT, Chan WC. Advances and challenges of nanotechnology-based drug delivery systems. *Expert Opin Drug Deliv*. **2007**, 4, 621-33.
[31] Lu H, Wang J, Wang T, Zhong J, Bao Y, Hao H. Recent progress on nanostructures for drug delivery applications. *J Nanomater*. **2016**,2016,20
[32] Kumari A, Singla R, Guliani A, Yadav SK. Nanoencapsulation for drug delivery. *EXCLI J.* **2014**,13,265-286.
[33] Fennell Evans, D., Wennerström, H. The colloidal domain: Where physics, chemistry, biology, and technology meet. VCH Publishers, New York **1994**
[34] Hughes G.A. Nanostructure-mediated drug delivery. *Nanomed.: Nanotechnol. Biol. Med.* **2005**,1,22–30
[35] Iqbal, P., Preece, J.A. and Mendes, P.M. Nanotechnology: The "Top-Down" and "Bottom-Up" Approaches. In Supramolecular Chemistry, **2012** (eds P.A. Gale and J.W. Steed).
[36] Fave G., Coste T.C., Armand M. Physicochemical properties of lipids: new strategies to manage fatty acid bioavailability *Cell. Mol. Biol*., **2004**, 50, 815-831.
[37] Torchilin VP. Multifunctional nanocarriers. *Adv Drug Deliv Rev*. **2012**,64,302–15.
[38] Chaudhari S. P., Dugar R. P. Application of surfactants in solid dispersion technology for improving solubility of poorly water soluble drugs. *J Drug Deliv Sci Technol* **2017**, 41, 68-77.
[39] Angelova A, Garamus VM, Angelov B, Tian Z, Li Y, Zou A. Advances in structural design of lipid-based nanoparticle carriers for delivery of macromolecular drugs, phytochemicals and anti-tumor agents. *Adv Colloid Interface Sci.* **2017**,249,331-345.
[40] Akbarzadeh, A., Rezaei-Sadabady, R., Davaran, S. *et al.* Liposome: classification, preparation, and applications. *Nanoscale Res Lett* , **2013**, 8, 102.
[41] Donsi F., Sessa M., Mediouni H., Mgaidi A., Ferrari G. Encapsulation of bioactive compounds in nanoemulsion-based delivery systems. *Procedia Food Science* **2011**, 1,1666-1671.
[42] Mehnert W., Mader K. Solid lipid nanoparticles: production, characterization and applications. *Adv Drug Deliv Rev*, **2012**,64, 83-101.
[43] H.M.C. Marques. A review on cyclodextrin encapsulation of essential oils and volatiles. *Flavour Fragr J*, **2010**, 25, 313-326
[44] Astray G, Gonzalez-Barreiro C, Mejuto JC, Rial-Otero R, Simal-Gándara J. A review on the use of cyclodextrins in foods. *Food hydrocolloids* **2009**,7,1631-1640.
[45] Sun C., Wei Y., Li R., Dai L., Gao Y. Quercetagetin-Loaded Zein–Propylene Glycol Alginate Ternary Composite Particles Induced by Calcium Ions: Structure Characterization and Formation Mechanism. *J. Agric. Food Chem.* **2017**, 65, 3934–3945

[46] Aleandri S., Mezzenga R. The physics of lipidic mesophase delivery systems. *Physics Today* **2020**, 73, 38.
[47] Fong C., Le T., Drummond C. J. Lyotropic liquid crystal engineering–ordered nanostructured small molecule amphiphile self-assembly materials by design. *Chem. Soc. Rev.* **2012**, 41, 1297
[48] H. Qiu, M. Caffrey, The phase diagram of the monoolein/water system: metastability and equilibrium aspects *Biomaterials* **2000**, 21, 223.
[49] Ramanathan M., Shrestha L.K., Mori T., Ji Q., Hill J. P., Ariga, K. Amphiphile nanoarchitectonics: from basic physical chemistry to advanced applications. *Phys Chem Chem Phys,* **2013**,15,10580.
[50] Larsson K, Fontell K, Krogh N. Structural relationships between lamellar, cubic and hexagonal phases in monoglyceride–water systems. Possibility of cubic structures in biological systems. *Chem Phys Lipids*, **1980**, 27, 321-328.
[51] Nagle JF, Tristram-Nagle S. Structure of lipid bilayers. *Biochim Biophys Acta*. **2000**,1469,159-95.
[52] Israelachvili J. N. Intermolecular and Surface Forces, **2011** 3rd Edition Academic Press.
[53] Fontell K. X-ray diffraction by liquid crystals amphiphilic systems, in "Liquid Crystals and Plastic Crystals", **1974**, Vol. 1, G.W.Gray and P.A.Winsor (Eds.)
[54] Angelova, A., Angelov, B., Deng, Y. Chapter 5 "Lipid Membranes: Fusion, Instabilities, and Cubic Structure Formation" In "Biological Soft Matter. Fundamentals, Properties and Applications", Nardin. C. and Schlaad H. (Eds.) John Wiley & Sons, Weinheim, 1st Edition, **2021**, pp. 117-152.
[55] Luzzati V. X-ray diffraction studies of lipid–water systems, **1968** D Chapman (Ed.), Biological membranes, vol. 1, Academic Press, New York, pp. 71-123.
[56] Luzzati V., Tardieu A., Gulik-Krzywicki T. *et al.* Structure of the Cubic Phases of Lipid–Water Systems. *Nature* **1968**,220**,** 485–488.
[57] Lindblom G, Rilfors L. Nonlamellar phases formed by membrane lipids. *Adv Colloid Interface Sci.* **1992**,41,101-25.
[58] Luzzati V., Delacroix H., Gulik A., Gulik-Krzywicki T., Mariani P., Vargas R. Chapter 1 The Cubic Phases of Lipids. *Current Topics in Membranes*, **1997**,44, 3-14, 14a, 14b, 15-24.
[59] Sadoc J.-F, Charvolin J. Infinite periodic minimal-surfaces and their crystallography in the hyperbolic plane. *Acta Crystallogr*. **1989**, A45, 10–20.
[60] Seddon J.M, Templer R.H. Cubic phases of self-assembled amphiphilic systems. *Phil. Trans. R. Soc.* **1993**, A. 344, 377–401.
[61] Hyde S.T., Andersson S., Larsson K., Blum Z., Landh T., Lidin S., Ninham B.W., The language of shape, The Role of Curvature in Condensed Matter: Physics, Chemistry and Biology, **1997**, Elsevier, Amsterdam.
[62] Wang J., Zhu M., Nie G. Biomembrane-based nanostructures for cancer targeting and therapy: From synthetic liposomes to natural biomembranes and membrane-vesicles. *Adv Drug Deliv Rev*, **2021**,178, 113974.
[63] Armstrong J.P.K., Holme M.N., Stevens M.M. Re-engineering extracellular vesicles as smart nanoscale therapeutics *ACS Nano*, **2017**,11, 69-83.
[64] Colzi I., Troyan A.N., Perito B., Casalone E., Romoli R., Pieraccini G., Škalko-Basnet N., Adessi A., Rossi F., Gonnelli C., Ristori S. Antibiotic delivery by liposomes from prokaryotic microorganisms: Similia cum similis works better. *Eur J Pharm Biopharm* **2015**, 94, 411–418.
[65] Gupta V., Gupta R., Grover R., Kanna R., Jangra V., Mittal A.J. Delivery of molecules to cancer cells using liposomes from bacterial culture, *J. Nanosci. Nanotech*. **2008**, 8, 2328-2333.
[66] Yang C., Zhang M., Merlina, D. Advances in plant-derived edible nanoparticle based lipid nano-drug delivery systems as therapeutic nanomedicines. *J Mater Chem B*, **2018**, 6, 1312.
[67] Clemente I., Menicucci F., Colzi I., Sbraci L., Benelli C., Giordano C., Gonnelli C., Ristori S., Petruccelli R. Unconventional and sustainable nanovectors for phytohormone delivery: Insights on *Olea europaea*. *ACS Sus Chem Eng* **2018**, 6, 15022–15031.

[68] Clemente I., Colzi I., Falsini S. Chapter "Lipid-Based Nanoformulations from Plants for Sustainable Drug Delivery", In "Novel Drug Delivery Systems for Phytoconstituents" 1st Eds, **2019**, CRC Press, 12 pp.
[69] Hu Q., Sommerfeld M., Jarvis E., Ghirardi M., Posewitz M., Seibert M., Darzins A. Microalgal triacylglycerols as feedstocks for biofuel production: perspectives and advances. *Plant J.* **2008**, 54, 621-39.
[70] Rodolfi L., Chini Zittelli G., Bassi N., Padovani G., Biondi N., Bonini G., Tredici MR. Microalgae for oil: strain selection, induction of lipid synthesis and outdoor mass cultivation in a low-cost photobioreactor. *Biotechnol Bioeng*. **2009**, 102, 100-12.
[71] Bondioli P., Della Bella L., Rivolta G., Chini Zittelli G., Bassi N., Rodolfi L., Casini D., Prussi M., Chiaramonti D., Tredici MR. Oil production by the marine microalgae *Nannochloropsis* sp. F&M-M24 and Tetraselmis suecica F&M-M33. *Bioresour. Technol.* **2012**, 114, 567–572.
[72] Clemente I., Bonechi C., Rodolfi L., Bacia-Verloop M., Rossi C., Ristori S. Lipids from algal biomass provide new (nonlamellar) nanovectors with high carrier potentiality for natural antioxidants. *Eur J Pharm Biopharm* **2020**, 158, 410-416.
[73] Menicucci F., Michelozzi M., Raio A., Tredici M., Cencetti G., Clemente I., Ristori S. Thymol-loaded lipid nanovectors from the marine microalga Nannochloropsis sp. as potential antibacterial agents. *Biocatal. Agric. Biotechnol*. **2021**, 32, 101962.
[74] Basnet P, Skalko-Basnet N. Curcumin: an anti-inflammatory molecule from a curry spice on the path to cancer treatment. *Molecules* **2011**,16,4567-98.
[75] Marquardt D, Kučerka N, Katsaras J, Harroun TA. α-Tocopherol's Location in Membranes Is Not Affected by Their Composition. *Langmuir* **2015**,31,4464-72.
[76] Wang R, Han J, Jiang A, Huang R, Fu T, Wang L, Zheng Q, Li W, Li J. Involvement of metabolism-permeability in enhancing the oral bioavailability of curcumin in excipient-free solid dispersions co-formed with piperine. *Int J Pharm*. **2019**, 561,9-18
[77] Chen S., Li Q., McClements DJ, Han Y., Dai L., Mao L., Gao Y. Co-delivery of curcumin and piperine in zein-carrageenan core-shell nanoparticles: formation, structure, stability and in vitro gastrointestinal digestion. *Food Hydrocoll* **2020**, 99, 105334
[78] Angelova A, Angelov B, Drechsler M, Bizien T, Gorshkova Y E., Deng Y. Plasmalogen-Based Liquid Crystalline Multiphase Structures Involving Docosapentaenoyl Derivatives Inspired by Biological Cubic Membranes. *Front. Cell Dev. Biol.* **2021** ,9,617984.
[79] Koifman, N.; Talmon, Y. Cryogenic Electron Microscopy Methodologies as Analytical Tools for the Study of Self-Assembled Pharmaceutics. *Pharmaceutics* **2021**, 13, 1015
[80] Zou L , Zheng B, Zhang R, Zhang Z, Liu W, Liu C, Xiao H, McClements DJ. Food-grade nanoparticles for encapsulation, protection and delivery of curcumin: comparison of lipid, protein, and phospholipid nanoparticles under simulated gastrointestinal conditions *RSC Adv.,***2016**, 6,3126.
[81] Cuomo F., Cofelice M., Venditti F., Ceglie A., Miguel M., Lindman B., Lopez F. In-vitro digestion of curcumin loaded chitosan-coated liposomes *Colloids Surf B* **2018**,168,29–34.
[82] Liu Y., Liu D., Zhu L., Gan Q., Le X. Temperature-dependent structure stability and in vitro release of chitosan-coated curcumin liposome. *Food Res Int* **2015**, 74, 97-105.
[83] Chu, B., Laser Light scattering: Basic Principles and Practice, Academic Press, **1992**.
[84] Lindner, P., Zemb, T., Eds. Neutron, X-Rays and Light Scattering Methods Applied to Soft Condensed Matter, North Holland Press, Amsterdam, **2002**.
[85] Boesecke P. Reduction of two-dimensional small- and wide-angle X-ray scattering data. *J. Appl. Crystallogr.* **2007**,40, 423-427.
[86] Narayanan, T., Sztucki M., Van Vaerenbergh P., Leonardon J., Gorini J., Claustre L., Sever F., Morse J., Boesecke P. A multipurpose instrument for time-resolved ultra-small-angle and coherent X-ray scattering. *J. Appl. Cryst.* **2018**, 51 ,1511-1524.
[87] Almgren M., Edwards K., Karlsson G. Cryo transmission electron microscopy of liposomes and related structures. *Colloids Surf A* ,**2000**,174, 3-21.

[88] Goldman M. Spin Temperature and Nuclear Magnetic Resonance in Solids. Clarendon, Oxford, **1970**.
[89] Charvolin J, Rigny P. Proton relaxation study of paraffinic chain motions in a lyotropic liquid crystal. *J Chem Phys* **1973**,58, 3999
[90] Lasic D.D. Magnetic Resonance Methods in The Studies of Liposomes. *Bull. Magn. Reson*. **1991**,13,3–13
[91] Archer W.R., Schulz M.D. Isothermal titration calorimetry: practical approaches and current applications in soft matter. *Soft Matter* **2020**, 16, 8760-8774.
[92] D'Aria F., Pagano B., Giancola C. Thermodynamic properties of hydroxypropyl-β-cyclodextrin/guest interaction: a survey of recent studies. *J Therm Anal Calorim* **2021**.
[93] Kamberi M, Nayak S, Myo-Min K, Carter TP, Hancock L, Feder D. A novel accelerated in vitro release method for biodegradable coating of drug eluting stents: Insight to the drug release mechanisms. *Eur J Pharm Sci.* **2009**, 37,217-22.
[94] D'Souza S. A Review of In Vitro Drug Release Test Methods for Nano-Sized Dosage Forms. *Adv in Pharm*, **2014**, 2014, 1–12.
[95] Janagam DR, Wang L, Ananthula S, Johnson JR, Lowe TL. An Accelerated Release Study to Evaluate Long-Acting Contraceptive Levonorgestrel-Containing in Situ Forming Depot Systems. *Pharmaceutics* **2016**,8,28.
[96] Markopoulos C, Andreas CJ, Vertzoni M, Dressman J, Reppas C. In-vitro simulation of luminal conditions for evaluation of performance of oral drug products: Choosing the appropriate test media. *Eur J Pharm Biopharm*. **2015**,93,173-82.
[97] McClements DJ, Li Y. Review of in vitro digestion models for rapid screening of emulsion-based systems *Food Funct*., **2010**,1, 32-59.
[98] Re R., Pellegrini N., Proteggente A., Pannala A., Yang M., Rice-Evans C. Antioxidant activity applying an improved ABTS radical cation decolorization assay. *Free Radic. Biol. Med.* **1999**, 26, 1231–1237.
[99] Bonechi, C., Donati, A., Tamasi, G., Pardini, A., Rostom, H., Leone, G., Rossi, C. Chemical characterization of liposomes containing nutraceutical compounds: Tyrosol, hydroxytyrosol and oleuropein. *Biophys Chem* **2019**,246,25-34.
[100] ISO 10995-5:2009 Biological evaluation of medical devices-Part 5: Tests for cytotoxicity: in vitro methods.
[101] Lamponi S, Baratto MC, Miraldi E, Baini G, Biagi M. Chemical Profile, Antioxidant, Anti-Proliferative, Anticoagulant and Mutagenic Effects of a Hydroalcoholic Extract of Tuscan Rosmarinus officinalis. *Plants (Basel)*. **2021**,10,97.
[102] Cruciani O., Mannina L., Sobolev A.P., Cametti C., Segre A. An improved NMR study of liposomes using 1-palmitoyl-2-oleoyl-sn-glycero-3-phospatidylcholine as model. *Molecules* **2006**, 11, 334–44.
[103] Bonechi, C.; Ristori, S.; Martini, G; Rossi, C. Study of Bradykinin Conformation in the presence of Model Membrane by NMR and Molecular Modelling, *BBA Biomembranes* **2009**, 1788, 708-16.
[104] Chen, Y.; Wu, Q.; Zhang, Z.; Yuan, L.; Liu, X.; Zhou, L. Preparation of Curcumin-Loaded Liposomes and Evaluation of Their Skin Permeation and Pharmacodynamics, *Molecules*, **2012**, 17, 5972-87.
[105] Ng, Z. Y.; Wong, J.-Y.; Panneerselvam, J.; Madheswaran, T.; Kumar, P.; Hsu, A.; Hansbro, N.; Bebawy, M.; Wark, P.; Hansbro, P.; Dua, K.; Chellappan, D.K. Assessing the potential of liposomes loaded with curcumin as a therapeutic intervention in asthma, *Coll. Surf. B*: *Biointerfaces*, **2018**, 172, 51-9.